A study of cell adhesion and Mechanosensitivity

by

Renu Vishavkarma

A thesis submitted to the Jawaharlal Nehru University

for the degree of Doctor of Philosophy

September 2015

DECLARATION

I, hereby, declare that this thesis is composed independently by me at Raman Research Institute, Bangalore, India, under the supervision of Prof. Pramod A. Pullarkat. The subject matter presented in this thesis has not previously formed the basis of the award of any degree, diploma, associateship, fellowship or any other similar title in any other University.

Prof. Pramod A. Pullarkat
Raman Research Institute

Renu Vishavkarma

CERTIFICATE

This is to certify that the thesis entitled **A study of cell adhesion and mechanosensitivity** submitted by Renu Vishavkarma for the award of the degree of DOCTOR OF PHILOSOPHY of Jawaharlal Nehru University is her original work. This has not been published or submitted to any other University for any other degree or diploma.

Dr. Ravi Subramaniam
Director
Raman Research Institute

Dr. Pramod A. Pullarkat
Thesis Supervisor

ACKNOWLEDGEMENTS

Joining as a Ph.D. student in RRI was like a turning point in my life. A number of people have contributed, directly or indirectly for the successful completion of this thesis work. I take this opportunity to thank all of them for their help and support.

The first in my acknowledgement list is my supervisor Dr. Pramod Pullarkat who introduced me to the field of interdisciplinary science. I thank him for the freedom he gave me to think and design experiments on my own, under his supervision. This has helped me grow as an independent researcher. I also wish to thank Prof. Joseph Samuel and Prof. Arun Roy for their valuable suggestions as the members of my advisory committee. The discussions with Prof. Yashodhan Hatwalne and Prof. V. A. Raghunathan were very helpful in concluding some of the work presented in this thesis. I wish to thank them for their valuable suggestions.

I would also like to acknowledge the technical staff of SCM, Dhasan, Ram, Ishaq, Murli, Raja for taking care of the day to day routine of the lab, to keep it going smoothly. I never had to worry about the complicated official procedures in the presence of RRI administrative staff and our group secretary Radhakrishnaji. I thank them for their support. Instrumentation would have not been this easy, if Narayan murthy and Achan would not have been there to help in RRI mechanical workshop. I thank them for their always ready to

help attitude and hard work. I would also like to thank my hostel-mates cum juniors, Jagdeesh, Amit, Sanjay, for the fun time we used to have in our hostel mess. It was because of Surya that I did not have to worry about vesicle preparation and micropipette pulling for one of the experiments towards the end. He was really a great help at a very crucial time and I am sincerely thankful for that.

I was lucky to always have wonderful lab-mates around. I would like to thank, Som, Venu, Chandrashekar, Roli, Alka, Susav, Serene, Nidhi, and Subham for just being there for me. Among all these people, I would like to acknowledgement the friendship, care and support that Giri, Anagha and Sushil have been giving me till date. They have never been less than a family for me in RRI.

I would also like to thank my family, which now includes Yogesh and my in-laws, for their constant support and belief in me. Lack of high education and presence of an orthodox environment in the family, had never stopped my parents from letting their daughter make her own choices. A note of thank is nothing, compared to what all they have done for me. I could not have reached so far, if they wouldn't have dared to go against the flow. I could just wish that they would always be proud of me.

Renu Vishavkarma
Bangalore
September, 2015

SYNOPSIS

Development of an embryo from a fertilized egg and maintenance against regular wear and tear in an adult organism, require a cell to divide, develop cell-cell or cell-substratum adhesion, migrate and differentiate. All these processes are controlled by biochemical and mechanical signals, that a cell receives from its surrounding. It is a well established fact now that *in vitro* these fundamental functions of a cell, can be controlled through the mechanical signals alone. These mechanical signals then in turn trigger cascades of signalling pathways inside the cell to make it respond to the mechanical cues in a particular way. Transmission of the mechanical force in a cell and the cellular response for mechanical cues is called mechanosensitivity. Our experiments attempt to understand certain aspects of cell adhesion and mechanosensitivity due to cell cytoskeleton, plasma membrane and cell adhesion. A comprehensive summary of the thesis is as follows.

Chapter I

The main cellular components that participate in transduction of the mechanical signals are the plasma membrane, cell substrate adhesion proteins and the cell cytoskeleton (an active biopolymer network). The first chapter of this thesis is a detailed description of the plasma membrane, cell cytoskeleton and cell adhesion. Other than

the structural and functional details of these three components, response of a cell to the mechanical signals from the surrounding is also discussed in this chapter, with an overview of earlier reported observations. The first chapter of the thesis also prepares the necessary background for the rest of the chapters in this thesis.

Chapter II

According to the earlier reports, stem cell differentiation can be controlled *in vitro* by controlling the ECM rigidity alone. The changes occurring at the genome level, when cells were grown on the substrates of different rigidities, were observed after 2-3 weeks. The change in morphology however, were noticed within 24 hours from the time when cells first came in contact with the substrate. The differences in morphology were seen in terms of the cell spreading on different rigidity substrates. It has also been observed earlier that the change in cell spreading, caused by varying substrate rigidity, also influences the nuclear shape. Nuclear and cellular geometries were reported to be correlated in these previous observations but this had never been quantified and tested before. We in our experiments have quantified this correlation for the mouse mesenchymal stem cells (mMSCs) and tested for its robustness over a number of cytoskeletal and nuclear perturbations. Similar type of correlation was also observed in case of 3T3 fibroblasts and C2C12 myoblasts between cell and nuclear geometries. Actin depolymerization, myosin

II inhibition and microtubule depolymerization were used to perturb cell cytoskeleton. For the nuclear perturbation, lamin A/C knock-down and inhibition of histone deacetylase were done on mMSCs. The correlation was found to be intact across all the perturbations mentioned above. These observation led to a conclusion that the nuclear shape is controlled by the cell shape alone. It does not matter how the change in cell shape is induced, change in the nuclear geometry always follows to fall on the cell spreading-nuclear projected area curve established through a number of experiments explained in detail, in chapter II.

The perturbation experiments, performed on mMSCs pointed towards a mechanical coupling between the cell spreading and the nuclear projected area. Confocal images of cells, grown on substrates with varying rigidities were taken to investigate this mechanical coupling. The nucleus was found to be sandwiched between two types of stress fibres. One beneath the nucleus in the flat basal part of the cell and the other passing over the nucleus, attached to the focal adhesion in basal part of the cells. The stress fibers that pass over the nucleus and can be seen in the apical section of the cell, are known as perinuclear stress fibres. The nuclear perturbation experiments, 80 nM Lat-A treatment and the previously reported results of laser ablation on perinuclear stress fibers, have shown that the disc like nucleus of well spread cells become nearly ellipsoid if the perinuclear stress fibers are either depolymerised or ablated. This suggests a normal compression of the nucleus by the cells, through

the perinuclear stress fibres. We also observed that the actin organization changes from the cortical actin to stress fibres gradually for the cells grown on soft, intermediate and rigid substrates. Therefore we hypothesize that the cell regulates the compressive forces on the nucleus by changing its actin organization from cortex to stress fibres to press on the nucleus for the enhancement of it spreading. Theoretical estimates and experiments were done to test this hypothesis of cell spreading dependent nuclear compression, responsible for the correlated changes in the cell spreading and nuclear projected area.

In agreement with the earlier reports, myosin II inhibition was found to enhance cell spreading in the case of cells grown on soft substrates and decrease the spreading for cells grown on rigid substrates. Cells grown on substrate with intermediate rigidity were observed to show a little difference in cell spreading. According to the previous reports, myosin II inhibition affects mechanosensitivity of the cells as rigidity dependent cell spreading, proliferation rate and differentiation were not seen in blebbistatin treated cells. The mechanism behind the antagonistic effect of blebbistatin treatment on cell spreading can also be explained through our nuclear compression model.

Chapter III

Membrane tension is one of the important mechanical property of the cell membrane. Membrane tension plays crucial role in regulation of cell motility, morphology and trafficking.

In chapter III, using the membrane tethers, pulled by optical tweezer, we first investigate the effect of cell spreading on static and dynamic membrane force, and then the tether force dynamics for pulling and retraction of a membrane tether. We report a number of novel observations, that need further investigations. A brief overview of the experiments done with the help of an optical trap, is as follows.

- **Dependency of static membrane tension on cell spreading.** Membrane tethers were pulled from 3T3 fibroblast cells, with different spreading. The cell spreading was controlled by growing the cells on adhesive patches of circular shape, prepared using micro-contact printing. Three spread area were used for the measurements of static membrane tension. We observed that the static membrane tension increases with increase in cell spreading.

- **Effect of cell spreading on dynamic membrane tension.** Dynamic force corresponds to the force experienced by an optically trapped bead, when it is pulling a tether from the plasma membrane at a constant speed. Two cell spreading areas 1800 μm^2, 314 μm^2 were used to investigate the behaviour of a constantly elongating membrane tether. Membrane tethers of length around 40 μm were pulled with two different speeds, 0.6 $\mu m/sec$ and 6 $\mu m/sec$.

- **Step pulling.** A tether was given a step pull of 5 μm, by moving the bead attached to the tether in a step. The step pulling

of a tether leads to a sharp rise in tether force which decays over a finite time. The peak heigh in these experiments were found to be depending on the length of the tether. E.g., peak for the second step–pull was observed to be smaller than that for the first step–pull. The difference between the peak height of two consecutive pulls was found to be decreasing with increasing tether length. The dependency of peak height on tether length was found to be unaffected even after actin depolymerization.

- **Cyclic strain.** 30–40 μm long tethers, pulled from 3T3 fibroblast cells were given + and − steps, to move the bead attached to the tether, away and towards the cell. This is equivalent to cyclic stretch and relaxation of the tether. We found that the tether force, after showing a sharp rise and dip for +ve and −ve step, respectively, comes back to the steady state force value.

- **Step retraction.** We, through our retraction experiments have aimed to explore the force dynamics of a retracting tether. A tether of around 40 μm in equilibrium with the cell membrane was retracted by moving the trapped bead attached to the tether, towards the cell, in steps of 5 μm. A sharp dip in force, followed by a force build up in membrane tether was observed. For the first few retraction steps, the building up of force was seen to be roughly exponential, but after a few steps the force retrieval becomes a two step process, as shown in fig. 3.23. We found that the actin structure of the cell, does not play any role in the tether force response to step relaxation. This suggests

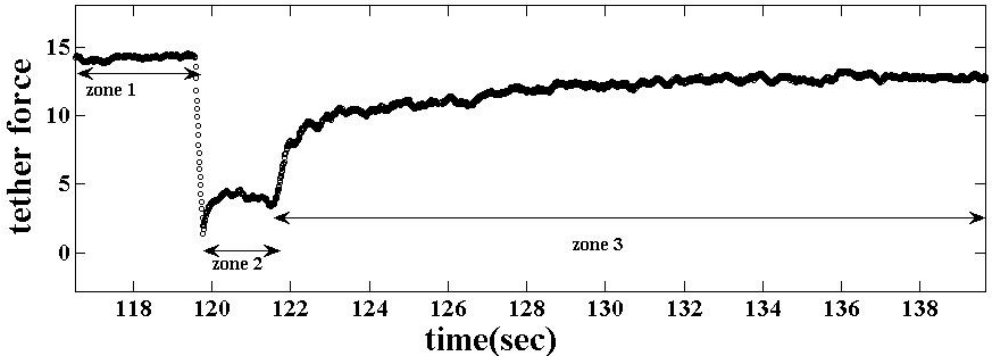

FIGURE 1: The force retrieval dynamics of a retracting tether when the trap is moved towards the cell in steps can be divided in three zones. Zone 1 represents the steady state tension of the tether before the step. Zone 2 is the duration for which the tether remains floppy. Zone 3 shows how the force retrieves in the tether as a function of time.

that the force retrieval at the trapped bead, due to step relaxation, might be a result of the intrinsic property of the lipid membrane alone.

In order to understand the two step relaxation, time lapse recordings were taken after a few retraction steps. We found that the first force retrieval step (Zone 2) is due to the floppiness appearing in the tether. The first step of force retrieval which takes around 1 sec, is due to the entropic properties of the floppy tether. Once the tether gets straightened, the force builds up in the tether to get an equilibrium between the tether force and the plasma membrane tension. An overall decrease in the membrane tension was also observed in these tether retraction experiments.

- **Dynamic tether retraction.** Long tethers of length around 40 μm, were pulled and then retracted back towards the cell with a constant speed of 0.2 $\mu m/sec$. We observed that the

tether force remains constant for some time and then starts decreasing. It suggests that the rate at which the tether membrane flows back to the cell membrane decreases as more and more excess membrane is made available to the cell membrane.The decrease in flow rate may be due to a decrease in membrane tension at the local scale.

- **Multiple tethers.** According to the earlier reports, a long tether pulled from one side of the cell causes a depletion of membrane reservoirs at the other side of the cell. This causes an increase in membrane tension at the other side. We, in our experiments could not see any such behaviour of membrane tension. We pulled 4–5 tethers, each of length 30–40 μm from different parts of cell membrane, and all the tethers were found to detect the same value for static membrane tension. Together, these experiments show never before reported response of the membrane tension to tether pulling and relaxation. Further experiments need to be done to explore the observed tether force dynamics for a better understanding.

Chapter IV

As discussed in the earlier section, the cytoskeletal in combination with the cell adhesion molecules, form the force sensing and generation machinery of a cell and hence makes a cell mechanosensitive.

This chapter aims to measure the adhesion strength of cells by using a cone and plate geometry based shearing device that we have designed in our lab. The device is compact, inexpensive, easy to use and can be combined with different types of microscopy techniques such as total internal reflection fluorescence (TIRF) and confocal, traction force microscopy (TFM). Unlike a passive material, a cell under shear is able to reorganize its cytoskeleton and change the distribution of its adhesion sites to oppose the stress caused by the shear. This happens when the applied shear is lower than the stress required to detach the cell. Another advantage of the device that we have designed is, live recording at high magnification which can be done while the cells are under shear. This advantage can be exploited to study the cytoskeletal reorganization and focal adhesion redistribution in adherent cells due to shear stress. This chapter includes design of the shearing device with details of its control, detection, alignment methods involved and its applications.

Prof. Pramod A. Pullarkat
Raman Research Institute

Renu Vishavkarma

Publications

- R. Vishavkarma, S. Raghavan, C. Kuyyamudi, A. Majumder, J. Dhawan and P.A.Pullarkat,
  '*Role of actin filaments in correlating nuclear shape and cell spreading*',
  Plos One DOI: 10.1371/journal.pone.0107895.

Contents

Chapter 1

Introduction

A cell is the basis of life. A multicellular life originates from a single cell. This single cell, i.e., the fertilized egg undergoes a number of divisions followed by migration of cells to form three germ layers. The cells in the three germ layers then differentiate and take the form of different organs to finally form a living organism. At the final stage of development we, the humans, are left with 200 different types of cells and 20 different types of organelles. Each of these 200 different type of cells are specialized to perform well defined tasks. In an adult body also these different types of cells undergo a cycle of life wherein they are born, live for some time, and then die. The birth, survival, and death of a cell depend on many biological and mechanical signals from the surrounding. The regular maintenance work, like replacing the dead cells during regular damages caused by injuries or diseases are carried out by the stem cells stored in different tissues in an adult body. A stem cell does not have any identity and it is not specialized to perform any particular task like a heart cell which

is specialized to beat or a neuronal cell which is functionalized to transmit the signals between the brain and rest of the body. A stem cell can either divide to give more stem cells or it can differentiate to become a specialized cell like a neuronal cell or a heart cell. Stem cells can be divided into three categories according to the number of lineages it can differentiate into: totipotent, pluripotent and multipotent [1]. A single cell that can divide and differentiate into all types of cells in an organism is called a totipotent cell. E.g., spores and zygotes. A zygote divides into a number of cells that makes embryo and placenta. The cells which divide and differentiate during embryogenesis are called pluripotent cells as they can differentiate into any cell type of an embryo, but not the protecting shell of the embryo. At the early stage of embryo development, all the mass of cells differentiate and reorganize into three germ layers. Each germ layer can further differentiate into limited cell types and therefore they are called multipotent cells. Multipotent cells are also present in an adult body. It is these cells that do the regular repair work in a developed organism. There are microenvironments in an adult body that act as storage houses for these cells. These microenvironments are called "niche". A niche signals the stem cells to make copies, migrate to the place where it is required and differentiate. The three main niche known in an adult body are bone marrow, muscle tissues and brain. The signal that instructs a cell to divide, migrate or differentiate can be biochemical or mechanical. Recently, it has been shown by a number of studies that these three processes of a cell can

be controlled by mechanical cues. Response of a cell to the mechanical cues from inside or outside the cell is called mechanosensitivity. The main cellular components that participate in the transduction of the mechanical signals are the plasma membrane, cell substrate adhesion proteins and the cell cytoskeleton (an active network).

This chapter includes an introduction to the cell membrane and the cell cytoskeletal, followed by an overview of adhesion and mechanosensitivity. Towards the end of this chapter, a brief introduction of rest of the chapters included in this thesis is provided.

1.1 Plasma membrane

The plasma membrane of a cell is what keeps the inside of the cell enclosed and separated from the surrounding. A cell membrane is a semi-permeable lipid bilayer with a number of proteins embedded in it. The membrane proteins act as the receptors to the biochemical or mechanical signals form the surrounding. The lipids in the membrane play active role in the regulation of membrane structures and biological functions [2–4]. The various parameters that define the mechanical properties of the plasma membrane are as follow.

- A very low shear modulus [5–7].
- Compressive elastic modulus = $10^3 N/m^2$ [8, 9].
- Bending modulus = $10^{-19} N.m$ [10–12].

The viscosity of the plasma membrane depends on its composition. The plasma membrane of a cell tries to maintain a cell specific membrane tension. Any modulation in membrane tension have been reported to affect cell motility [13–15], morphology [16, 17], and trafficking [18]. The plasma membrane also has a number of ion channels, that are sensitive to the membrane tension. An increase in membrane tension can result in activation of these ion channels [19].

1.2 Cell Cytoskeleton

The second component of the force sensing machinery of the cell is the cell cytoskeleton.

The cytoskeleton is a network of filamentous protein polymers that are interconnected with cross linker proteins [20]. There are mainly three type of filamentous polymers that constitute the cytoskeleton: microfilaments or actin filaments, microtubules and intermediate filaments. In a cell, the length of each type of filament depends on assembly and disassembly rate of their respective subunits, as shown in fig. 1.1.

The basic functions of the cytoskeleton are to provide shape to the cell, transport intracellular cargo, sensing and responding to the external forces. Together with the adhesion complexes (discussed later), the cytoskeleton makes the major force sensory machinery of the cell. The detailed description and functions of different components of the cell cytoskeleton are as follows.

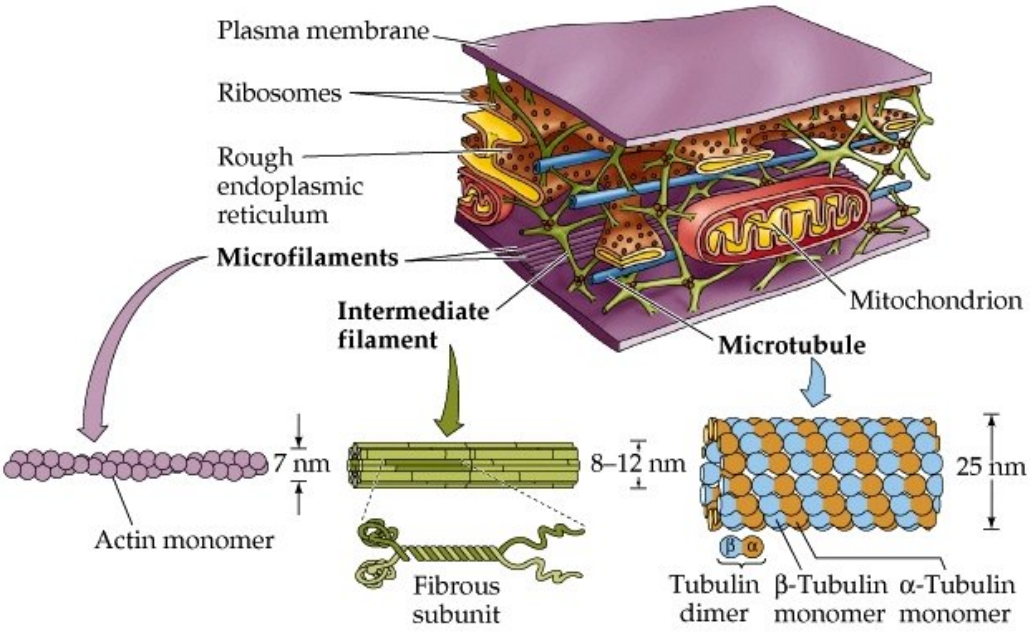

FIGURE 1.1: The cytoskeletal of a cell is composed of three types of biopolymer filaments that are essential for maintaining the cellular shape and functionality. The three type of filaments are actin filaments/microfilaments, microtubules and intermediate filaments. Images is adopted from– http://jindetres.blogspot.in/2013/05/disturbios-celulares-2.html

1.2.1 Microtubules

Microtubule filaments are hollow cylinders of 25 nm typical diameter and approximately 5 mm of persistent length. Each microtubule filament is composed of 11-16 protofilaments. A single protofilament is nothing but tubulin dimers connected end to end. Each tubulin dimer has two subunits called α tubulin and β tubulin as shown in fig. 1.1. Microtubules are the stiffest cytoskeletal fibres. As the tubulin dimer adds only in one direction, microtubules have a polarity. The end of the microtubule where tubulin dimer polymerizes and β-tubulin is exposed is called the + end and the other end where α-tubulin is exposed is called the − end. It is the + end of the microtubule where the assembly or disassembly takes place. The −

ends are clustered together at the microtubule organizing centre or centrosome. The basic functions of a microtubule are as follows.

- Microtubules form long distance tracks for the transport of the cargo inside the cell. The cargos are carried by dynein and kinesin family of motors, on these tracks as shown in fig. 1.2(a).

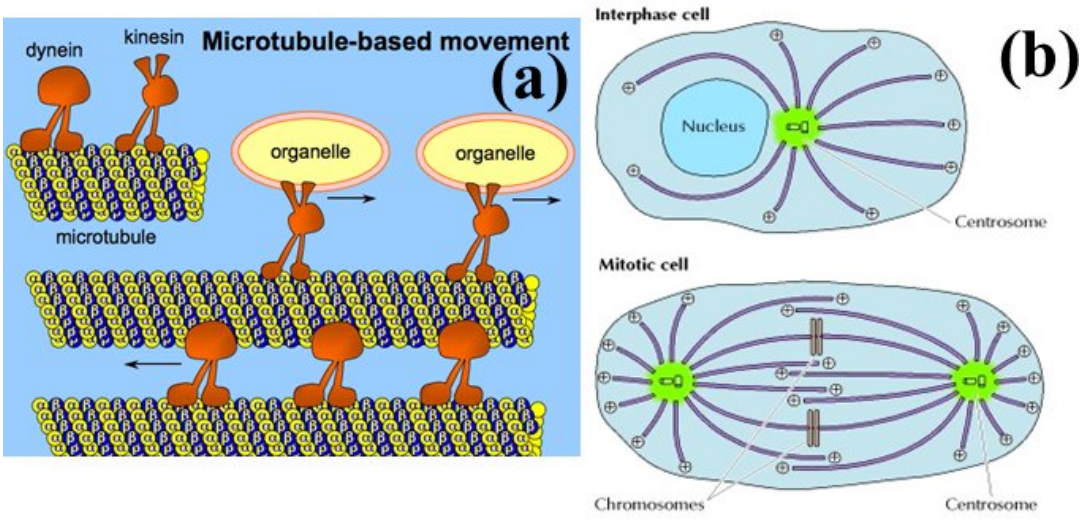

FIGURE 1.2: (a) Microtubules form tracks for the transport of the cargo. Transport is effected by microtubule associated motor protein dynein & kinesin using energy derived from ATP hydrolysis. Image courtesy http://plantphys.info/plant_physiology/cytoskeleton.shtml. (b) The configuration of the microtubules in a cell in the two stages, interphase and cytokinesis, of cell cycle. Image courtesy, The Cell : A molecular approach, 2000 [21]

- It plays a crucial role in cell division with the formation of spindles to separate chromosomes into two identical sets as shown in fig. 1.2(b).

1.2.2 Actin filaments

An actin filament is made up of two protofilaments, each called F-actin, wound together in a right handed helix as seen in fig. 1.1. Subunit of actin filament, G-actin has a specific conformation and can attach only in a particular orientation. Thus, the filament has an intrinsic orientation and polarity. An actin filament can either shrink or elongate at both the ends according to the local concentration of actin monomers near the end. The dynamics of addition or removal of monomers is faster at the + end than at the − end. The average length of an actin filament is decided by the difference in critical concentration of cytosolic monomers (C_c) and the concentration of monomers at the two ends (C_c^+ and C_c^-) of the actin fiber. For C_c greater than C_c^+ and C_c^- both the ends of actin filaments grow and for C_c smaller than C_c^+ and C_c^- both ends shrink and the filament position moves at a constant velocity. Actin filaments undergo a process known as treadmilling. Treadmilling occurs when the + end of the filament is growing and the − end is shrinking. At the steady state treadmilling, the rate of growth of actin filament at one end is equal to the rate of shrinkage at the other end. The nucleation of actin polymerization is done by Arp2/3 [22] for branched actin filaments, e.g., filaments in lamellopodia, and formins [23] for the unbranched actin filaments, e.g., actin fibres that make stress fibres.

Actin filaments can have two conformations in a cell. With the help of cross-linking proteins the actin filaments can either form bundles

or make random networks. Bundles of actin is what is found in stress fibres whereas the actin network constitute the cell cortex that lies beneath the cell membrane. Few examples where actin is required in a cell are as follows.

- Bundles of closely spaced actin filaments binds to the tips of filopodia to make them stiff. The plus end of the actin bundles are oriented towards the filopodia tip and helps them grow by generating forces through polymerization.
- Growth of the branched actin filaments close to the plasma membrane pushes the lamellopodia of the cell, in forward direction during cell migration [24].
- When a cell makes stable adhesion to the substrate, it develops bundles of actin fibers called the stress fibers. Anti-parallel stress fibers with their + end towards opposite side of the cell are able to slide when connected with molecular myosin motor. This sliding of stress fibres provides contractility to the cell which plays a crucial role in mechanosensitivity.
- The contractile actin network, i.e., the cortical actin, lies just beneath the plasma membrane and provides shape and rigidity to the cell.
- Together with myosin motors, actin filaments form contractile rings to separate the daughter cells during cell division.

- Since the actin filaments are also polarized like microtubules, they also contribute to the myosin mediated transport of the cargo inside the cell.

1.2.3 Intermediate filaments

Fibrous subunits that are extended dimers overlap to form unpolarized cables called intermediate filaments. These are the most flexible and high tensile strength fibers of the cytoskeleton with a typical diameter of 8-12 nm. As they do not posses any polarity, they have no contribution in directed transport of intracellular cargos. A cell has a number of different types of intermediate filaments that can broadly be grouped into five classes [25]: 1) type I (acidic) keratins, 2) type II (basic) keratins, 3) vimentin and desmin, 4) α-internexin and neurofilaments, and 5) lamins. Intermediate filaments from different classes form a network to carry out different tasks in a cell. For example, keratin intermediate filaments form network in airway endothelial cells to resist shear stress [26]. Lamins are found in the nucleus and are essential for its mechanical integrity. Phosphorylation of nuclear lamins dissolves nuclear envelope at the beginning of mitosis [27]. Neurofilaments that embed or surround the microtubules in neuronal cells are the key players in controlling the radius of the axon.

1.2.4 Motor proteins

Motor proteins are the molecular motors that move/walk on the cytoskeletal filaments for either intracellular transport or force generation within the cytoskeleton. Microtubule oriented transport is performed by kinesin and dynein motors whereas the molecular motors associated with actin are called myosins. In most cells, kinesin motor walks towards the + end of the microtubule and dynein walks towards the − end. Myosins, on the other hand, mostly walk towards the + end of the actin filaments, except myosin VI. In this chapter we are concerned with myosin motors. A detailed description of myosins is as follows.

1.2.4.1 Myosin

Myosins are the motor proteins that move along actin filaments by ATP hydrolysis. A myosin motor may have one or two heads depending on the class it belongs to, and a tail. The head hydrolyse ATP, makes attachments and moves along the actin filaments. Depending on the sequence of amino acids in the motor domain, myosins can be divided into 20 groups. The so far well explored myosin classes are myosin I, myosin II, myosin V and myosin VI. Assemblies of myosin II motors slides the anti-parallel actin filaments which may be either in the form of stress fibres or in the actin filament network. Heads of bipolar myosin II complex attached to two anti parallel actin filaments result in acto-myosin contractility of the cell as shown in

fig. 1.3(a). The acto-myosin based contractility plays important role

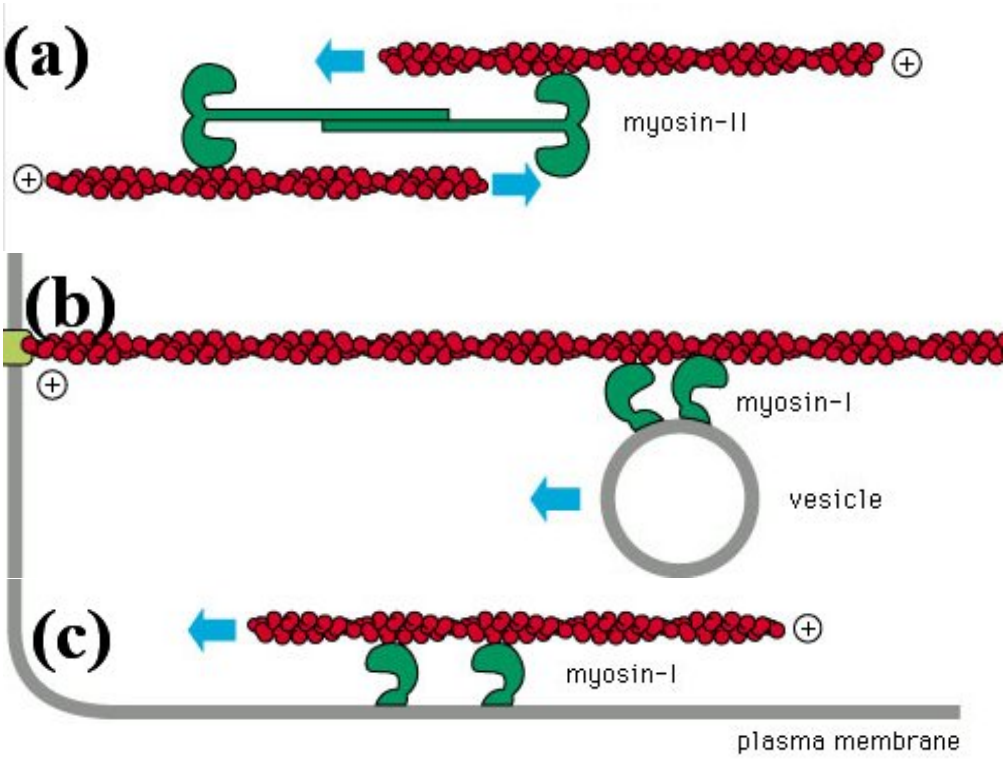

FIGURE 1.3: (a) Bipolar myosin II complex attached between two anti parallel actin filaments makes the filaments slide against each other and cause contractility. (b) & (c) Myosin I has only one motor domain that can bind to the actin filament and move towards its + end. The neck of myosin I is either attached to the plasma membrane or to a cargo. Image courtesy: http://www.bio.miami.edu/tom/courses/bil360/bil360goods/16_muscle.html.

in force sensing or generation, retraction of the rear end in cell migration, formation of contractile rings to separate the daughter cells during cell division, etc.. The actin mesh under the plasma membrane is also contractile due to its association with myosin II motors.

Myosin I ,V and VI either connect cell membrane to the actin filaments to move the membrane in forward direction during cell migration or attach to the vesicles to participate in intracellular organelle movement as shown in fig. 1.3(b), 1.3(c) and 1.4.

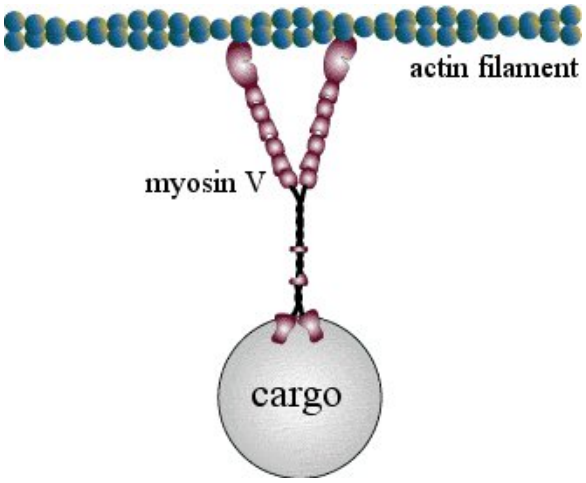

FIGURE 1.4: The globular heads with heavy chain attach to myosin V move along actin filaments by ATP hydrolysis. The heads at the other end of myosin V generally binds to the cargo for intracellular transport. Image is adopted from http://www.bumc.bu.edu/phys-biophys/people/faculty/moore/moore-laboratory/research/m5background/.

1.3 Cell adhesion

Cell adhesion is the anchoring of the cell to the extra cellular matrix (ECM). Cell adhesion is non-uniform, environment and time dependent. The longer a cell is in contact with its surrounding, the better adhesion it would make, until a saturation level of adhesion is reached. Environment dependency includes the effects of chemical composition and the mechanical properties of the ECM on cell adhesion. Cells grown on plain glass with different protein coatings have been found to show difference extent of cell spreading and hence difference in cell adhesion [28]. A cell binds to the adhesion proteins on the ECM through discrete patches of the transmembrane proteins called integrins. These integrins are attached to focal adhesion complexes inside the cell. The focal adhesions are in turn attached to the actin filaments and therefore the cytoskeletal network of the cell.

Together, focal adhesion complexes and actin-myosin network forms the force sensory machinery of the cell as shown in fig. 1.5 [29]. Sensing the forces or stress from the surrounding and generating signals to behave in a surrounding dependent manner is done by the cells through this machinery.

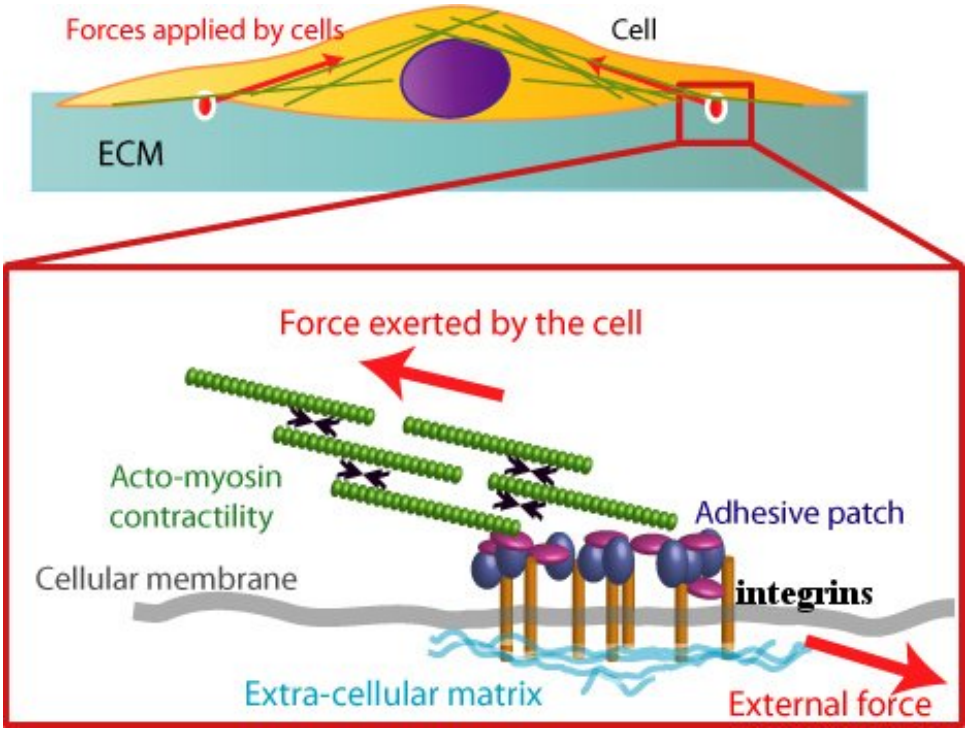

FIGURE 1.5: Connection made via adhesion molecules (proteins) that are clustered to form tiny patches. Image courtesy http://www.cs.stedwards.edu/chem/Chemistry/CHEM43/CHEM43/CellAdhesion/integrinregulation.htm.

1.3.0.2 Focal adhesion complexes

Focal adhesion are known to be very dynamic in nature. The chemical composition, size, assembling and disassembling rate of focal adhesions depend on the chemical or mechanical signals they receive from the surrounding. Acto-myosin contractility of the cell act as the key player in focal adhesion kinetics [30]. Recruitment of vinculin

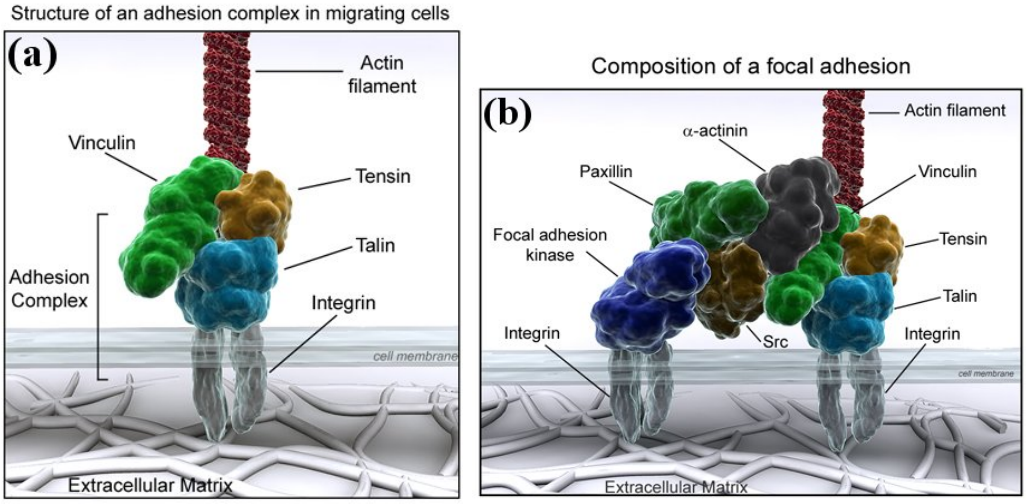

FIGURE 1.6: (a) and (b) show the difference in the molecular structure of nascent focal adhesion and mature focal adhesions. Image is adopted from http://www.reading.ac.uk/cellmigration/adhesion.htm.

to focal adhesion complexes by focal adhesion kinase is mediated by myosin contractility induced paxillin phosphorylation [31]. Inhibition of myosin II has been shown to prevent the formation of mature focal adhesion complexes and disassembly of the existing ones [32–34]. When a mechanical force is applied on the cell, the focal adhesion complex responds in number of ways. The maturation and disassembly of focal adhesions depend on the mechanical stress in the surrounding [35, 36]. The binding of vinculin to talin in a focal adhesion complex has also been shown to get enhanced if a stretch is applied to the talin rod [37]. This in turn strengthen and stabilizes the focal adhesions. The various components that constitute focal complexes and mature focal adhesion can be seen in fig. 1.6. The various functions of different proteins in a focal adhesion complex are as follows.

- **Vinculin:**: It regulates and transmits mechanical forces between integrins and cell cytoskeleton [38].
- **Talin:** It comprises of a N terminal head domain, neck and a rod domain. It makes multiple connections with the integrins, plasma membrane, actin filaments and vinculin. It acts as a vinculin binding protein [39].
- **Paxilin:** It controls adhesion and organization of internal cytoskeleton by bringing together the signalling molecules, regulatory proteins and the structural components. It also acts as a vinculin binding site in focal adhesion complex [40].
- **Taxin:** It forms bridges to maintains tension between the actin filaments and integrins [41].

1.4 Mechanosensitivity

A cell responds in number of ways to the mechanical cues in its surrounding. These mechanical cues generally include substrate rigidity, stress, shear, geometric constraints, substrate topography etc. As a response to these mechanical cues, a cell can open the ion channels present on its membrane [42], change cytoskeletal organization, increase/decrease acto-myosin contractility, modify the cell-ECM adhesion [43], etc. Regulation of these parameters of the cell by mechanical forces controls the previously mentioned processes, i.e., migration, proliferation, apoptosis, differentiation etc. A pictorial

representation of the machinery that governs the cellular response to mechanical forces is as shown in fig. 1.7. The various effects caused

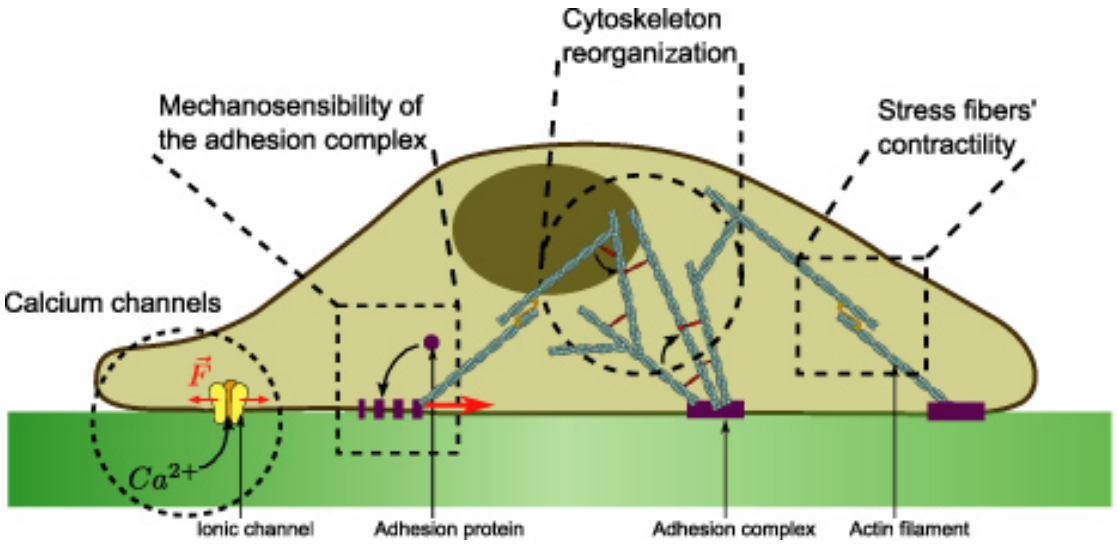

FIGURE 1.7: When an external mechanical signal is given to a cell, it responds in a number of ways. Cellular response to given external mechanical cue is dictated by the stress-activated channels on cell membrane, acto-myosin contractility, cytoskeletal organization and cell-ECM adhesion. These signals can be transmitted to the nucleus either by direct coupling or via biochemical means. Image is adopted from Ladoux and Nicolas, 2012 [43].

by mechanosensitivity are discussed below.

1.4.1 Stem Cell Differentiation

Engler et al., in 2006 showed that mesenchymal stem cells (MSCs) grown on substrates with rigidity varying from 1 kPa to 100 kPa differentiate differently [44]. Cells on polyacrylamide gels of rigidity 1 kPa and 60 kPa were shown to differentiate to give neurons and bone cells respectively. The correspondence of substrate rigidity to stem cell lineage specification is shown in fig. 1.8. It is shown that the stem cells starts showing the stiffness dependent changes in morphology, within few hours of their contact with the substrate as shown in

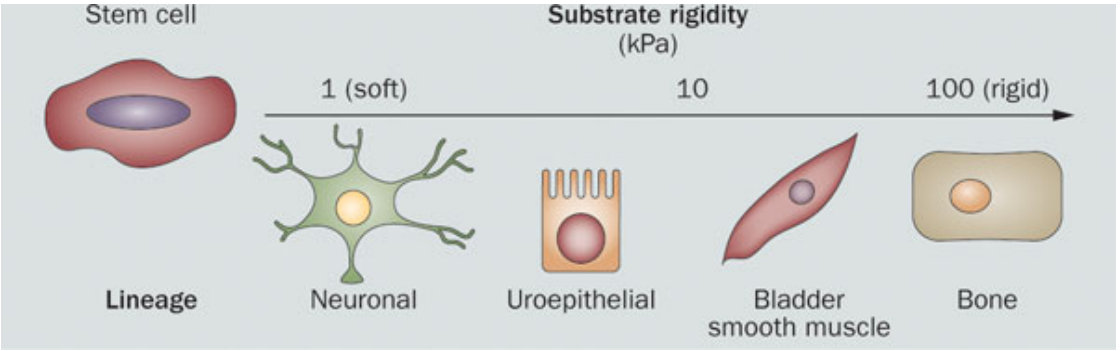

FIGURE 1.8: It has been observed that the stiffness of the substrate should match the stiffness of the cellular niche [45] to give a lineage commitment. The stiffness of the niche for a bone cell is different from the niche for a neuronal cell. A cell growing on the rigidity of a neuronal niche can not differentiate into anything other than a neuron. Image is adopted from Nature Review Urology [46].

fig. 1.9. The changes at genome level takes place in 3 to 4 weeks [44].

Other than substrate rigidity, stem cells differentiation has also been found to get affected by compressive loading [47], level of confluency and therefore cell shape [48] and geometric constraints [49, 50]. Monolayers of human MSCs (hMSCs) grown on a circular patch showed commitment to different lineages depending on the radial distance [49]. Cells near the center became osteocytes whereas cells near the periphery committed to adipogenic differentiation. Moreover, the monolayers of different shapes and curvature also showed differentiation depending on space coordinates as shown in fig. 1.10(a–f). On single cell level, hMSCs grown on adhesive rectangles of equal area but various aspect ratios and same area patterns with five vertices but different edge curvature, have been shown to give different osteogenesis and adipogenesis profiles [50] as shown in fig. 1.10(g) & (h).

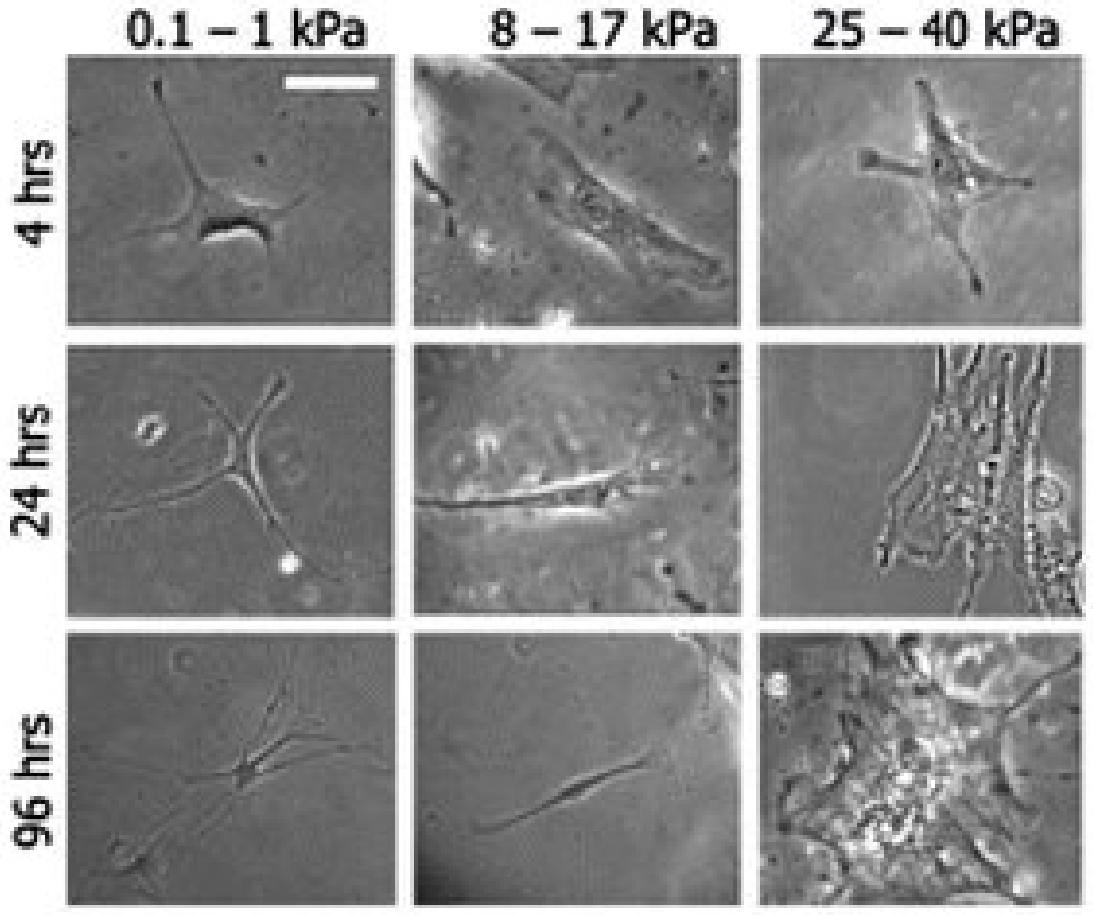

FIGURE 1.9: Cells grown on substrate with low Young's modulus (0.1–1 kPa) were shown to develop more branch like morphology as compared to the cells grown on hard substrate. The number of branches increase as the cells proceed to differentiate into a neuron. The cells on the substrates with intermediate rigidity (8–17 kPa) were observed to get a polarity and found to differentiated into muscle cells after a few weeks. The hardest substrates (25–40 kPa) used, were seen to induce large spreading in cell and the a morphology of an osteoblast. Image is take form Engler et. al, 2006 [44]

Mechanosensitivity is not the phenomenon restricted to stem cells only. It also has an effect on other cell types in terms of changing contractility, shape, migration speed and cell division rate. A few of these changes that can be induced in any cell type by changing substrate rigidity are as discussed in the following subsections.

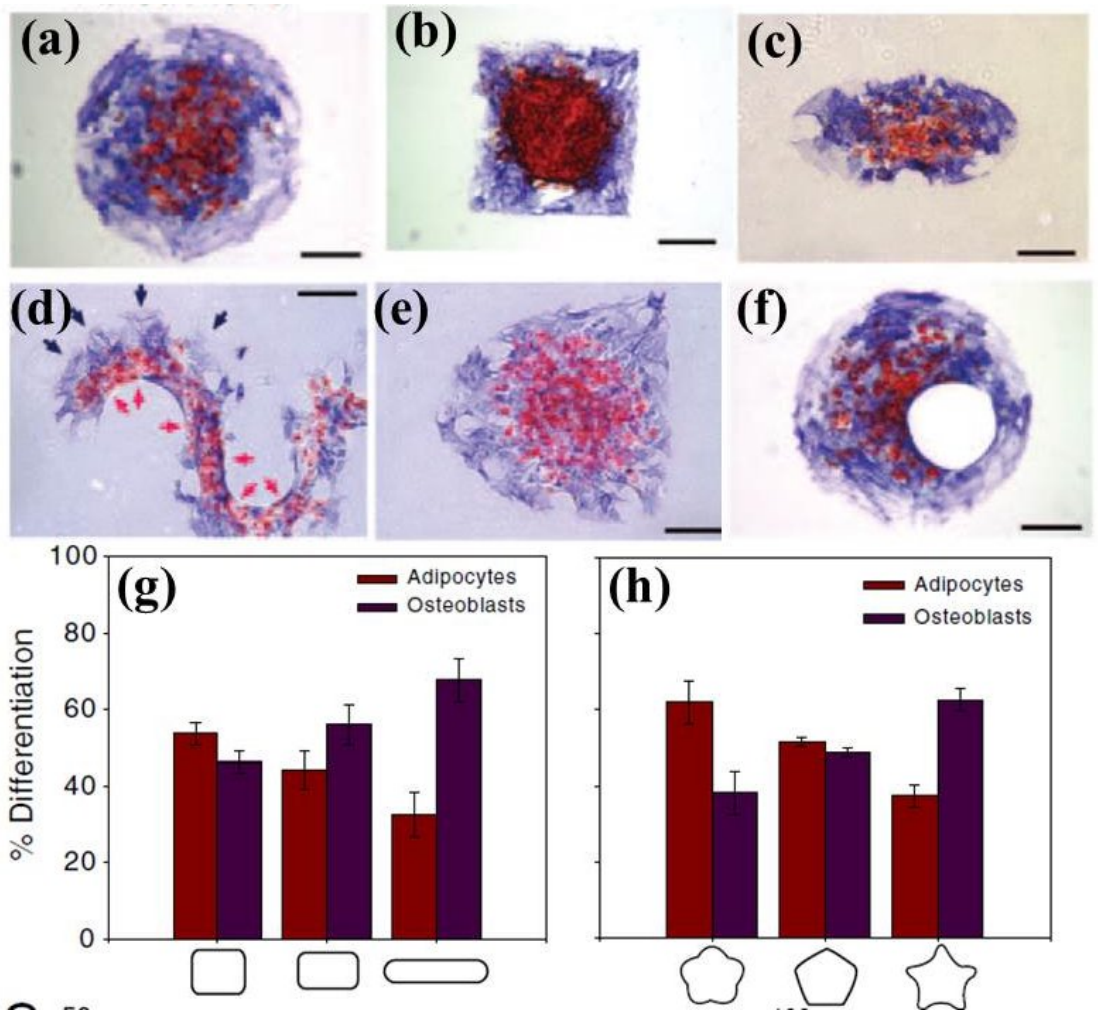

FIGURE 1.10: (a–f) Monolayers of hMSCs show position and curvature dependent differentiation when grown on adhesive patches of different shapes [49]. (g) & (h) Change in aspect ratio or subcellular curvature changes the profile of differentiation in hMSCs monolayers of equal area [50]. Blue and red color represent osteogenic and adipogenic differentiation, respectively.

1.4.2 Cell migration

Cell migration plays a crucial role in tissue formation during embryogenesis, wound healing, immune responses and spreading of disease e.g., cancer metastasis. Generally chemical or mechanical cues are required to navigate a cell in a particular direction. Cell migration is a multistep process that involves protrusion of lamellopodia in the direction of migration, formation of new focal contacts and their

maturation or turnover followed by disassembly of focal adhesion and retraction of cell at the rear end [51]. The protrusion and contraction of the cell is accompanied by cytoskeletal reorganization as shown in fig. 1.11. The speed of cell migration depends on many chemical and

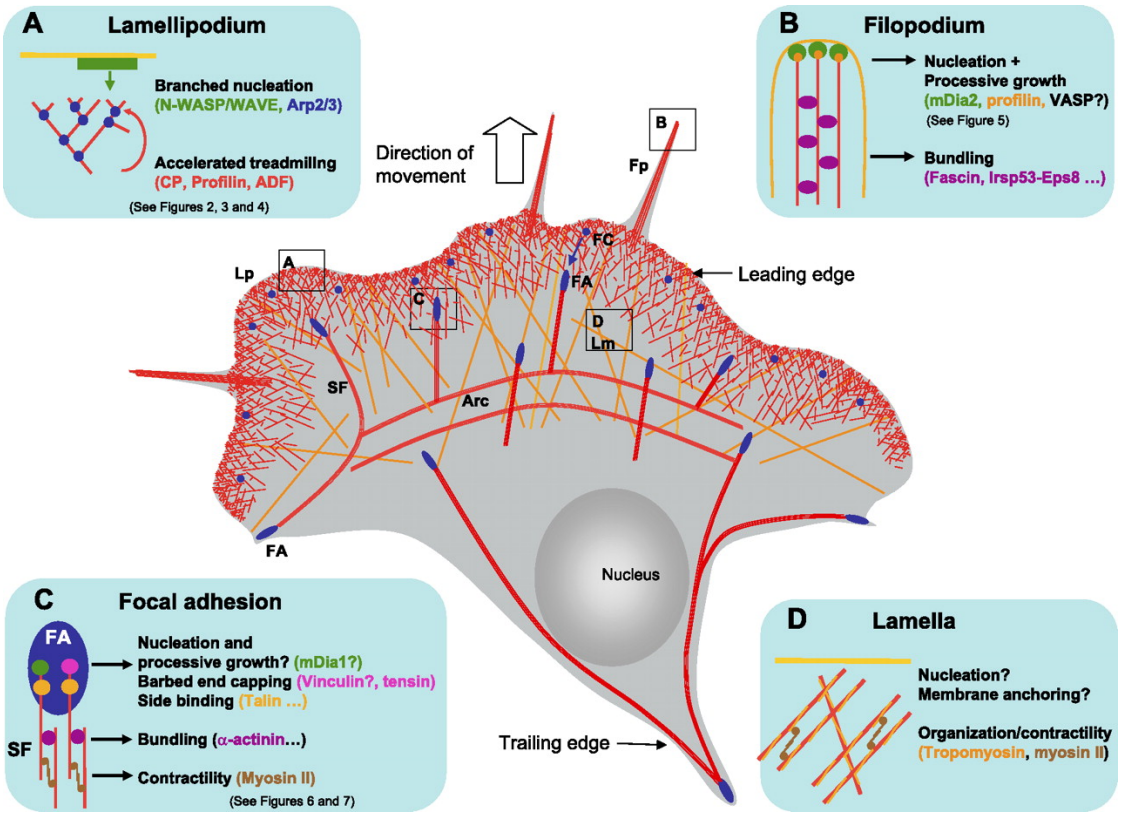

FIGURE 1.11: Cell migration starts with the generation of filopodium and lamellipodium, followed by focal contact formation and movement of lamellipodium in the forward direction. Image is taken from Clainche and Carlier, 2008 [52].

mechanical factors. The migration speed also depends on cell type and cell contractility [53]. For example cells like neurons and human embryonic kidney cells are almost non motile whereas fibroblasts are the cells commonly used for cell migration assays. Fish keratocytes are the fastest moving cells that have been generally used for migration related studies. One of the mechanical factor that influences cell migration speed is substrate rigidity. Cell migration speed is

proportional to the substrate rigidity. The migration speed of a fibroblast cell has been found to be higher on a hard substrate as compared to a soft substrate, with high membrane fluctuations on soft substrate [54]. hMSCs, when grown on substrates with rigidity gradient, were found to migrate to give a density distribution [55]. More number of cells were observed towards the hard side of the substrate as compared to the soft side.

1.4.3 Cell proliferation

Cell division rate has also been shown to have a substrate rigidity dependence. Cells growing on rigid substrates divide faster than the cells grown on the compliant substrates [56]. Mih J.D. et. al. [57] showed that the proliferation rate of a cell is coupled to its spread area. Cells with low proliferation rate showed an increase in cell division rate once the cell spreading is increased by reducing cell contractility by inhibiting myosin II, as shown in fig. 1.12. Inhibition of myosin II in cells grown on gels of varying substrate rigidity induces rigidity independent spreading [57]. Hence, cells on rigid substrate and compliant substrate spread to almost equal extent. Moreover, the difference in migration speed and rigidity dependent lineage specification is also not to be seen once the cells are treated with the myosin inhibitor Blebbistatin [44]. This indicates that the mechanosensitivity is an acto-myosin driven phenomenon, and in the absence of contractility cell can no longer sense the substrate stiffness.

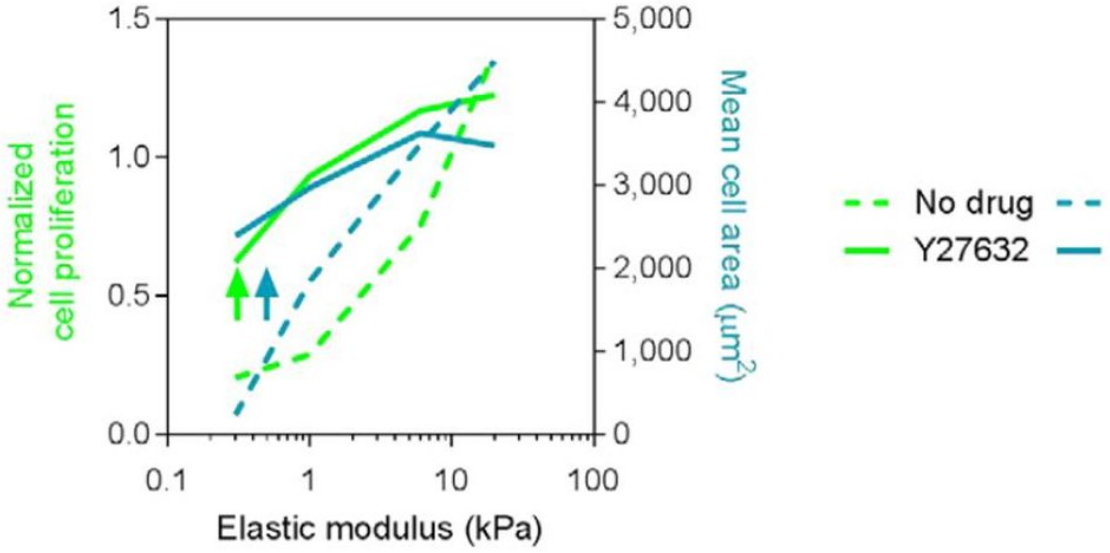

FIGURE 1.12: Cells grown on soft substrates show an increase in cell spreading and proliferation rate after Y27632 treatment [57]. The drug reduces cell contractility by inhibiting ROCK.

All the experiments related to stem cell differentiation indicate that the differentiation has a strong dependency on shape and size of the cell. ECM rigidity is one parameter that can induce change in morphology and spreading area of the cell. The argument that mechanosensitivity is related to cell shape and size is strengthen by the experiment where the contractility of the cell is reduced, which resulted in an increase in cell spreading and proliferation rate on compliant substrates [57]. Even the migration speed of a cell increases with a decrease in cell contractility [53]. All these experiments suggest that mechanosensitivity of a cell may not be a rigidity driven phenomenon per se, but a cell spreading dependent process. As the ultimate change at genome level has to happen in the nucleus, the changes in cell shape should give corresponding changes in nucleus

also. These correlated changes can either be in terms of direct mechanical coupling of cell and nucleus, or via biochemical signalling pathways.

In Chaper 2, we have explored the mechanical coupling between the cell geometry and the nuclear geometry in mMSCs. These are the multipotent cells taken from the bone marrow and are capable of differentiating into a number of lineages [58].We at first quantified the correlation between the cell spreading and the nuclear projected area. The robustness of the correlation was tested under various cytoskeletal and nuclear perturbations. We found that the coupling between the cell spreading and the nuclear projected area remains unperturbed across all perturbation experiments. This pointed towards a mechanical coupling between the cell spreading and nuclear projected area, which was investigated through confocal imaging of the cells on different rigidity substrates. We through our observations, hypothesize that the cell applies a compressive force on the nucleus to increase its spreading via a set of stress fibres, called the perinuclear stress fibres. Cell changes its actin organization from cortical actin to bundled actin to regulated the compressive force on the nucleus, for a correlated change in cell spreading and nuclear projected area. These perinuclear stress fibers pass over the nucleus and are anchored to the substrate through focal adhesions at the two ends [59]. The hypothesis of different extent of nuclear compression for different cell spreading was tested using theoretical estimates and our novel nuclear compression experiment. The nuclear compression

model also explains the antagonistic effect of myosin II inhibition on the spreading of cells, grown on soft and rigid substrates.

In Chapter 3, we have explored the dynamics of the force response for pulling and retraction of a tether from 3T3 fibroblast cells. It is known (as discussed earlier) that the substrate rigidity affects the cell spreading which in turn influences the functionality of the cell. Therefore, our initial experiments, reported in this chapter were aimed to investigate the effect of cell spreading on static and dynamic membrane tension of a cell. We grew cells on adhesive circles of 40 and 20μm, and without patterns, and performed membrane tension measurements using the optical trap. The next set of experiments showed that the height of the peak which appears in a force curve due to the step pull, depends on tether length. The mechanism by which the membrane flows to the tether in tether pulling experiments are well explored but the literature lacks the understanding of the tether retraction. We, through a set of experiments, investigated the dynamic response of the retracting tethers. Tether was retracted by moving the bead attached to the tether, towards the cell, along the tether length. The novel observations of step pulling and step retraction reported in this chapter need further experiments and theoretical estimates to give an understanding of the mechanisms involved.

In chapter 4, we explain the design and control of a compact, inexpensive and versatile shearing device to apply fluid shear stress

on fibroblast cell. The cell shearing device is based on the principle of cone-plate rheometer. The shearing device can be used as a detachment assay to measure the adhesion strength of different cell lines, for different surface and drug treatments. Our experiments regarding the cell detachment showed the existence of a threshold shear stress for cell detachment. For a shear stress, less than this threshold, the device can be used to study cell cytoskeletal reorganization and focal adhesion redistribution, under fluid shear. This is possible as high magnification live imaging is an advantage of the shearing device that we have designed. Detecting cancerous cells using the cell detachment curves and combining the device with microscopy techniques such as confocal and total internal reflection are the directions planned for the future of the shearing device.

In chapter 5, we give an overview of the thesis with list of questions that need to be explored by further experiments and theoretical estimates.

Chapter 2

Role of actin filaments in correlating cell spreading and nuclear geometry

Introduction

It is well known that substrate properties like adhesion and elasticity can influence cellular morphology, function and organization at a fundamental level [60–63]. Neuronal cells, for example, show a preference for soft substrates with moduli close to that of the brain, cardiac cells beat best on the substrates with heart like elasticity [45] and the fibroblasts show an affinity for stiffer substrates in terms of growth and migration [64]. Lineage specification of a stem cell is also known to get influenced by substrate rigidity [44, 55, 65]. Soft substrates favour differentiation into neuronal cells whereas stiff substrates generate osteoblasts [44]. Even the conditions of cell spreading alone may influence the process of lineage determination, e.g., cells grown

to different levels of confluency have been shown to differentiate into different lineages [48]. Cells cultured on different rigidity substrates and those cultured to different level of confluency have one thing in common — a varying degree of cell spreading. Both, the substrate rigidity and the confluency put a constraint on the extent to which a cell can spread [44, 60]. Direct application of mechanical stresses to the cell nucleus has also been reported to influence the gene expression. A cell under compression (using AFM cantilever) was shown to differentiate into osteoblast [47]. Nuclear architecture has also been shown to be regulated by the cytoskeletal stresses [59, 66–68]. In case of cells grown on adhesive islands of different aspect ratios, nuclear shape was found to change in accordance to the cell geometry, e.g., an elongated cell was observed to have elongated nucleus [68].

In adherent cells, nuclear deformations are coupled to the cell cytoskeleton, especially via actin stress fibers through LINC complexes [59, 69, 70]. The mechanisms by which nuclear deformations are regulated in a substrate dependent manner, and the exact role of cytoskeleton in this process is only beginning to be understood. There could be two possible mechanisms to explain the coupling between the cellular and the nuclear geometry via cytoskeleton: (a) compressive loading due to stress fibers running over the nucleus [59], and (b) lateral pulling by the direct coupling between adhesion proteins and nuclear membrane via cytoskeletal components [71]. Experiments where cells were grown on adhesive islands of different shapes

or adhesive strips show that variation in cell spreading or cell's aspect ratio is transmitted to the nucleus by actin stress fibers which results in nuclear deformation [59, 66, 68]. It has been demonstrated that when cells are spread on highly anisotropic patches, the nucleus is elongated along the long axis of the pattern and actin stress fibers running on either sides of the nucleus are responsible for the observed deformation [68]. Stress fibers have also been observed to run over the nucleus, and ablation of these fibers result in reorganization of nuclear structures [59, 70]. All these results point towards a mechanical connection between the actin cytoskeleton and the nucleus, which could regulate nuclear deformations. In this process of mechanotransduction, myosin II seems to be playing a key role as cell differentiation is observed to get hindered by its inhibition using the inhibitor, Blebbistatin [44]. The proliferation rate of cells, which depends on substrate rigidity has also been observed to become independent of substrate rigidity after myosin II inhibition. Cells on the soft substrates were therefore shown to be having higher proliferation rate after blebbistatin treatment [57].

Further, it is known that cell spreading and nuclear geometry are related and change in a correlated manner when growth conditions are changed or cells are detached using trypsin [71, 72]. But the mechanism which links nuclear deformation to cell spreading is not understood.

In this chapter, we explore the mechanism that links cell spreading to nuclear deformation. We would first start with quantification of

the correlated changes in cell spreading and nuclear projected area followed by the investigation of possible reasons for the correlation. We then propose a mechanism by a quantitative model, with an experiment to support the mechanical aspect of the correlated behavior. In our myosin inhibition experiment, we observed a loss of mechanosensitivity in cells. We also attempt to explain this using our nuclear compression model.

2.1 Correlated changes in cell spreading and nuclear geometry

Mainly three completely independent types of experiments were performed to quantify the correlated changes in cell spreading and nuclear projected area. In the first experiment, cell spreading was influenced by changing the substrate rigidity. In the second and third experiments spreading was recorded as a function of time, during growth and retraction, respectively. In all the experiments, cell spreading and nuclear projected area were recorded and plotted for the quantification of the correlation between the two. Experimental details and results are as follows.

2.1.1 Changes induced by substrate rigidity

Mouse Mesenchymal Stem Cells (mMSCs) were cultured on the polyacrylamide (PAA) gel substrates of different rigidities to quantify the

dependency of cell area and nuclear projected area on substrate rigidity. It was observed that mMSC plated on substrates with different stiffnesses exhibit increased cell spreading with increase in stiffness in range of 3 to 70 kPa as shown in Fig. 2.1(a). The maximum stiff-

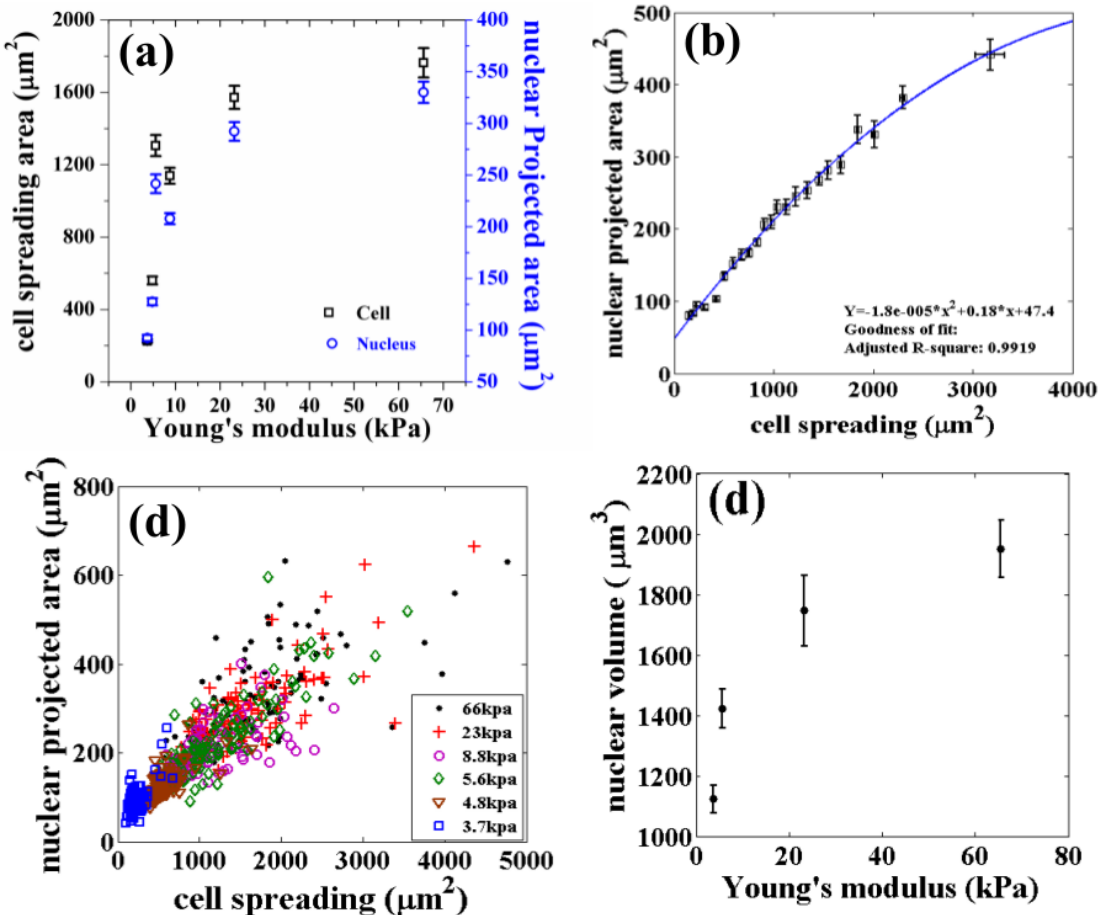

FIGURE 2.1: (a) Variation in cell spreading and nuclear projected area as a function of Young's modulus of the substrate. Each point is an average taken over 100 cells. (b) Dependence of nuclear projected area on cell spreading obtained after putting all the data from all rigidities together and then taking a bin over $40\mu m^2$ for cell spreading. (c) Scatter plot of the two areas of individual cells obtained from different substrates. Note that the spread in cell area increases with substrate stiffness and a linear trend can be seen towards higher stiffness. (d) Nuclear volume as a function of the elastic modulus of the substrate. Error bars in all the plots represent standard error.

ness sensitivity is in the 3 to 20 kPa range. This agrees with the observations in previous studies by various groups [44, 61, 63]. We observe that the nuclear projected area also follows a similar, highly

correlated, behavior with stiffness (Fig. 2.1(a)). Figure 2.1(b) shows how the nuclear projected area increase with increase in cell spreading. This plot is obtained by binning all the data from different substrates according to their cell spreading area. The raw data from individual substrates is shown in Fig. 2.1(c).

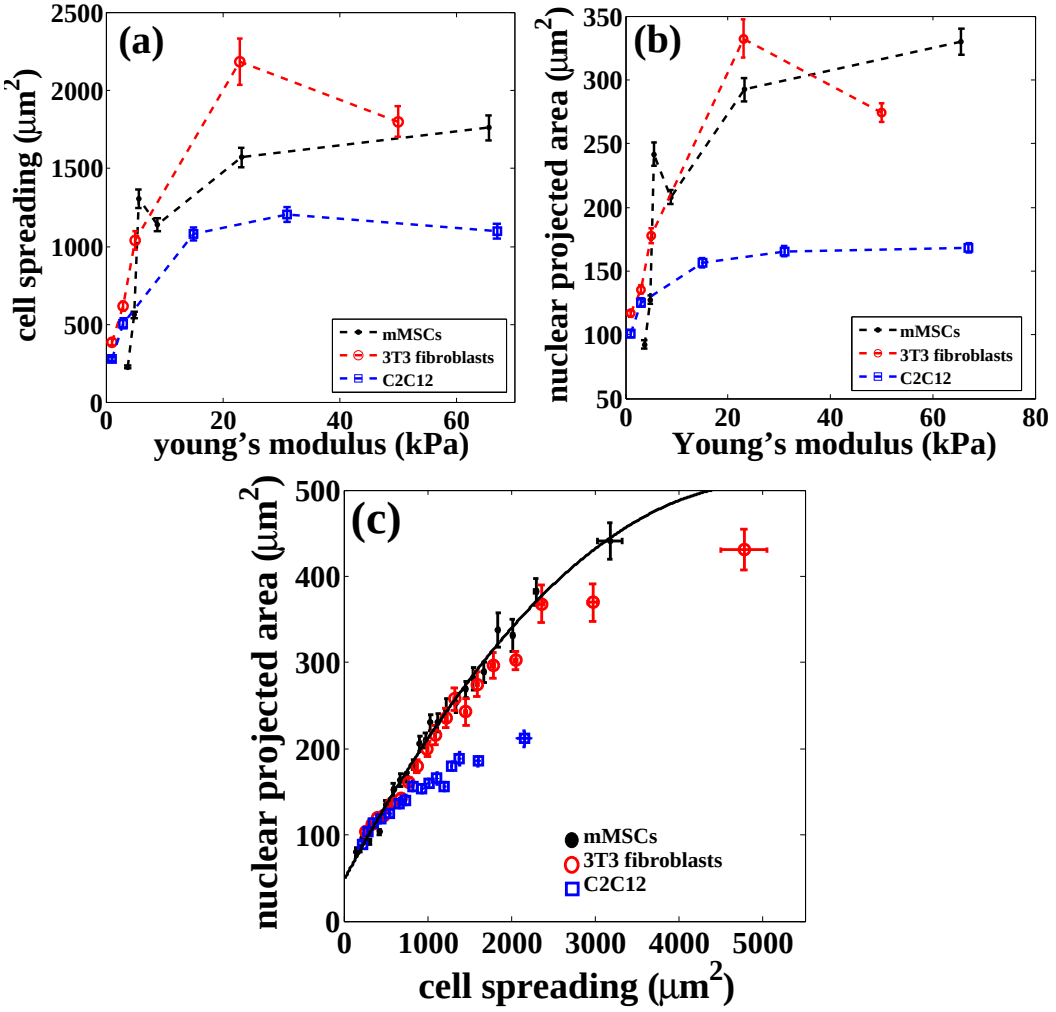

FIGURE 2.2: (a) & (b) Change in cell spreading and nuclear projected area respectively as a function of substrate stiffness for mMSCs, 3T3 fibroblasts and C2C12 myoblast cells. Each point is an average of around 100 cells. (c) correlation between cell spreading and nuclear projected area holds even for different cell types. Error bars shown are the standard errors in measurements.

In order to check if a similar relation would hold for other differentiated cell types, we performed experiments using 3T3 fibroblast and

C2C12 cells cultured on substrates with different rigidities. We found that the correlated behavior of the two projected areas hold even for these cells but with different functional dependence, as shown in Fig. 2.2(a),(b) & (c).

2.1.1.1 Substrate stiffness dependence of nuclear volume

It is clear from Fig. 2.1(d) that the nuclear volume shows a trend very similar to the cell and nuclear projected area, when cells are plated on substrates of varying elastic moduli. This increase in volume with stiffness could have important implications on nuclear compactness and hence in the regulation of gene expression. However, the volume change cannot be understood purely based on elastic deformation models. Moreover, when well spread cells on stiff substrate were detached using trypsin, the initially flattened nucleus became rounded within a minute, without any measurable change in its volume (See fig.2.3). This suggests that short time scale shape relaxations occur at constant volume. Growth effects and changes in osmotic pressure due to changes in DNA compactness might play a role in the observed volume effect seen in Fig. 2.1(d).

In order to further explore the relation between cell spreading, cytoskeletal organisation and nuclear deformation we performed the following experiments using mMSCs.

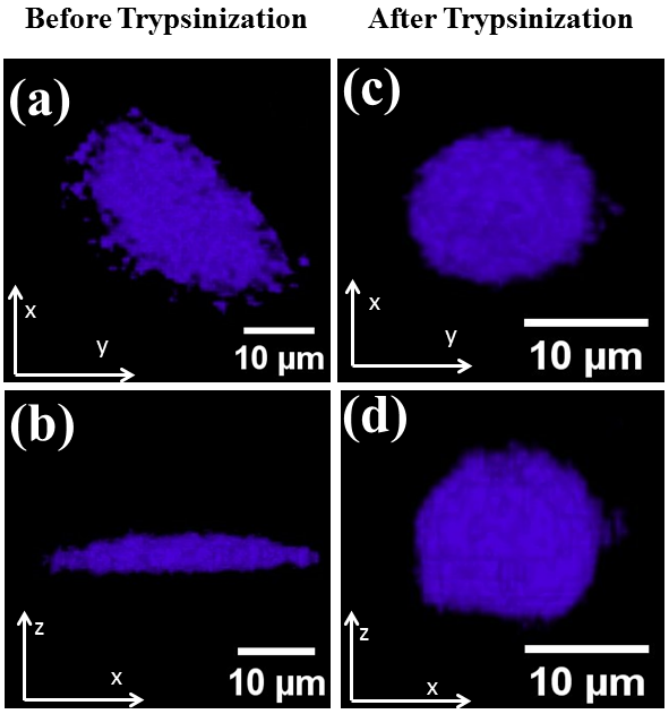

FIGURE 2.3: Projected area in two perpendicular planes, i.e., x-y and x-z plane of the substrate (a) & (b) before and (c) & (d) after, trypsin treatment. Volume was calculated using ImageJ plugin, using z-stacks and it was found to be constant.

2.1.2 Correlated nuclear deformation in cell spreading area as a function of time

In the first experiment, the mMSCs were grown on PAA substrates of different rigidities. In order to check the dependence of nuclear deformation (projected area) on cell spreading in a manner which is independent of substrate properties, we plated mMSCs on cell culture treated petri dishes (Nunc) and recorded the cell and nuclear areas as a function of time as cell spreading progressed. Once again a nearly identical relation between the two recorded areas was obtained as shown in Fig. 2.4(a) and 2.4(b). Nine tissue culture dishes were prepared at the same time and observed at different times to avoid

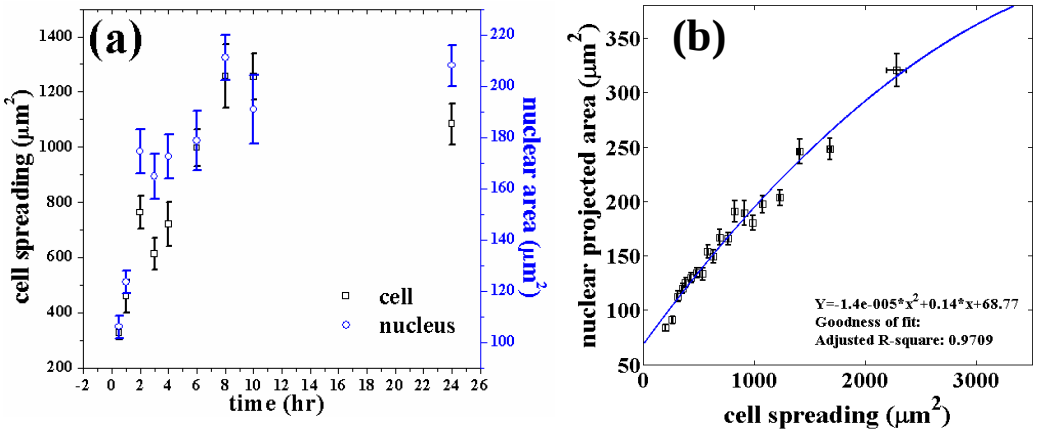

FIGURE 2.4: (a) Cell area and nuclear area as a function of time for cells grown on plastic surfaces for up to 24 hours. (b) Relation between the two areas obtained from the data shown in Fig. 2.4a. This plot is obtained by binning the cell areas of all 500 cells into bins of n=20.

keeping cells outside the incubator for long.

2.1.3 Correlated nuclear deformation in detaching or retracting cells as a function of time

This experiment represents an antagonistic experiment to the one performed in section 2.1.2, where growing cells was recorded as a function of time. Here, cell spreading is induced to decrease as a function of time by trypsin deadhesion [73] and the following cell and nucleus deformations were recorded as a function of time while cell area kept shrinking. Phototoxicity was the main problem for the live imaging of the retracting cells. For all static experiments we had used the cytoplasmic marker Calcein AM and Hoechst33342 to make cell and nucleus respectively fluorescent. It was found that the continuous exposure to light to cells treated with Calcein and Hoechst33342, affects the cells and they no longer detach on trypsin

treatment. In order to solve this problem, phase contrast images of the shrinking cells were taken for calculating cell area and minimum possible amount of nuclear dye (0.3 $\mu l/ml$) was used. As seen in Fig. 2.5, the correlation between cell and nuclear projected area is nearly maintained during the entire deadhesion process. This experiment also reiterate the fact that there is a correlation between cell spreading and changes in the nuclear projected area (deformation), irrespective of the way one changes the cell spreading.

In order to find the reason or the cytoskeletal/ nuclear component inside the cell responsible for the coupling between the cellular and nuclear projected area, different perturbations were performed on cytoskeletal and nuclear components.

2.2 Cytoskeleton perturbations

It was observed that it does not matter how the increase/decrease in cell spreading is induced, nuclear geometry always follows the trend to maintain the cell area and nuclear projected area coupled, to give a master curve which is the fit shown in fig. 2.1(b). In order to explore the role of cytoskeleton in correlating the cellular and nuclear geometry, we perturb the following three main cytoskeleton components in mMSCs: (a) Actin, (b) Microtubules and (c) Myosin II. Actin and microtubule depolymerization were done on the cells grown on fibronectin coated cover glass but myosin II inhibition was

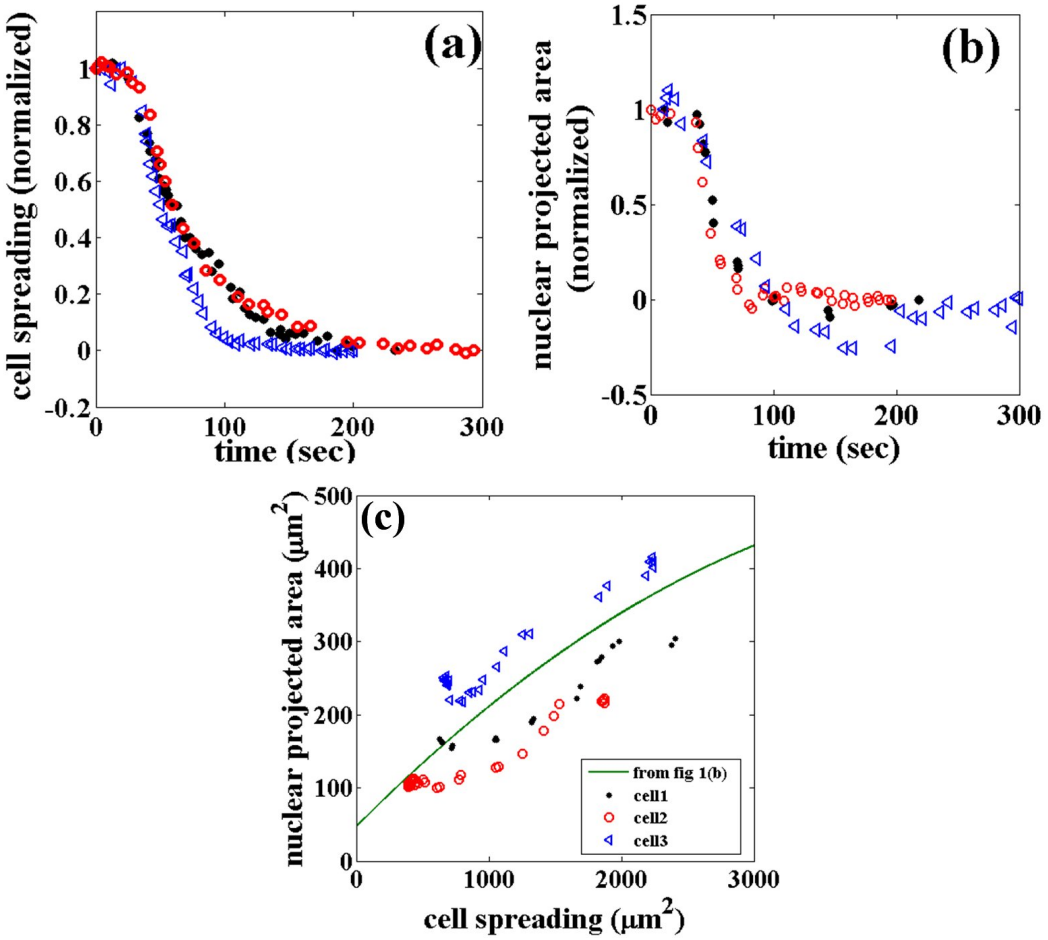

FIGURE 2.5: (a, b) Changes in cell spreading and nuclear projected area (normalized values) as a function of time, obtained from individual cells (different symbols) during trypsin mediated deadhesion. Normalization is done using the formula $1-[A_{initial}-A(t)]/[A_{initial}-A_{final}]$. (c) Variation in nuclear projected area as a function of cell spreading for the same cells. The line is the same fit as in Fig. 2.1b, and is plotted for comparison. In some cases, nuclear area shows an undershoot where the area decreases below the final value as seen in (b). Moreover, in some cases cell shrinkage precedes nuclear shrinkage as can be seen in (c).

done on gels of different rigidities. The results of these perturbations are summarized in Fig. 2.6.

Actin depolymerisation in a cell is dose dependent, and for this reason, two concentrations of LAT–A 80 nM and 0.67 μM were used to perturb actin in mMSCs. A well spread cell is known to have two sets of actin fibres– basal and apical. The apical stress fibers run

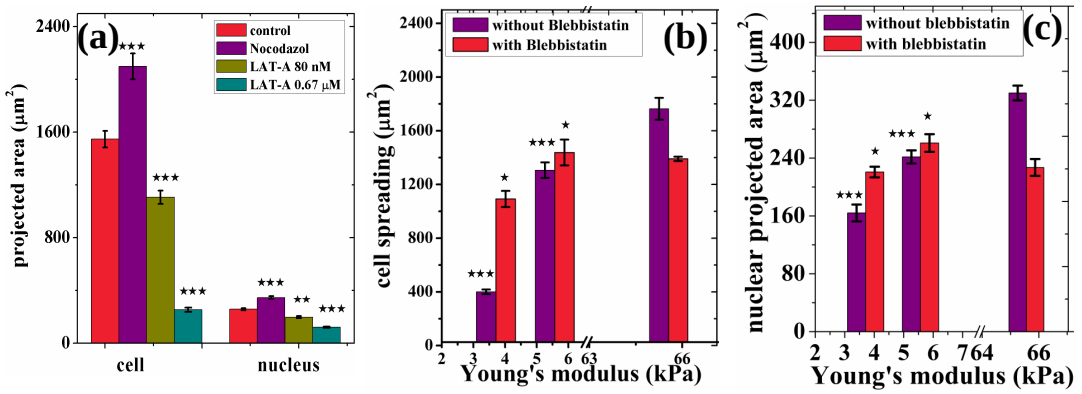

FIGURE 2.6: (a) Changes in cell and nuclear projected areas after microtubule disruption using Nocodazole and actin depolymerisation using Latrunculin-A. (b, c) Variation in the two areas after treatment with blebbistatin to deactivate myosin-II. Note that the substrate sensitivity is significantly diminished after mysosin-II inhibition. Further, for all drug treatments, a change in cell area causes a proportional change in nuclear area.

over the nucleus and hold it at its position. Cell treated with lower concentration of LAT–A were found to have actin depolymerisation only in the apical stress fibers as shown in Fig. 2.7. Disappearance of actin stress fibers from the apical region resulted in a reduced cell spreading with a concomitant reduction in nuclear projected area. Higher concentration of 0.67 μM results in much more extensive disruption of actin skeleton and more drastic reduction in nuclear and cell area as seen in fig. 2.6(a).

Cells were treated with 17 μM nocodazole (noco) for 30 min to depolymerize microtubules. The cell spreading was observed to be increasing with a corresponding increase in nuclear projected area, after noco treatment.

Inhibition of non muscle myosin II was done using 20μM blebbistatin. For Blebbistatin treatment, cells grown on substrates with

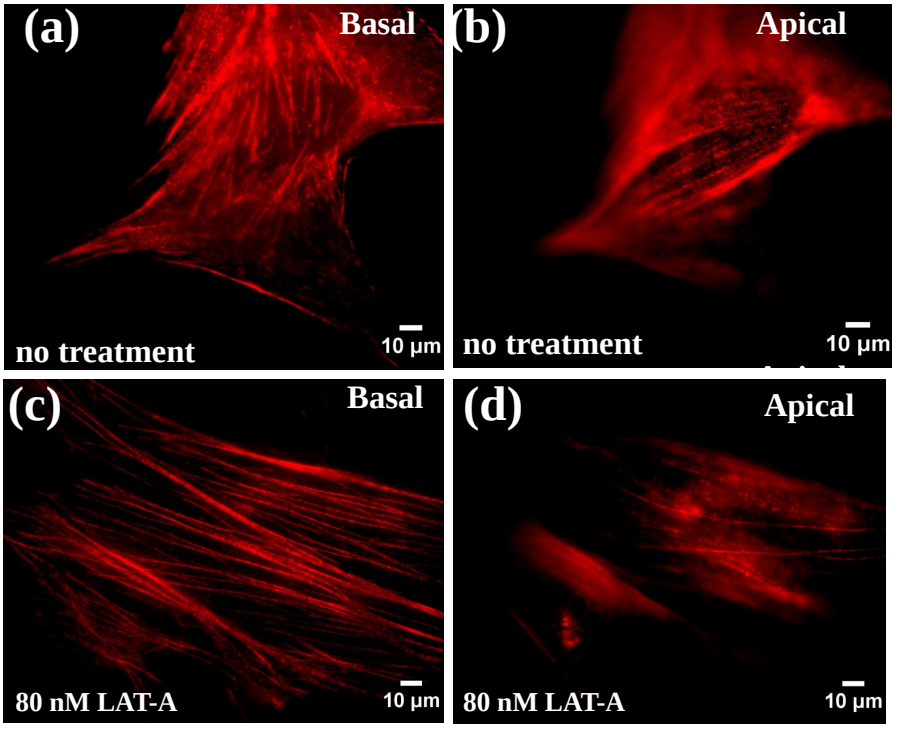

FIGURE 2.7: Confocal images showing the organization of actin stress fiber in basal and apical region respectively (a & b), in a controlled cell and (c & d) in a cell treated with 80 nM of LAT–A. The number of stress fibers over the nucleus, i.e., in the apical section, can be seen to be reduced drastically in case of LAT–A treatment.

different rigidities were used. As can be seen in fig. 2.6(b) & (c), non muscle myosin II inhibition in mMSC makes cells insensitive towards the changes in elastic modulus of substrates and cells change their spreading to get an optimum projected area with a corresponding change in nuclear projected area to fall along the master curve in Fig. 2.1(b).

All changes in cell area after cytoskeletal perturbation occurred concomitant with a change in nuclear area, always respecting the master curve, as shown in fig. 2.12.

2.3 Actin distribution and nuclear geometry

Confocal microscopy, using Ziess LSM 510 Meta was used to look at the correlation between the actin organization and nuclear deformation. Scan was done along the cell height, using Ziess LSM 510 Meta confocal microscope (in CIFF, NCBS). Z-stacks, taken using confocal microscope, were then used to reconstruct 3D projection of the actin structure and nucleus of cells grown on substrates with different rigidity. Detailed confocal imaging revealed the following.

On stiff substrates we observe two types of actin stress fibers. One set runs parallel to the substrate and lies very close to the plane of the substrate. These stress fibers lie below the nucleus (basal stress fibers). The other set ran over the nucleus (dorsal/perinuclear stress fibers) with the ends anchored at the substrate (Fig. 2.8(c) and 2.8(k)). Thus, the nucleus is tightly sandwiched between these two sets of stress fibers. Nucleus also showed a change in geometry from disc like (Fig. 2.8(d) & (e)) on a stiff substrate to ellipsoid on a compliant substrate (Fig. 2.8(i)& (j)). The nucleus appeared to be compressed between these two sets of stress fibers and is highly flattened on stiff substrates. This is similar to the observation made by Khatau et. al., 2009 [59]. As the stiffness is reduced, cell spreading, organization of either type of stress fibers, and nuclear deformation changed systematically as shown in Figs. 2.8 and 2.10. A precise quantification of the stress fiber density and thickness as a function of stiffness proved difficult since the distinction between stress fibers

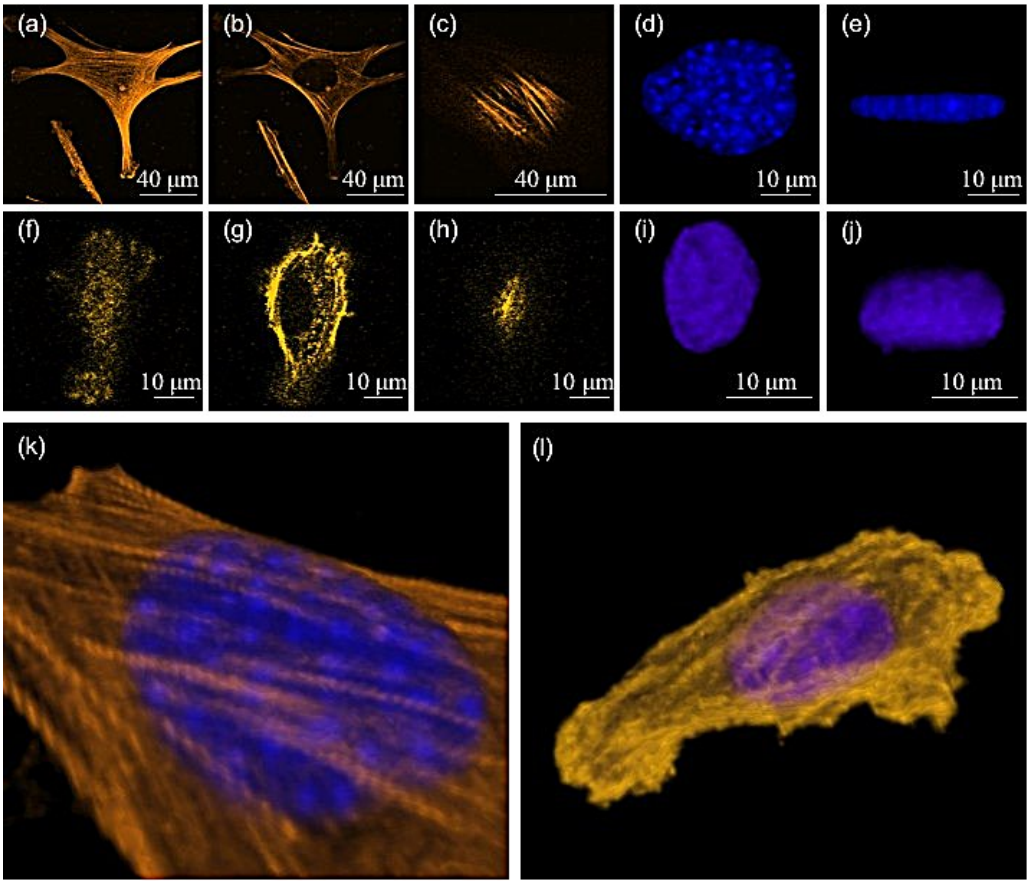

FIGURE 2.8: (a, b, c) Confocal images of a cell on a 70 kPa stiffness substrate. The images show actin filaments close to the plane of the substrate, in an approximate mid plane, and just above the nucleus respectively. Stress fibers running over the nucleus are clearly visible on the upper most region as in 2.8c. (d, e) The nucleus of the same cell projected in the plane of the substrate and in a perpendicular plane respectively. (f–j) Similar observations of a cell spread on a soft substrate (3 kPa). Note the difference in the nuclear shape compared to the upper set. (k, l) 3D reconstruction of confocal images showing perinuclear stress fibers running over the nucleus in the case of the first cell (stiff substrate) and a predominantly cortical actin mesh in the case of the second cell (soft substrate). Images in k and l are 3D reconstructions of the cells shown in a–e and f–j respectively.

and background actin (cortex) became poor rapidly as the gel stiffness was reduced. As an estimate, on the hardest substrates, intensity line-cuts reveal 10±2 fibers running over the nucleus as can be seen in fig. 2.9. On the softest substrates (3 kPa) no stress fibers were

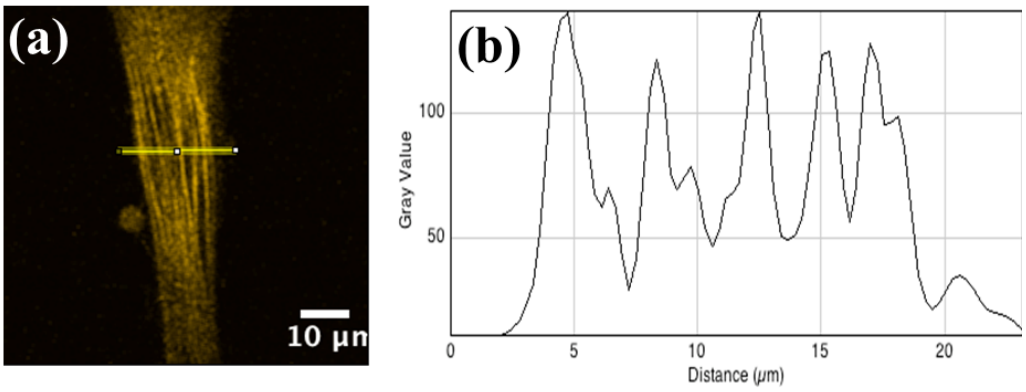

FIGURE 2.9: An estimate of the number of stress fibers can be obtained by measuring the intensity profile across the cell as shown in (a). The line width is 5 pxl. and the image was smoothened slightly using Gaussian Blur of 2 pxl. size using ImageJ to reduce noise. The line profile thus obtained is shown in (b).

visible and instead actin was distributed as an inhomogeneous cortical layer (Fig. 2.8(l)). The nucleus in this case was almost spherical as shown in fig. 2.8(i) and fig. 2.8(j). These observations suggest that the nuclear deformation seen on stiff substrates may be due to a compressive loading of the nucleus by perinuclear stress fibers. Along the similar lines, cells grown on adhesive rectangular strips were found to be more and more elliptical with an increasing length to width ratio [59]. Using analytic estimates, the authors have argued that increasing lateral compression of the nucleus with increasing length to width ratio is responsible for the observed elongation. From this, we hypothesize that a reduction in stress fiber number and tension

in these fibers may be responsible for the correlated reduction in nuclear compression and cell spreading, as elaborated in the following sections.

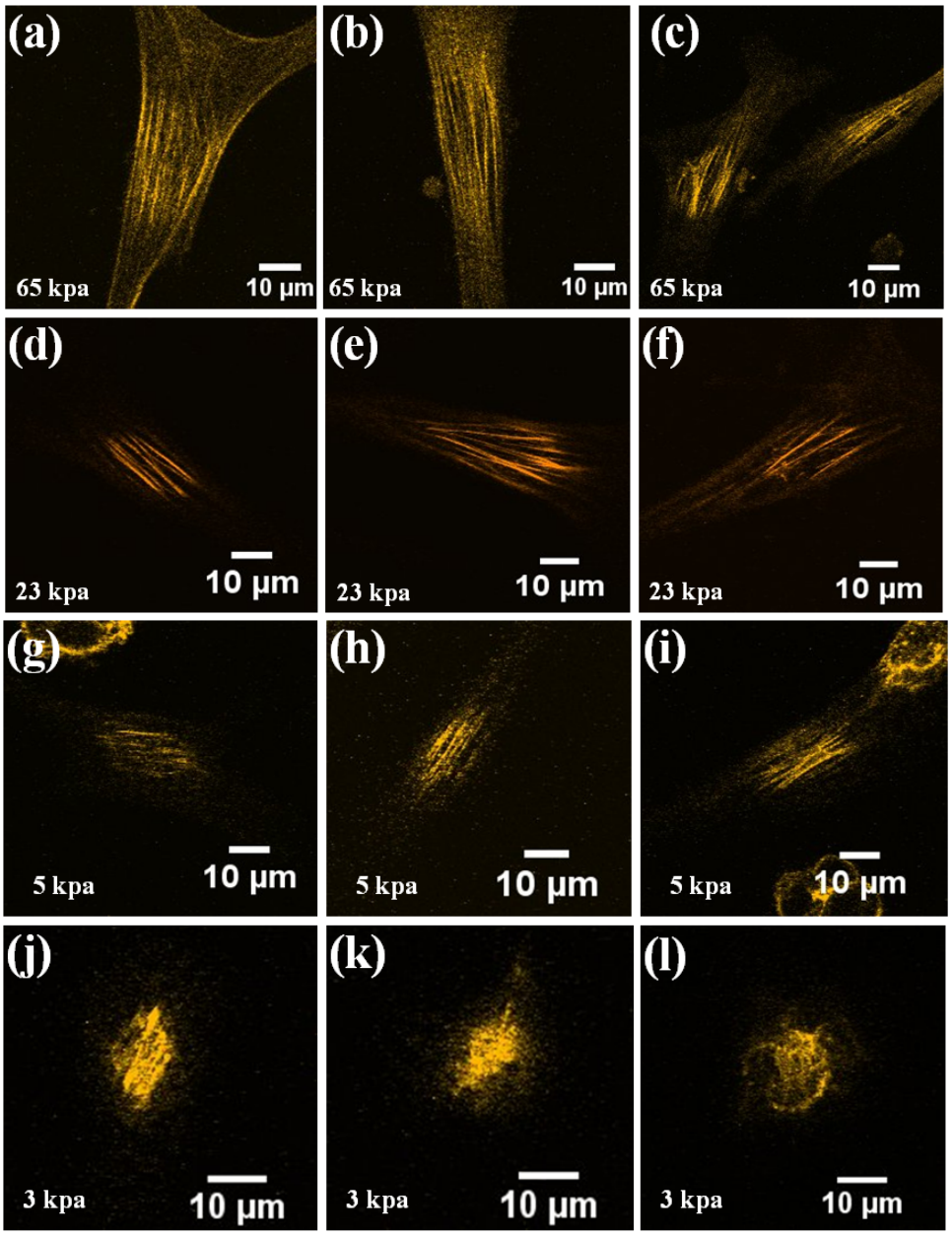

FIGURE 2.10: Images showing the typical variation in stress fibers distribution or actin organization for cells grown on substrates with different rigidities. (a-c) 65 kPa, (d-f) 23 kPa, (g-i) 5 kPa and (j-l) 3 kPa.

2.4 Nuclear perturbation experiment

Apart from cytoskeletal perturbations, we also performed nuclear perturbation experiments similar to that performed in Khatau et al. [59] for fibroblast cells. As per the nuclear compression hypothesis, cell spreading should get affected by the alteration in nuclear stiffness or compactness. Therefore, we chose lamin knockdown and inhibition of histone deacetylase activity to perturb mMSC nucleus.

2.4.1 Lamin a/c knockdown

Lamins form the skeleton of the nucleus which is responsible for giving shape and providing mechanical integrity to the nucleus [74]. Lamin network is found just beneath the nuclear membrane. Amount of lamin in a cell nucleus is known to scale with tissue stiffness [75]. A nucleus, rich with lamin A has also been reported to be more rigid than the one devoid of it [76]. Therefore the knockdown of lamin A/C decreases the nuclear stiffness. A decreased nuclear stiffness should result in an enhanced cell spreading which we did not see in our experiment, instead we observed a reduction in cell spreading. The reason for a reduced cell spreading with softening of the nucleus is disruption of LINC complexes caused by lamin knockdown as observed by Khatau et at. [59]. A broken lamin network, caused by siRNA knockdown breaks the mechanical connection, i.e., the LINC complexes between the perinuclear stress fibres and the nuclear skeleton. This causes disappearance of the perinuclear stress fibres as can

be seen in fig. 2.11(g) & (h). This reduces the compressive loading of the nucleus by a large amount due to which the nucleus bulges out and forces the cell to reduce its spread area. The bulging nucleus after lamin knock down can be seen in fig. 2.11(i). The procedure adopted to knockdown lamin A/C is explained in detail in section 2.9. Even after this perturbation, the cell and nuclear projected areas remain correlated and unperturbed as shown in Fig. 2.12.

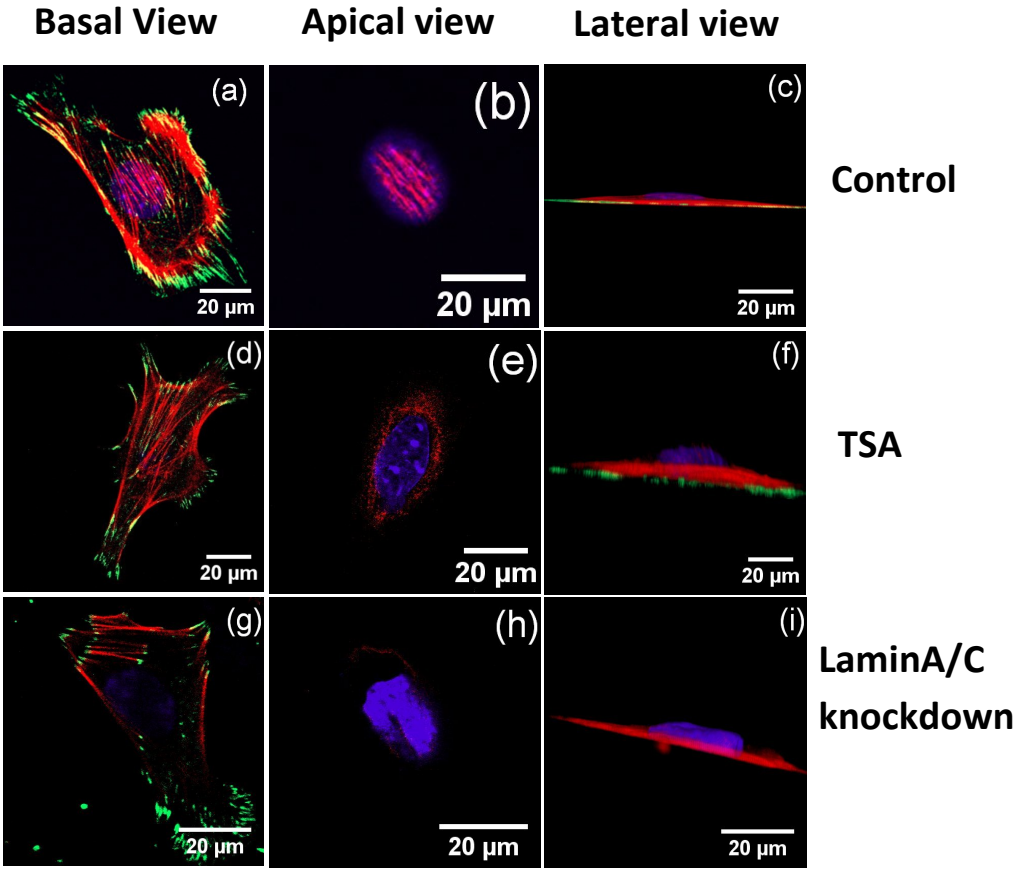

FIGURE 2.11: Confocal slices of cells after nuclear perturbations (Control, TSA treatment and lamin A/C knock down). All the cells were cultured on coverslips. Actin filaments, nucleus and focal adhesions are labelled in red, blue and green colors respectively.

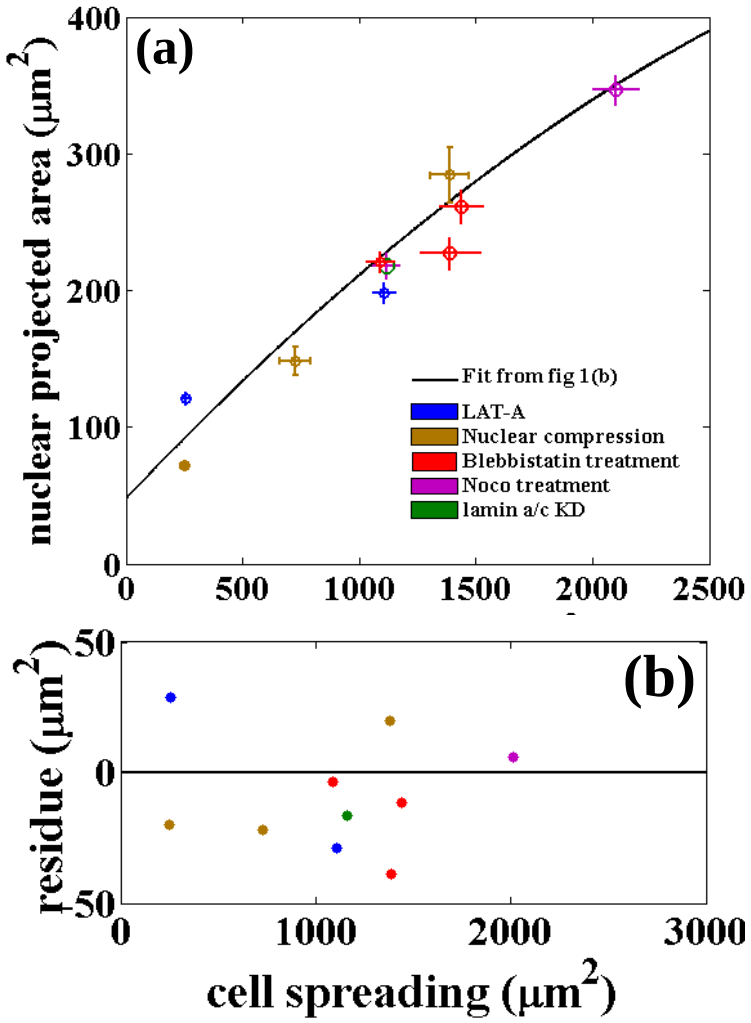

FIGURE 2.12: Change in cell spreading seems to be changing the nuclear projected area to follow the trend shown in Fig. 2.1b. In this plot, control represents cell grown on fibronectin coated cover glass. Brown color represents the myosin II inhibition experiment, where cells were grown on substrate with different rigidity and then treated with Blebbistatin as in Fig. 2.6(b) and 2.6(c).

2.4.2 Histone deacetylase inhibition

Histones play a crucial role in keeping the nucleus compact by making long DNA wind around them in the nucleosome as shown in Fig. 2.13. Histone deacetylases (HDAC) are the enzymes that remove acetyl groups from an ϵ-N-acetyl lysine amino acid on a histone and

makes the DNA wrap around the histone more tightly. Trichostatin–A (TSA) is an organic compound that inhibits the HDAC activity and therefore loosens the DNA wrapping around the histones and alters the nuclear packing. Experiments with TSA treatment to de-

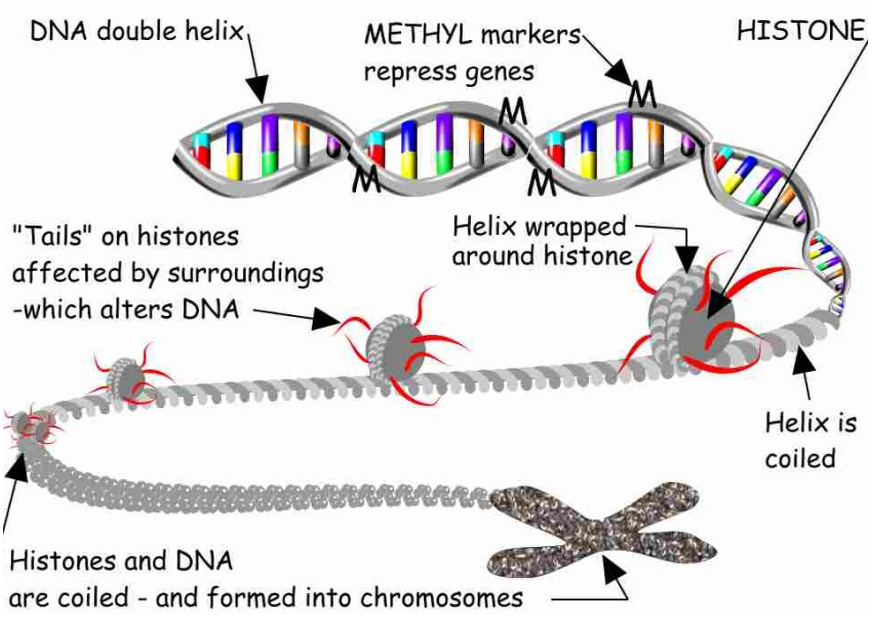

FIGURE 2.13: Winding of DNA around the histones in a chromosome. The image is adopted from http://homepage.ntlworld.com/malcolmbowden/histones.htm.

condense DNA revealed a significant reduction in the nuclear projected area accompanied by a corresponding decrease in cell area (Fig. 2.14). An increase in nuclear thickness and a prominent protrusion of the nucleus on its apical surface, similar to lamin A/C knock down and 80 nM LAT–A treatment, was also observed with TSA treatment (Fig. 2.11(f)). Although perinuclear stress fibers appear on some cells, their numbers were highly reduced (Fig. 2.11(d), 2.11(e)). So far, through all our experiments of different perturbations, we could not pin down on any cytoskeletal or nuclear component which could decouple the two quantities, i.e., cell spreading

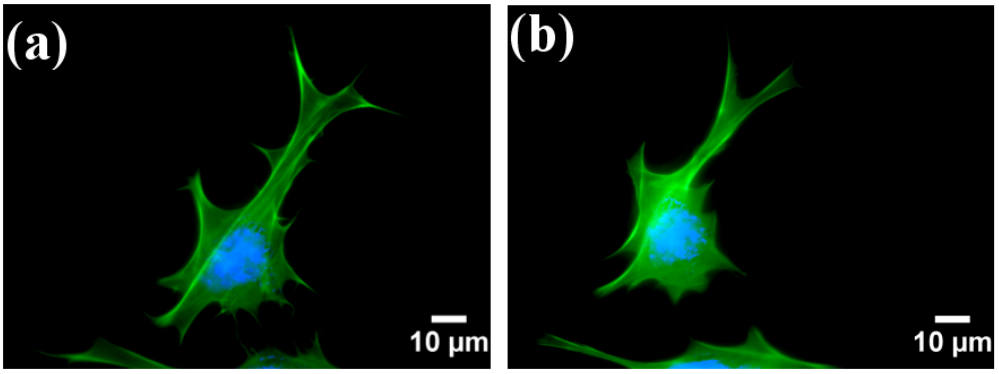

FIGURE 2.14: Effect of TSA on mMSCs. (a) and (b) are the composite images of a cell and the corresponding nucleus before and after 5 hrs of TSA treatment.

and nuclear projected area. This indicated towards the mechanical coupling of cellular and nuclear geometry. Analyzing the above results collectively as seen in fig. 2.12, we make a theoretical estimate of the relation between perinuclear stress fiber density and nuclear deformation. An estimate of compressive forces required to deform the nucleus was done before making theoretical estimates.

2.5 Estimates of Compressive forces on nucleus

In order to estimate the normal forces acting on the nucleus due to actin stress fibers in a spread cell, we had deployed two methods. The description of the two methods are as follows.

2.5.1 Using micropipette

The Perinuclear stress fibers are the rope like structures, anchored at the two ends and going over the cell nucleus. When actin is disrupted either by drug treatment as done in the cytoskeletal and

nuclear perturbation experiments or by ablating the stress fiber as done by Khatau et al., 2009 and Nagayama et al., 2011 [59, 70], the nucleus seemed to be bulging up with a reduction in nuclear projected area. In that case it was expected that the nucleus, due to its elastic behavior on short time scale, will exert a force in perpendicular direction (to the substrate), and this can be probed if a soft cantilever is put in contact with the apical surface. This could give an estimate for the compressive loading on the nucleus due to the stress fibers. As for the experimental set up, thin glass pipettes of about 3μm tip diameter were pulled using a pipette puller and was used as a probe to be in contact with the apical surface of the cell as shown in Fig. 2.15(a). The thin tip of the glass pipettes were bent

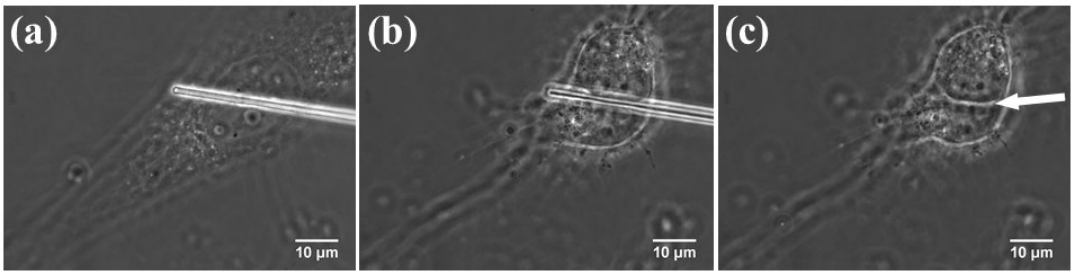

FIGURE 2.15: (a) Image of a well spread cell under the glass pipette. (b) Retracted cell after Lat-A treatment. The image was taken after 20 minutes of treatment. (c) It can be observed that the pipette cause a depression in the nucleus. Instead of pushing the pipette in the upward direction, the cell deformed and made way for the pipette to make a depression, shown by the arrow.

at an angle by heat treatment in order to place them almost parallel to the apical plane of the cell as shown in fig. 2.16. Cells were grown on cover slips for about 24 hrs before the experiment. After bringing the needle/glass pipette in contact with the top most point in cell's contour using the micromanipulator, as shown in Fig. 2.15(a), they

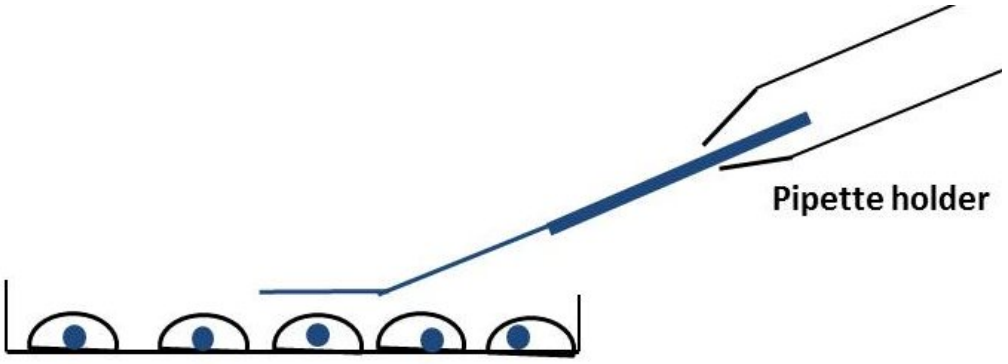

FIGURE 2.16: The tip was bent by heating the glass rod. It was done to keep the rod parallel to the plane of the dish while keeping it in contact with the apical surface of the cell.

were treated with 0.67μM Lat-A to disrupt the actin structure inside the cell and recorded for 30 minutes. Two types of observations were recorded: (a) if the pipette is placed slightly off the centre of the cell, the cell slipped out of the pipette by moving laterally, (b) if the pipette was placed exactly at the centre it made a groove on the cell when the nucleus tried to bulge out after Lat-A treatment, as shown in Fig. 2.15(b) and (c). We could not see any deflection in the needle to get a measure of compressive loading due to rounding up of the cell nucleus. There could have been two reasons for this: 1) the excess stiffness of the glass needle or 2) softening of the cell in the absence of actin structure. We then tried to estimate the normal force using traction force microscopy and a simple model as discussed in the following sections.

2.5.2 Traction Force Microscopy

This method requires cell to be grown either on a bed of flexible micro-pillars or on deformable substrates like PAA gels. In case of measuring traction force microscopy using micro-pillars, the stiffness of the substrate is varied by varying the length or diameter of the micro-pillars. Long pillars behave as soft substrate whereas short pillars are equivalent to hard substrate. The force generated by a cell on a micropillar can be calculated as [77]

$$F = \left[\frac{3\pi E r^4}{4L^3}\right] \Delta x \tag{2.1}$$

Where, E= elastic modulus of the elastomer used to prepare pillars; r = radius of the pillars; L= height of the pillars, and Δx = deflection in pillar caused by cell traction. The deflection in micro-pillars of different lengths gives the traction force generated by the cell as shown in fig. 2.17.

The other way to estimate the traction force is by mapping the deformation field of PAA gel of known modulus caused by a cell. Fluorescent beads of diameter 200 nm embedded in the gel are used as the marker to measure the deformation field. It is known that a cell grown on the surface (x–y plane) of a gel, applies a traction on gel in 3D [79]. Other than the x and y deformation of the gel, a z direction deformation has also been observed. We, in our measurements, were interested only in the traction values in the x-y plane. The standardised protocol for preparation of gels for TFM involves

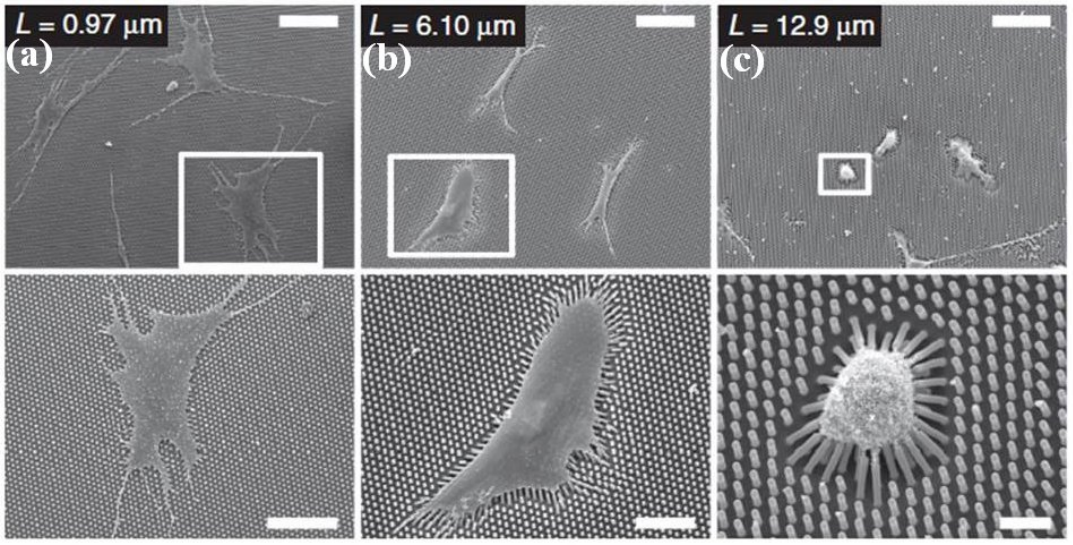

FIGURE 2.17: Substrate with micropillars of different length is equivalent to substrate of different rigidities. (a) Very small pillars can be deflected only by a small amount and therefore a bed of small pillars act like hard substrate and cells spread well on them. (b) & (c) Larger the height more would be the deflection in the pillars caused by the cells. A large deflection in pillars opposes cell spreading and therefore pillars with large height act like the low rigidity substrates. Image courtesy Fu J. et al., 2010 [78]

mixing of beads with the gel solution. Gels prepared by these methods have beads in all focal planes and therefore generally give wrong estimates with traction measurement codes. We, in our protocol, have developed a way to have beads only in one plane, i.e., the plane just below the cells. The detailed protocol for the gel preparation is as follows.

- Cleaned coverslips were coated with 20 μg/ml fibronectin solution, as it is cell adhesion compatible, for 30 min. This was done to make the coverslips hydrophilic to stop flying of beads from coverslips while spin coating. A typical bead density used for TFM is shown in fig. 2.18(c).

- After fibronectin coating, coverslips were spin coated with a solution of 200 nm fluorescence beads at 1200 RPM for 3 min. Bead solution was prepared in HBSS and density was adjusted to have about 15 beads in an area of 100 μm^2.

- These coverslips were then used as the top plate for gel preparation as described in PAA gel preparation and characterization protocol in later section.

- Once the gel is cured, ECM coating using fibronectin was done, as described later.

- Cells were cultured at a very low density to get a single cell in field of view of a 100x objective.

- Once the cells were well spread (after 8-10 hrs), they were transfected with Vinculin-venus using lipofactamin as described in Vinculin transfection protocol and incubated at 37 °C with 5% CO_2 for 48 hrs before doing TFM.

- For TFM, beads under a cell were imaged before and after trypsinization and the Matlab code (written by Iva Marija Tolic-Norrelykke and was kindly given to us by Dr. Namrata Gundiah, IISc) described in the reference [80] was used to calculate the displacement field and the traction field under mature focal adhesions (FA). A Typical bead distribution, displacement map with corresponding cell and focal adhesion labelling used for TFM are shown in fig. 2.18.

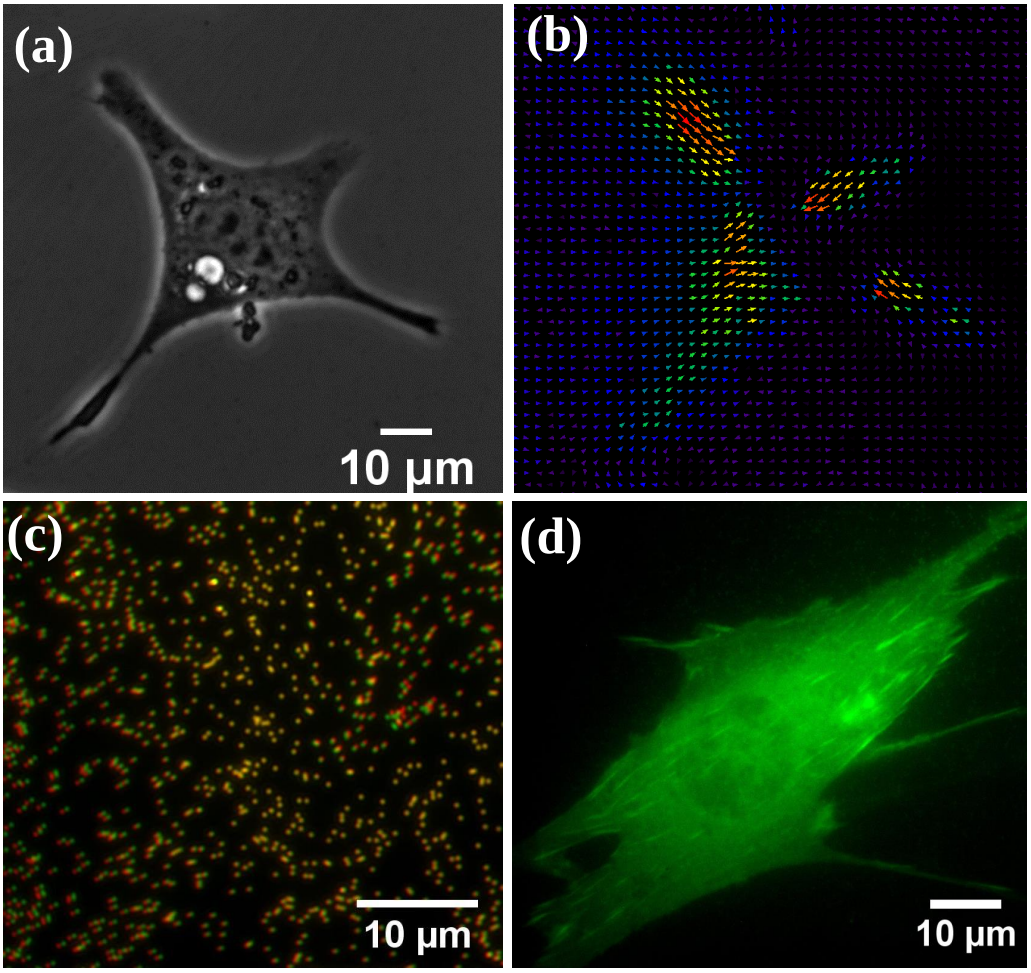

FIGURE 2.18: (a) and (b) are the images of a cell grown on a 23 kPa substrate and the corresponding displacement map respectively. (c) Two images with bead position before and after trypsinization are overlapped to show the bead displacement after cell detachment. Beads given red color are at the position after trypsinization whereas the beads given green color are the beads before cell detachment. (d) mMSC after vinculin transfection to label focal adhesions under normal fluorescence microscopy.

- The Matlab code was able to draw a boundary around the region of interest and make displacement outside the boundary equal to zero. We defined a boundary around a focal adhesion to estimate traction per FA point. "N" number of FA points were chosen from 15–20 cells and a distribution of traction was obtained (fig: 2.19).

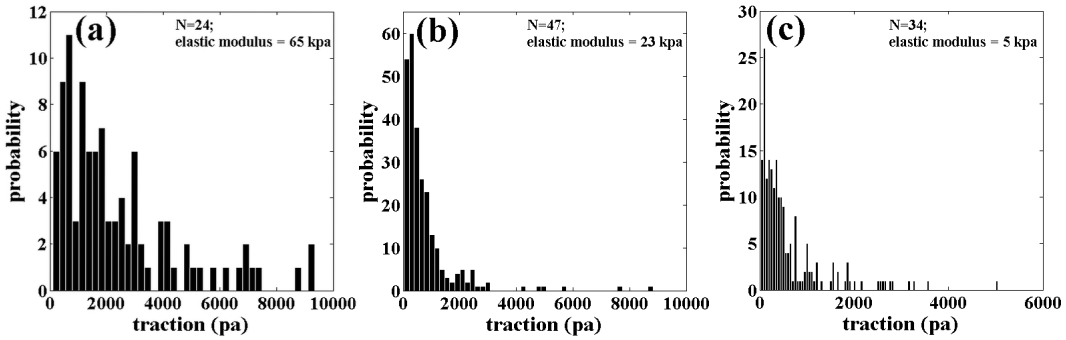

FIGURE 2.19: (a–c) Distributions for estimated traction under "N" number of FA points for different rigidities.

- The average FA area for mature focal adhesions was found to be 4 μm^2 and forces due to these were calculated by multiplying the average traction per unit area with average area of FA.

These traction force values were used to estimate the compressive loading on the nucleus as described in the next section.

2.6 Nuclear Compression Model

Here we present a quantitative analysis of the compression mechanism to determine how well it accounts for the observations. The estimates are made using Tatara's theory [81, 82] because of the large strain observed in confocal images. At large strain, the deformation of an elastic object goes beyond the elastic limit and Hook's law, i.e., strain proportional to stress no longer holds. Tatara's model relates stress and strain for the deformation of an elastic object beyond elastic limits. To get the estimates of compressive load we make the following simplifying assumptions.

- Perinuclear stress fibers run over the nucleus in symmetric fashion and are anchored at either ends to the substrate. Tension in these fibers generate a normal stress on the nucleus (fig. 2.20(b)). The ground state (uncompressed state) of the nucleus is taken to be a sphere.

- Stress fibers running over the nucleus are assumed to be equivalent to a continuous sheet generating normal compression as shown in the schematic Fig. 2.20(a).

- Slipping and friction, if any, between the stress fibers and the nucleus are ignored. No slipping is supported by the fact that the stress fibers are connected to the nucleus via LINC complexes as discussed in [59].

- Nuclear volume is assumed to be constant during nuclear compression and the deformation is assumed to be elastic (viscosity is unimportant in dictating the final shape), as supported by the trypsin de-adhesion experiments. This assumption ignores effects like changes in DNA synthesis or changes in the folded structure of the nuclear membrane as discussed in [66] and [68], respectively. This assumption should be especially valid for short time scale experiments like trypsin de-adhesion, dynamic cell spreading, cytoskeletal perturbations, etc.

The traction force per stress fiber is obtained for different substrate stiffness from the Traction Force Microscopy data. The mean traction force f_t per fiber is 9.2 nN for 65 kPa, 4.4 nN for 23 kPa, and 2.8

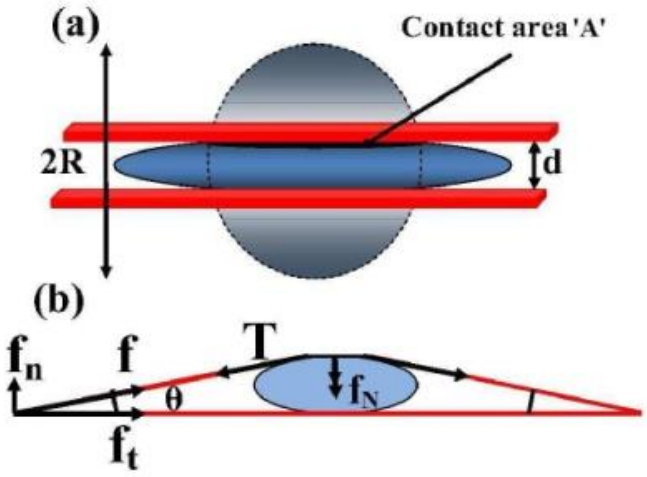

FIGURE 2.20: (a) Schematic showing nuclear deformation under uniform loading. The undeformed nucleus has a radius R. After loading the contact area with the plate is a and the nuclear height is d. (b) Schematic showing how normal stresses arise due to a perinuclear stress fiber.

nN for 5 kPa substrate rigidity (Fig. 2.19). This reduction in traction force with substrate stiffness is in agreement with earlier works [62, 78, 83]. We estimate the normal force acting on the nucleus due to one stress fiber as follows. From Fig. 2.20(b), $f_n = f_t\, tan\theta$, where f_t is the traction force and θ is obtained from confocal images. Therefore, the normal compression acting on the nucleus due to one stress fiber is given by $f_N = 2f_t\, tan\theta$. The normal force due to all the perinuclear fibers add up to give the net compressive loading on the nucleus. Stress fiber numbers vary from about 10 $\pm$ 2 (n = 15) for cells on stiff substrates to no visible fibers on the softest substrate (see Fig. 2.8 and 2.9). The net compressive load on the nucleus for stiff substrates (assuming 10 stress fibers) is calculated to be around 30 nN. We now use Tatara analysis for a sphere compressed between two plates [84] to check whether such a loading can

cause the observed deformation. According to this model [81, 82]

$$\alpha = \frac{3(1-\nu^2)F}{2Ea} - \frac{2Ff(a)}{\pi E}, \tag{2.2}$$

where $\alpha = 2R - d$ is the approach (see Fig. 2.20), ν = Poisson's ratio, a = contact radius, E = elastic modulus of the nucleus, F = compressive load, and

$$f(a) = \frac{2(1+\nu)R^2}{(a^2+4R^2)^{\frac{3}{2}}} + \frac{1-\nu^2}{(a^2+4R^2)^{\frac{1}{2}}}\ , \tag{2.3}$$

where R, d and a are taken from confocal images. Using the above expressions, we obtain the Young's modulus of the nucleus to be 0.4 kPa. This is comparable to the value obtained for stem cells in recent work [75]. This means that the nuclear deformations arising from the variation in the cell spreading can be explained by the normal pressure exerted by the perinuclear stress fibers as was hypothesized in [59]. On softer substrates, both the stress fiber density and traction forces reduce as observed, resulting in reduced compressive loading and hence less nuclear deformation. A recent study using epithelial cells on adhesive islands of different aspect ratios and a 2D-model has shown that lateral stress fibers can generate forces large enough to account for geometry-dependent nuclear deformations [68]. This is analogous to the normal compression in our case.

2.7 Nuclear compression experiment

A cell growing on a hard substrate tend to be stiff and on a compliance substrate tend to be soft. The cell can do these adaptations, by changing its spreading. The nucleus being the elastic inclusion inside the cell, limits the extent upto which the cell can spread. It means if an external load equal to the normal compression due to stress fibers, is applied on cell cortex of a poorly spread cell, the cell should show an increase in its spreading. In order to verify this experimentally, we applied a normal compression on cell cortex and studied resultant changes in nuclear and cellular deformation. The experimental arrangement is shown schematically in Fig. 2.21(a). For this, we developed a simple technique which uses plano-convex lenses of focal length 400 mm and weights 0.97 and 1.07 grams to apply a normal pressure on the nucleus. As compared to a flat surface, a lens eliminates the need for alignment of the two surfaces (the curved surface of the lens and the coverslip with cells). For a low curvature lens (long focal length), the surface can be approximated to a locally flat one in comparison to the length scale of a cell. The lens, placed in the culture dish over a monolayer of cells (30–40% confluent), exerts a pressure proportional to its weight with a radial distribution around the bottom most point of contact. At the point of contact, the surface can be assumed to be perfectly parallel to the coverslip. The point of maximum pressure is easily determined from the interference pattern (Newton's rings) generated by reflected, green, monochromatic light from the curved surface of the lens and the upper surface of the

coverslip as shown in Fig. 2.21(b). This illumination is done using the fluorescence imaging unit of the microscope without an emission filter. The weight of the lens is chosen to apply a gentle pressure without damaging the cells. For this experiment, mMSCs were cultured for 8 hrs, on coverslips coated with 0.05 μg/ml of fibronectin (low concentration) to obtain an intermediate level of spreading before the application of pressure. Observations were made under the lens and outside the lens. As soon as the lens is placed on the cells, the cells began to spread. In some cases the cells exhibited extensive blebbing for a short period similar to that seen in normal cell spreading. The cell spreading reach a steady state within 15 min. Images of the cells under external compression are shown in Fig. 2.21(d) and (e). It is observed that a compressive loading of the cortex results in flattening of the nucleus and an increase in cell spreading. Remarkably, the data for cell and nuclear areas obtained for the two different compressive loads fall on the master-curve as shown in Fig. 2.12.

Below, we make an estimate of the normal compression on the cells due to a lens of mass m. The maximum pressure due to the lens (at the central point) is given by

$$p_{max} = 3F/(2\pi a^2), \tag{2.4}$$

where $F = mg$ is the force and a is the contact area between the lens and the layer of cells and is given by

$$a = \left[\frac{3F}{8}\frac{(1-\nu_1^2)/E_1 + (1-\nu_2^2)/E_2}{1/d_1 + 1/d_2}\right]^{1/3} \tag{2.5}$$

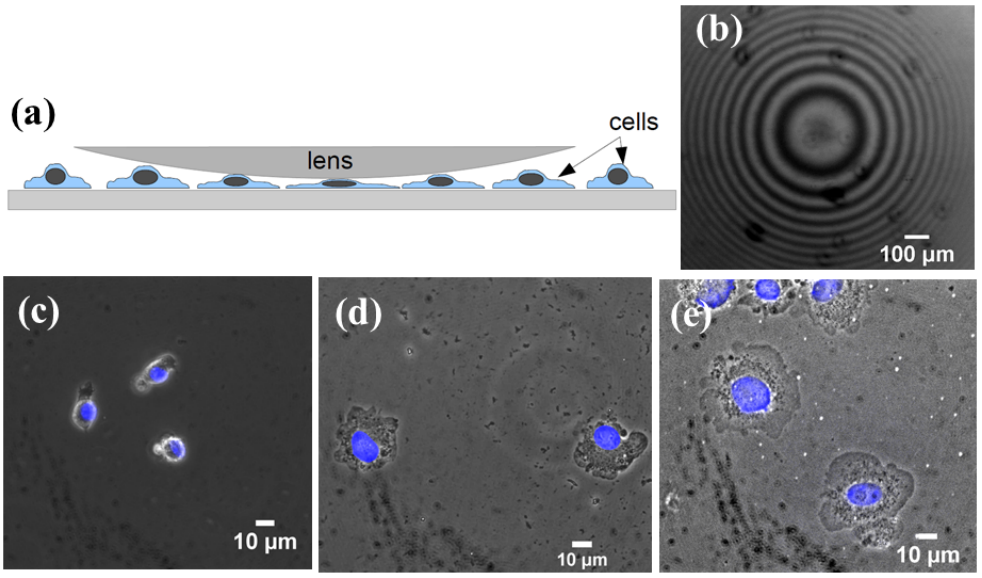

FIGURE 2.21: Phase contrast images showing the effect of a compressive load on cells applied using a convex lens. (a) Schematic showing the experimental set up, with a lens carefully placed over the monolayer of poorly spread cells. (b) The image of the Newton's rings observed due to the interference between the reflected light from the bottom surface of the lens and top surface of the bottom plate with cells. (c) Poorly spread cells due to low concentration of fibronectin coating of the bottom surface. (d) & (e) Cells subjected to a compressive load with lenses of different weight. In (e) the nuclei are flattened and the cells are much more spread than in (d) due to a higher compressive load.

as discussed in [85, 86]. Here, $\nu_1 = 0.3$ and $\nu_2 = 0.5$ are the Poisson's ratios for the lens and the cell respectively, $E_1 \simeq 50$ GPa and $E_2 \simeq 0.5$ kPa are the corresponding Young's moduli, $d_1 = 400$ mm is the diameter of the intending object (twice the radius of curvature of the lens), and $d_2 = \infty$, since the cell layer is flat. F can be calculated as,

$$F = m'g = mg - F_b \tag{2.6}$$

$$F_b = (\rho V_l)g = \left(\rho \frac{m}{\rho_l}\right) g$$

substituting in eq.5, we get

$$m' = \left(1 - \frac{\rho}{\rho_l}\right) m$$

F_b is the buoyant force on lens; m=1.06g, mass of the lens; V_l is the lens volume and ρ, ρ_l are the densities of the cell culture medium and glass respectively. This gives $p_{max} \simeq 25$ pN/μm^2. If we assume the cells to be a confluent layer and a cell-lens contact radius of 10 μm per cell, the force per cell is about 7 nN. Since the cells are only 30–40% confluent, the actual value could be a few times higher as the weight of the lens is supported by fewer cells. This is then comparable to the compressive force estimated earlier from traction force values which is about 3 nN per stress fiber and several of these stress fibers may be acting on the nucleus. Thus, the compressive force exerted by the lens is of the same order of magnitude as that generated by stress fibers. The data obtained from the compression experiment when plotted along with master plot (fig. 2.22) showed a remarkably good agreement and supports compression of nucleus against lateral pulling.

2.8 Discussion and Conclusion

Recent study on fibroblasts cultured on elongated adhesive stripes of varying width has shown that perinuclear stress fibers running over the nucleus can regulate nuclear shape [59, 87]. Further, it has been shown that endothelial cells grown on highly elongated adhesive

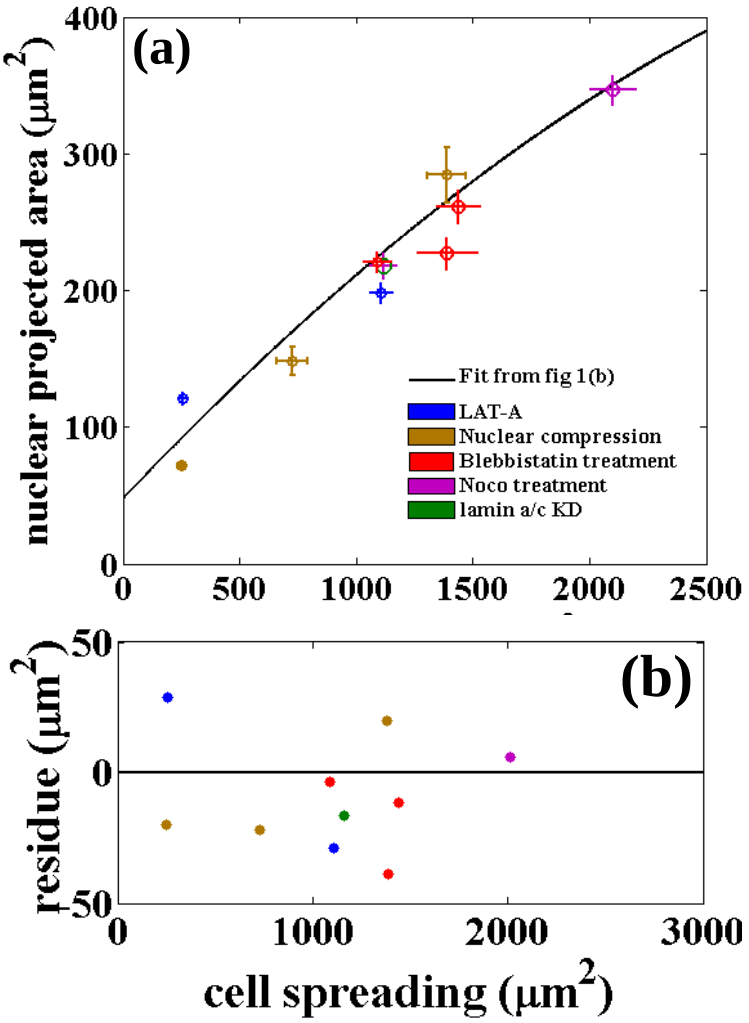

FIGURE 2.22: Change in cell spreading seems to be changing the nuclear projected area to follow the trend shown in Fig. 2.1b. Compressive force applied on the nucleus, using the lens, flattened the nucleus and induced an increase in cell spreading. The deformation in he nucleus and change in cell spreading were coupled to follow the master curve, similar to all perturbation experiments.

islands exhibit lateral actin stress fibers which can generate active tension resulting in the deformation of the nucleus [68], as shown in fig. 2.23. It is shown that the nuclear geometry depends on the aspect ratio of the adhesive island that dictate cell shape. These and similar results reveal the role of stress fibers in regulating nuclear geometry and the influence of cell shape in this [59, 68–70]. However, how the actin cytoskeleton or stress fibers influence cell spreading is not clear.

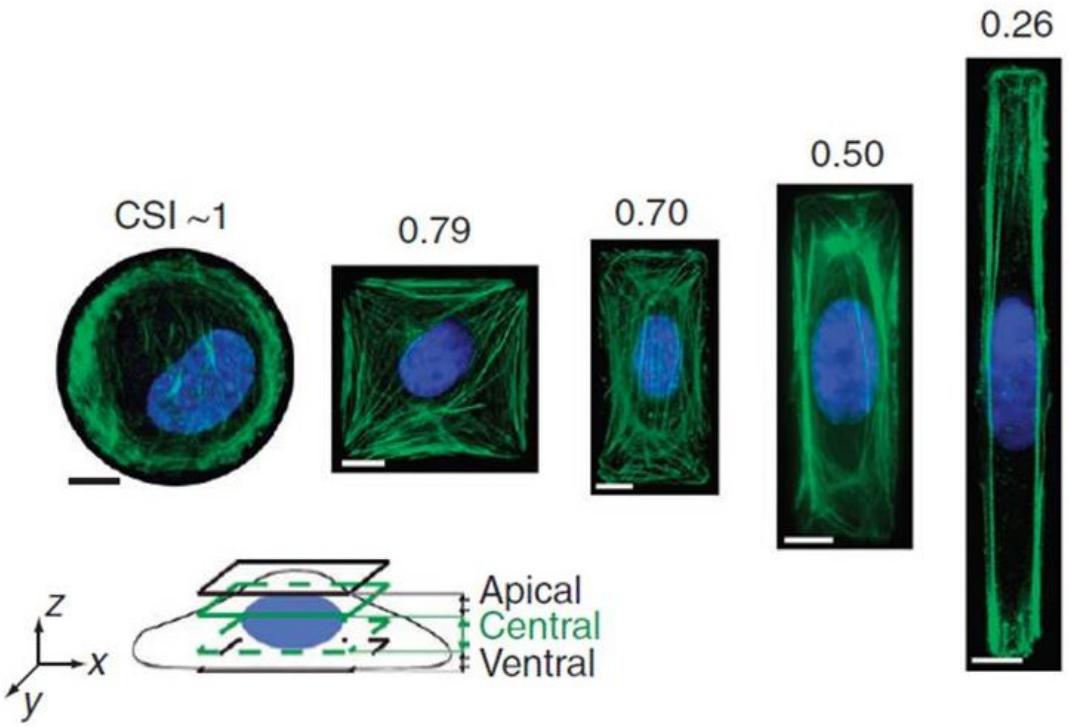

FIGURE 2.23: CSI stands for cell shape index. It was observed that the lateral stress fibers in elongated cells, apply a lateral compression on the nucleus to change its shape. Image is taken from Versaeval et al., 2012 [68]

It has been known for some time that cell spreading and nuclear geometry are related [71, 72] but the mechanism for this coupling remains poorly understood. In this chapter we have explored this aspect by adopting a wide range of quantitative methods.

2.8.1 Cell and nuclear projected areas are robustly coupled and follow a Master Curve

Measurements of cell spreading and nuclear projected area, which is a measure of nuclear deformation, show a robust correlation between the two. These two quantities are related over the entire measurement range. In order to test the robustness of this relationship

under different spreading conditions, we measured the cell and nuclear spread (i) using cells seeded on gels of varying stiffness, (ii) by monitoring the two areas as cell spreading progressed on fibronectin coated glass surfaces, (iii) during trypsin mediated de-adhesion. All these experiments show quantitatively very similar behavior. In order to check if the two areas can be de-coupled by perturbing the cytoskeletal structure or the actin-nucleus linkages we performed a series of such experiments. Remarkably, actin or microtubule depolymerization, inhibition of active stresses by myosin-II inactivation and perturbation of nuclear–actin linkages, all resulted in variations in cell spreading respecting the same relation between nuclear and cell areas as seen in normal cells. All these data follow a master-curve without the need for any scaling as shown in Fig. 2.12.

2.8.2 Perinuclear stress fibers regulate cell spreading as well as nuclear shape

Next, we explored how nuclear deformations may be coupled to cell spreading. Imaging the actin cytoskeleton reveals that a number of perinuclear stress fibers run over the nucleus in well spread mMSCs, similar but lower in number compared to that reported for fibroblasts [59]. When cells were imaged on gels of different stiffnesses, the number of these fibers shows a correlation with the extent of cell spreading, decreasing from about 10 in fully spread cells to no detectable stress fibres in the lowest range of cell spreading (softest gel). The model shows that these stress fibers can generate enough

tension to deform the nucleus as seen in experiments. In poorly spread cells, stress fibers are replaced by a cortical actin layer below the membrane. These observations suggest that the compression of the nucleus by actin stress fibers may be the primary cause for the observed nuclear deformation dependent changes in cell spreading. Compression of the nucleus by applying an external load using the lens-technique demonstrates this mechanism. Indeed, the application of an external compressive loading over the nucleus resulted in increased nuclear and cell spreading. Remarkably, the data agrees well with the master-curve Fig. 2.12. These results reveal the importance of perinuclear stress fibers in coupling nuclear deformation to cell spreading as elaborated in the next section.

2.8.3 Nuclear compression by stress fibers aid cell spreading

Together, our results show that a compressive loading of the nucleus by stress fibers is a mechanical regulating factor that dictates cell spreading. This can be explained as follows. A nucleus is an elastic inclusion inside a cell. In the absence of a nucleus, as in the case of cell fragments, cells are able to spread to an almost flat structure, maximizing the extent of spreading. In normal cells, the nucleus prevents the cell from reaching this maximally spread state, since deforming the nucleus costs elastic free energy. The cell achieves

an intermediate state of spreading, which is dictated by the elastic deformability of the nucleus (its Young's modulus) and the substrate mediated adhesion. However, if the nucleus is compressed by an external force, the cell is able to spread to a greater extent as shown by the nuclear compression experiment using lens. In a normal cell plated on an adhesion promoting substrate, this compression is brought about by the perinuclear stress fibers as discussed in the modeling section. This is schematically shown in "Fig. 2.25". This simple mechanism may account for the observed correlation between cell spreading and nuclear compression by stress fibers. Similar arguments have been made previously to understand early stages of cell spreading dynamics but without considering stress fiber mediated nuclear compression [88, 89]. The early stage cell spreading here in these reports had been shown to follow the dynamics similar to the spreading of a liquid drop [88]. It had been shown to follow a power law and had been argued with quantitative model that the early stage cell spreading is governed by its mesoscopic structural and material properties [89]. If the extent of actin stress fibers compressing the nucleus is reduced or if the contractility is blocked, the nucleus becomes more rounded and, thereby, reduce the ability of the cell cortex to spread out due to surface mediated forces. This agrees well with our data, the confocal observations, cell response to cytoskeletal or myosin-II perturbation experiments (Fig. 2.6) and nuclear compression experiment. When perinuclear stress fibers are absent, as in cells on gels, lamin knock-down cells or cells treated

with low levels of latrunculin, the nucleus bulges out and exert an outward pressure on the cortex (membrane plus any cortical actin mesh) causing a reduction in spread area. In all these perturbation experiments a reduction in nuclear projected area occurs concomitant with a reduction in cell area and the data follows the same master curve (Fig. 2.12).

Pulling forces generated by stress fibers terminating on the nucleus may be ruled out on two accounts [71]: (i) confocal images do not show any cusp-like deformations at the attachment points which are expected if the nucleus is stretched by localized tensile stresses and (ii) these stress fibers which are attached to only one focal adhesion complex and terminate on the nucleus have a unipolar organization of actin and cannot generate contractile stresses [90, 91]. On the other hand, experiments have shown indentation of the nucleus due to perinuclear stress fibers attached to the substrate at both ends which is expected in case of compressive stresses [70].

2.8.4 Role of Myosin-II in regulating cell spreading

One of the more remarkable observations is that myosin-II inhibition produces antagonistic effects on cells plated on stiff and soft substrates as can be seen in fig. 2.6(b), fig. 2.6(c) and fig. 2.24. Cells grown on stiff substrates decrease their spread area when myosin is inhibited whereas those plated on soft substrates show increased spreading when treated with blebbistatin. This may be understood

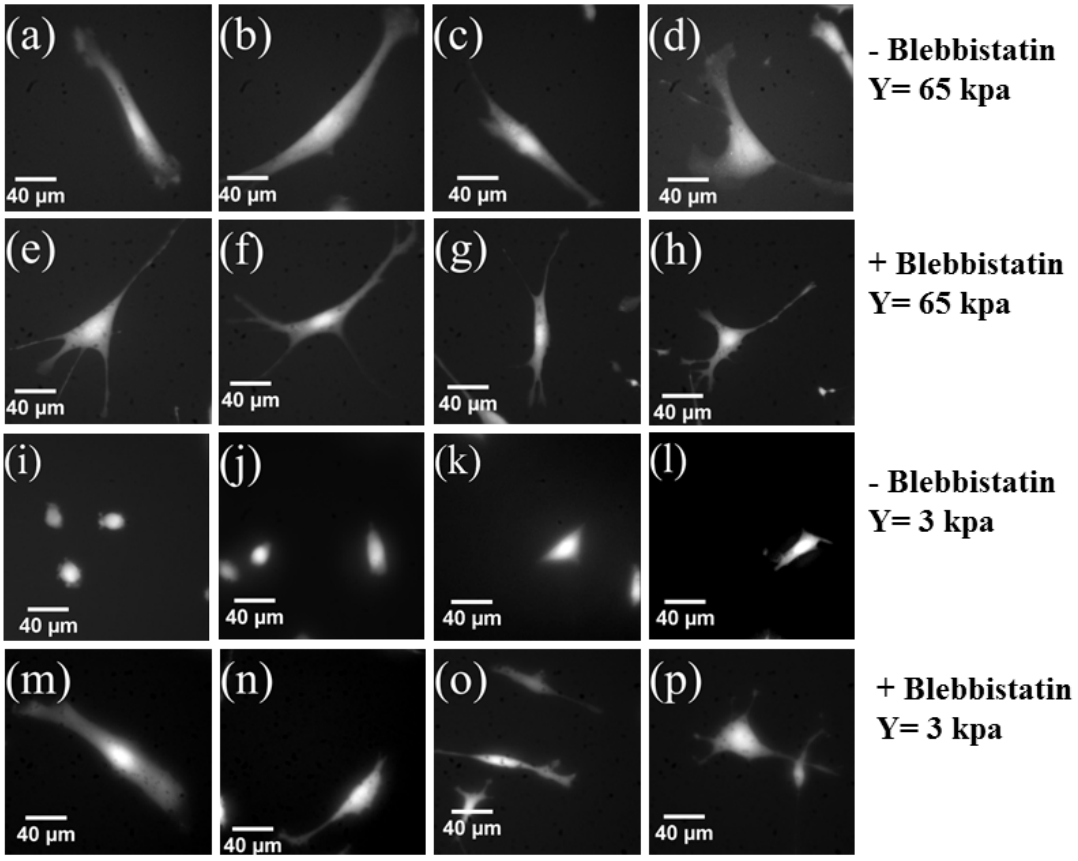

FIGURE 2.24: (a)–(d) Cells grown on the PAA gel with elastic modulus 65 kPa. (e)–(h) Cells grown on substrate with rigidity 65 kPa show a little reduction in spreading after blebbistatin treatment. (i)–(l) Poorly spread cells on substrate with elastic modulus 3 kPa. (m)–(p) After blebbistatin treatment a drastic increase in cell spreading was observed in the poorly spread cells grown on 3 kPa PAA gel.

as follows. Stress fiber numbers are high on stiff substrates and perinuclear fibers help cells spread better as already discussed. Blebbistatin treatment causes disassembly of stress fibers and therefore the compressive loading of the nucleus by perinuclear fibers (Fig. 2.26). This results in decreased cell spreading as discussed above. On soft substrates, on the other hand, actin is mostly in the form of a cortical mesh. In presence of phosphorylated myosin such a cortex is contractile and hence acts as an active elastic shell [92]. This cortical tension tries to maintain a spherical shape for the cell while adhesive

forces try to increase spreading and hence cause deformation (see, for example, [93]). Inhibition of myosin-II drastically reduce cortical tension [92]. Relaxing this active tension by inhibiting myosin tips the balance towards better spreading. The mechanism by which the acto-myosin structure organizes as stress fibers on stiff substrates (well spread cells) and as cortical actin on soft substrates (poorly spread cells) require further investigation. In summary, the exper-

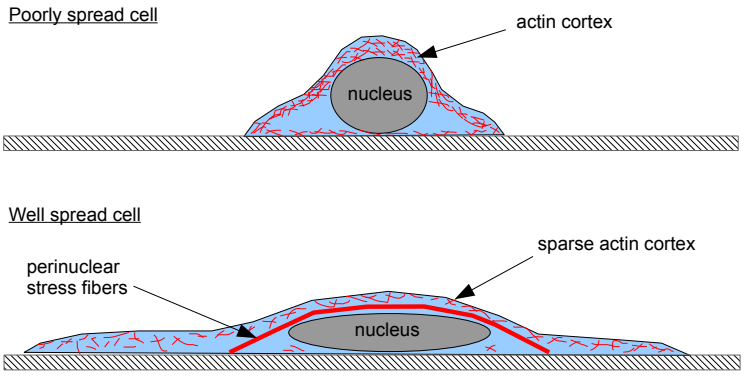

FIGURE 2.25: Schematic showing how nuclear compression helps in cell spreading. Flattening the nucleus by perinuclear stress fibers (or external load as in the case of lens experiment) allows the cell to spread to a greater extent. In the absence of such a compressive loading of the nucleus, the nucleus exerts an upwards force on the cell cortex which constraints cell spreading due to balance of adhesive and elastic forces.

iments reported here demonstrate a tight quantitative relationship between nuclear deformation and cell spreading in mMSCs. Using independent methods we showed that this relation holds irrespective of the way cell spreading is altered, under cytoskeletal and nuclear perturbations, and holds across different cell types. With the help of observations and a simple theoretical model, we hypothesize that compressive loading of the nucleus by perinuclear stress fibers can

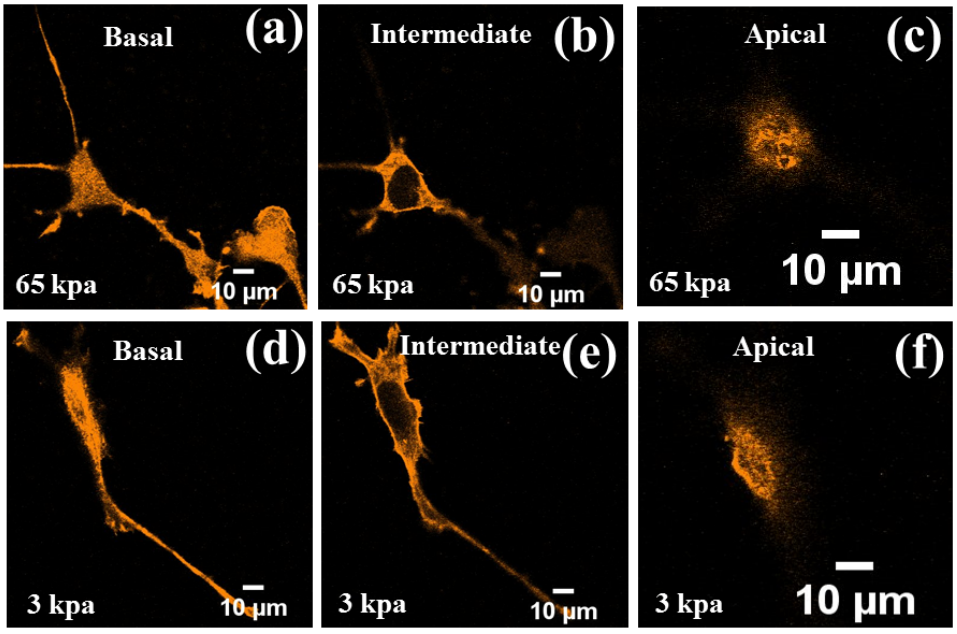

FIGURE 2.26: Images showing that stress fibers are absent in cells treated with blebbistatin irrespective of substrate rigidity.

account for the increase in cell spreading with higher nuclear compression. This is demonstrated by a simple method to apply external compression to the nucleus. While these experiments help us understand how perinuclear stress fibers aid in cell spreading, understanding how the formation of stress fibers depend on substrate properties and how gene expression profile depends on nuclear geometry requires further investigations. Also, mechano-chemical coupling mediated by signalling pathways resulting in feedback processes have to be investigated to obtain a more complete picture of the role played by actin stress fibers in regulating cell and nuclear shape. However, we believe that these experiments and analyses capture the main physical mechanisms that regulate cell and nuclear deformations in a tightly coupled manner.

2.9 Methods

2.9.1 Polyacrylamide (PAA) substrate preparation

PAA gels of about 300μm thickness were prepared on 18 mm activated circular coverslips. For activation, cleaned coverslips were kept in a solution consisting of 90% (v/v) absolute ethanol, 8% deionized Millipore water and 2% 3-Aminopropyltrimethoxysilane (Sigma) for 30 to 45 min., rinsed with Millipore water, incubated at 120 °C for 1 hr and finally treated with 0.5% Gluteraldehyde solution for 30 min. After rinsing, the coverslips were used as the rigid bottom plate for the gel preparation, within 24 hr. Substrate rigidity was controlled by adjusting the percentage of Bis-acrylamide (Sigma) from 0.5% to 0.03% in a solution of 10% Acrylamide (Sigma) and cured at room temperature[94]. To get a flat and smooth top surface of the PAA gels, hydrophobic coverslips were used. To make the coverslips hydrophobic, coverslips were kept in a desiccator with few drops of trichlorosilane (sigma) in an eppendrof cap for 15-20 min in a fume hood. The desiccator was covered by a glass plate to stop the vapours generated by trichlorosilane from escaping. The vaporized silane deposits on the coverslips and makes them hydrophobic. After the silanization, coverslips were washed with millipore water and heated at 120 °C for 1 hr.

The characterization of the PAA substrates was done using two well established techniques: 1) atomic force microscopy (AFM) and 2) ball indentation. The comparison of the values of Young's modulus

obtained from these two methods is as shown in Fig. 2.27. The Hertz formula was used to calculate the Young's modulus for both the methods i.e., ball indentation and AFM.

$$E = \frac{3(1-\nu^2)F}{4\delta^{3/2}R^{1/2}} \tag{2.7}$$

where E is the Young's modulus, $\nu = 0.45$ is the Poisson ratio[95], F is the normal force, δ is the measured indentation of the ball and R is the radius of the ball or the radius of curvature of the AFM tip.

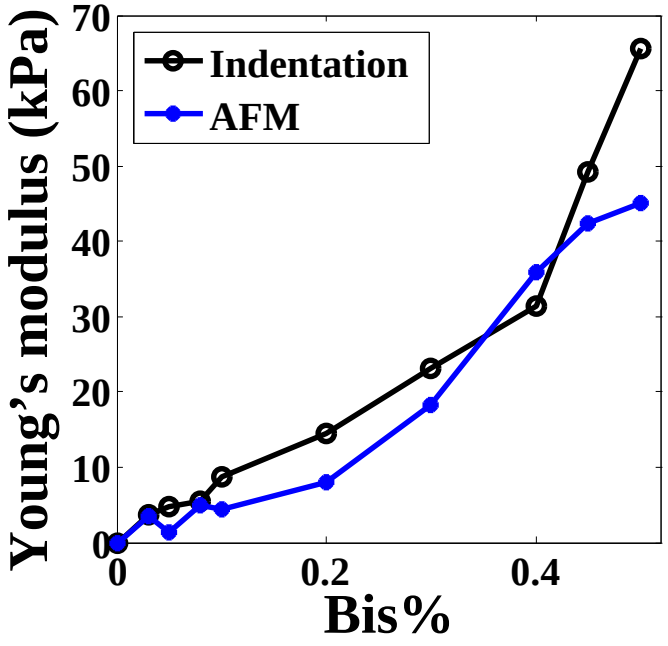

FIGURE 2.27: Figure shows a comparison between the two methods of measuring elastic moduli of PAA gel substrates.

For the ball indentation method, a solution of 2 μm fluorescent beads in 1 ml HBSS was spread over the gel surface as a surface marker. Then a steel ball of radius 1.59 mm and weight 0.129 grams was

placed on the surface as indenter. Indentations were measured using a calibrated microscope focus arrangement.

Indentation values for the calibration using AFM (Shivprasad Patil's lab in IISER Pune) were taken by applying a constant force on the gel surface using a spherical tip cantilever over a scanning area of $100X100\mu m^2$. The spring constant of the cantilever was 0.2 N/m and the diameter of the spherical tip was 1 μm. This scanning was done to check if there are significant inhomogeneities, especially in weaker gels when probed at the scale of a focal adhesion.

It is to be noted that PPA gel can give same value of elastic modulus for different percentage ratios of Acrylamide and Bis-Acrylamide. For example, 3%, 4% and 5% Acrylamide with 0.1%, 0.06% and 0.03% Bis-Acrylamide respectively will give a PAA gel with Young's modulus around 1 kPa. While preparing soft gels, i.e., of elasticity less than 3 kPa, it is very crucial to choose the ratio of Acrylamide and Bis-Acrylamide in gel solution as many ratios were shown to have cracks in gel substrates after polymerization as discussed in Saha et al., 2010 [96]. Among all three percentage ratios, which are mentioned above, only first could polymerize into crack free gel surface.

2.9.2 ECM coating for PAA gels

- Wash the gel surfaces with HBSS to remove non polymerized acrylamide, as it is toxic to the cells.

- Wash gels with 50 mM HEPES buffer at pH 8–8.5 two times.

- Prepare 1 mg/ml sulfo-SANPAH stock solution by dissolving 50 mg of sulfo-SANPAH powder in 50 ml of 50 mM HEPES buffer at pH 8–8.5 in dark and immediately store at $-20\,^{\circ}\mathrm{C}$ after wrapping the aliquots with aluminium foil, to protect them from light. Dilute each aliquot by 3 times in 50 mM HEPES pH 8-8.5 buffer and use immediately (do not keep at room temperature for more than the minimum time required to complete the whole procedure of coating). Pipette a small quantity (nearly 200 μl for the gel surfaces prepared on 18 mm square cover slips) of diluted sulfo-SANPAH solution onto the gel surface, enough to cover the gel surface and place them under 365 nm UV lamp for 15min or till the solution turns from reddish orange to dark brown. The UV lamp (Pierce; Thermo scientific) was kept at a height of 6-10 inches from the gel with sulfo-SANPAH.

- Wash with 50 mM HEPES and irradiate under UV with sulfo-SANPAH solution once again as done in the previous step and then wash with 50 mM HEPES at least two times.

- Prepare 50 $\mu g/ml$ fibronectin solution in 50 mM HEPES buffer pH 8-8.5 from 1 mg/ml stock solution and pipette 200 μl of this solution on the top of the gels prepared on 18mm square coverslips.

- Carefully place the gels at 37^oC for over night incubation. The protein solution should remain at the top of gel surface during incubation and the gel should not become dry. To prevent drying of gel, the incubation was done with humidity control.
- After incubation, wash the surfaces with HBSS 2-3 times and use them for cell culture.

2.9.3 Immunostaining

Following steps were taken to label vinculin, actin and nucleus in cells. All the confocal images were taken with fixed immunostained cells.

- Add 4% Paraformaldehyde (PFA), prepared in 1% Phosphate buffered saline (PBS), to cell and incubate at room temperature (RT) for 15 min.
- Wash the cells with PBS three times. All the washes should be gentle and quick (without incubation). After fixation, cells can be kept in PBS, at 4 °C.
- To permeabilize cells, add 0.1% Triton x100, prepared in PBS for 10 min and incubate at RT. Give three quick washes.
- Add blocking buffer (5% BSA + 5%FBS) to cells and incubate at RT for 1 hr.

- Remove blocking buffer and add primary antibody anti-vinculin (Sigma Aldrich, cat. no. V9131) and leave for 1.5 hr. The dilution used for anti-vinculin primary antibody was 1μl in 500μl of PBS.

- Wash with PBS+0.1% Tween20 solution two times and with only PBS once. Each wash should be of 10 min duration.

- Add secondary antibody Alexa fluor 488 (Molecular Probes, Invitrogen) with a dilution 1:600 for mMSCs and 1:800 for 3T3 fibroblasts. Incubate at RT for 1 hr.

- Remove secondary and wash the cells two times with PBS + 0.1%Tween20 solution and once only with PBS. All three washes were quick washes.

- To stain actin fibers and nucleus, working solution containing Rhodamine Phalloidin (Rh-Pl) and Hoechst33342 was prepared from stock solutions. Concentration of stock solution was 1 mg/ml for both Hoechst33342 and Rh-Pl, To make stock solutions Methanol and HBSS were used to dissolve Rh-Pl and Hoechst33342, respectively. To prepare 1 ml of working solution 0.025 μl of Rh-Pl stock and 0.5 μl of Hoechst33342 was added in 1 ml PBS.

- Working solution was added to the culture and cells were incubated at RT for 20 min.

- Wash with PBS two times with each wash of duration 10 min.

- Mount the sample and observe.

2.9.4 siRNA Transfection to knock down lamin A/C

- Prepare two vials A and B with 300 μl of pre-warmed Opti-MEM.
- In A, add 20μl siRNA (20μM stock prepared in siRNA Buffer) and in B add 25 μl of Dharmafact. Incubate both the vials at RT for 5 min.
- Gently mix the contents of the two vials in a tube and incubate at RT for 30 min.
- Take 70–80% confluent culture in a 90 mm disk, remove media and drop-wise add the solution prepared in previous step to the culture.
- Add 2.4 ml of pre-warmed Opti-MEM to the culture and incubate at 37 °C with 5% CO_2 for 5 hr.
- After 5 hr, remove Opti-MEM and add complete cell culture media to the dish and leave in incubation at 37 °C with 5% CO_2 for 48 hr.

  siRNA used in the experiments is labelled with DY-547 (Cy3 analog)- Absorbance/Emission Max= 557/570 nm and gives a positive correlation of cytoplasmic fluorescence with transfection efficiency as shown in Fig. 2.28. This fluorescence was used as an indicator of lamin knock down in mMSCs.

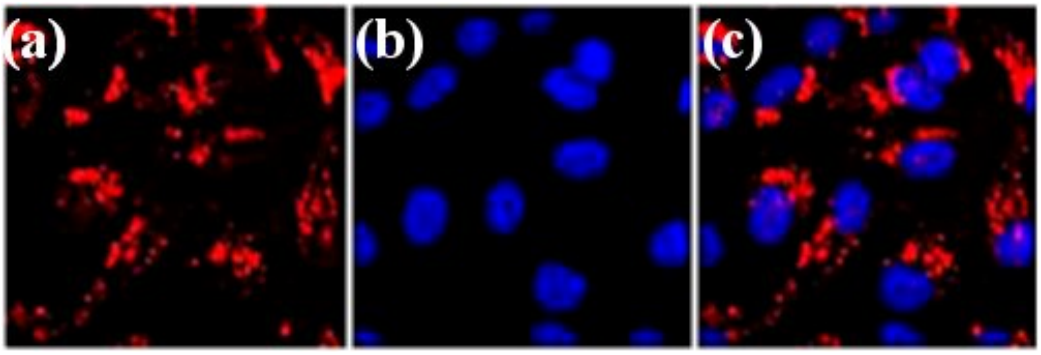

FIGURE 2.28: The cytoplasmic fluorescence, visible in cells after 48 hrs of transfection. (a) Cytoplasmic fluorescence, caused by lamin A/C knock-down. (b) Nucleus labelled using Dapi. (c) Merged image of (a) & (b). The image is adopted from http://dharmacon.gelifesciences.com/sirna/siglo-lamin-a-c-sirna-human-mouse-rat/

2.9.5 Transfection protocol

This protocol is for the transfection of 60–70% confluent culture in a 35 mm dish and needs fine tuning for different plasmids and different cell type. The following protocol was used to label vinculin in cell grown on PAA substrates for TFM.

- Remove the cell culture medium from the dish and add pre-warm Opti-MEM. Incubate the cells for 20–30 min at 37 °C with 5% CO_2.
- Take 200 μl of Opti-MEM media in two vials of 500 μl and label them as A and B. In A add 1 μg of plasmid DNA and in B add 2–5 μl of lipofectamin and let the solution stand for 5 min.
- Gently mix the solution in two vials and incubate at room temperature for 15 min.

- Add the solution to the cell culture and incubate at 37 °C with 5% CO_2 for 5 hours.
- After 5 hrs of incubation change the medium and incubate again for 24-36 hrs to see any expression.

2.9.6 Image acquisition and analysis

Confocal imaging was done using Ziess 510 Meta confocal microscope in CIFF, NCBS. For confocal imaging, cells were fixed, permeabilized and then labelled, for actin, focal adhesions and nucleus. Image analysis to quantify cell spreading area and nuclear projected area was done using a custom written Matlab code. The code involved conversion of grayscale images into binary images by applying a threshold to the grayscale values and then finding area using an inbuilt Matlab function "regionprops". Fiji-Just ImageJ plugins http://fiji.sc/Fiji were used for analysing the phase contrast images from trypsin experiment and calculating the volume from the confocal z-stacks. Z-stacks were acquired using the confocal microscope with a resolution of 0.6 μm (for thick cells) to 0.2 μm (for thin cells) (about 50 slices per cell). The object counter plugin of Fiji-Just ImageJ was used to calculate the nuclear volume. The plugin adds the voxels in each slice of the z-stack of an object to give volume.

Chapter 3

Dynamics of membrane tension

Introduction

A cell membrane is what keeps the inside of the cell packed and separated from the outside environment. A cell membrane or plasma membrane, is basically a lipid bilayer with a number of proteins embedded in it. The lipids in the membrane play an active role in the regulation of membrane structures and biological functions [2–4]. The membrane of a cell, though behaves like a 2D-liquid, also has certain mechanical properties. According to the fluid mosaic model for plasma membrane, the lipids and the proteins embedded in the membrane can freely diffuse in the plane of the membrane. As per the reported mechanical properties, the plasma membrane has a very low shear [5–7] and a high lateral compression elastic modulus ($10^3 N/m^2$) [8, 9]. The viscosity of the membrane depends on its composition, for an erythrocyte it has been reported to be in the range 0.36–2.1 $10^3 Pas$ [9]. Membrane tension is also one of

the well documented mechanical property of a cell. A cell always maintains the membrane tension associated with it. Any change in the membrane tension leads to the change in a number of functions in a cell. These functions are mainly related to the regulation of cell motility [13–15], morphology [16, 17] and trafficking [18]. The rate of exocytosis and endocytosis have been reported to get influence by the change in membrane tension [18, 97]. Increase in membrane tension increases the exocytosis rate and decrease in tension increases endocytosis rate to maintain the cell specific membrane tension. A typical image of a cell membrane can be seen in fig. 3.1. This chapter

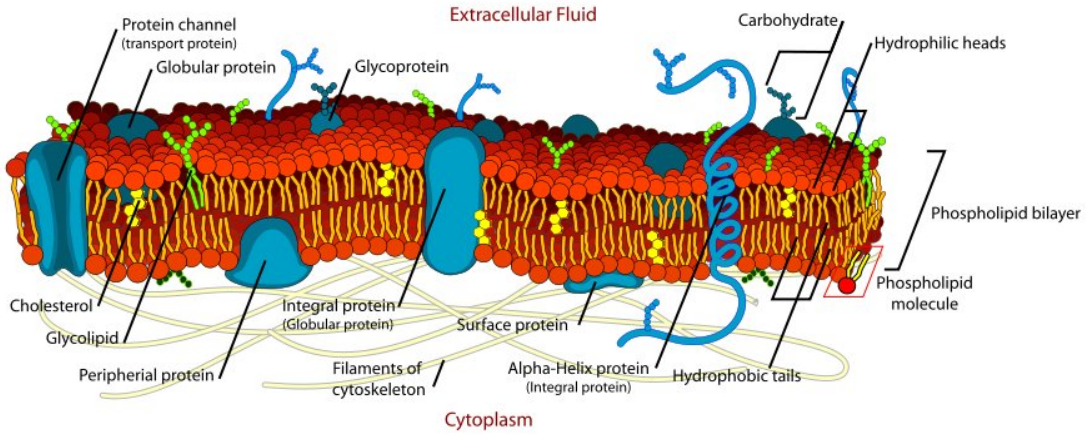

FIGURE 3.1: The cell membrane is a phospholipid bilayer with a number of transmembrane proteins embedded in it. Image courtesy http://en.wikipedia.org/wiki/Cell_membrane

includes a few measurements of the membrane tension in 3T3 fibroblast cell as a function of cell spreading. Static and dynamic tether force were measured, using an optical trap, to see the dependency of membrane tension on cell spreading area. Experiments that led to some interesting findings while investigating the force dynamics of a tether, pulled or retracted in step are also reported in this chapter.

3.1 Methods to quantify membrane tension

There are various methods that can be used to measure membrane tension of the lipid bilayer in case of cells or vesicles. The explanation of these methods are a follow.

3.1.1 Compression

Compression of cells, lipid vesicles, urchin eggs and red blood cells is one of the oldest methods to measure the membrane tension [8, 11, 98]. In this method, the cell or the vesicle is compressed between two rigid plates and tension is measured through the well established contact mechanics for the deformation of the elastic objects, as shown in fig. 3.2(a), using the following equation.

$$T = \frac{F/A}{1/R_1 - 1/R_2} \tag{3.1}$$

where, A= πD^2.

3.1.2 Micropipette Aspiration

In the case of micropipette aspiration a negative pressure is applied at the membrane surface using a glass pipette of diameter about a few microns to pull a part of the membrane inside the pipette to measure the membrane tension, as shown in fig. 3.2(b). The following formula can be used to measure membrane tension, in the

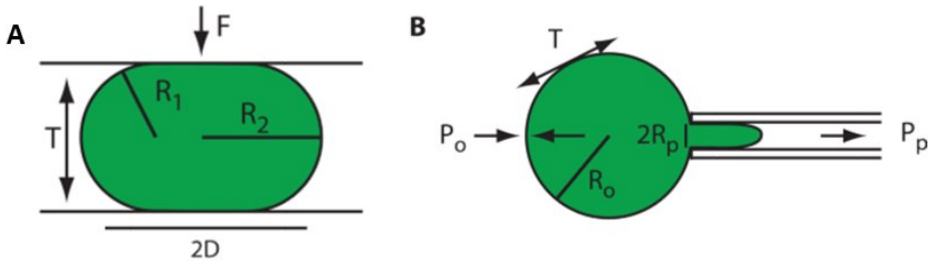

FIGURE 3.2: Micropipette aspiration has been extensively used to explore the mechanical properties of the membrane in vesicles. (a) Compressing a vesicle can also give a measure of the properties of its membrane. (b) A tube like structure pulled from the membrane with the help of a micropipette gives a measure of the membrane tension. Image is taken from Trends in Cell Biology [99].

case of micropipette aspiration.

$$T = \frac{P_o - P_p}{2(1/R_p - 1/R_o)}. \tag{3.2}$$

3.1.3 Pulling a membrane nanotube

A membrane nanotube (tether), pulled from a vesicle or cell membrane gives an estimate of the membrane tension and membrane dynamic response at the same time. A membrane tube can be pulled from a cell surface by letting a bead to make contact with the membrane surface first and the pulling it away to draw a membrane nanotube. The bead in contact with the membrane can be pulled either using another glass pipette or an AFM tip as shown in fig. 3.3 & fig. 3.4 [100] or an optical tweezer [101] as shown in fig. 3.4. Holding the object using one pipette and pulling tether with another pipette with the bead as shown in fig. 3.3, is used to measure the membrane tension and membrane dynamics of suspended cells or vesicles [102]. The equation that can be employed to calculate membrane tension

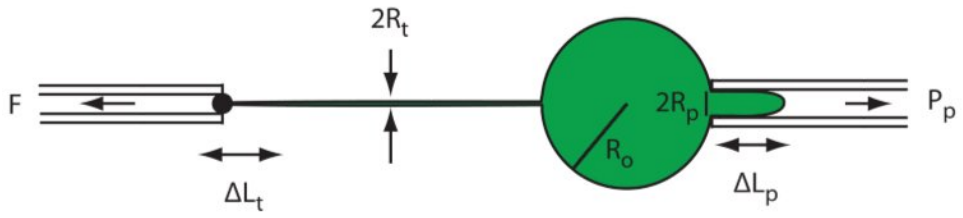

FIGURE 3.3: Micropipette aspiration as shown can be used to pull membrane tubes from a suspended cell or a vesicle [99].

in the case of suspended cells or vesicles using the method shown in fig. 3.3, is as follows.

$$R_t = R_p(1 - R_p/R_o)(\Delta L_p/\Delta L_t) \tag{3.3}$$

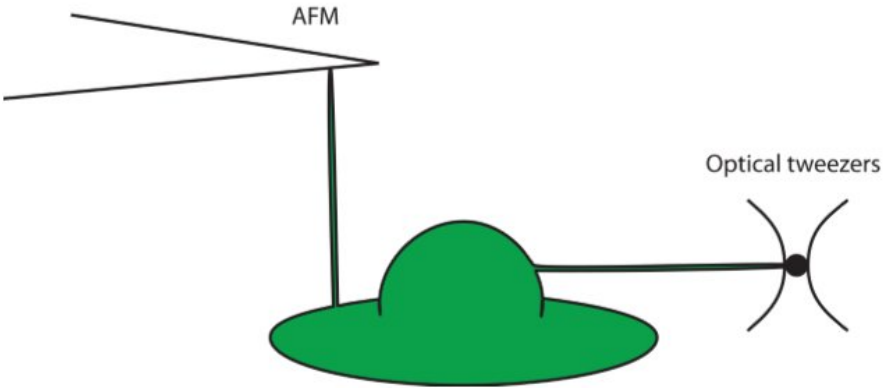

FIGURE 3.4: Membrane tubes can be pulled from adhered cells, using either an AFM tip or an optically trapped bead [99].

Force measurements in case of AFM and the optical trap are done using Hook's law $F = -k\Delta L$. Where, ΔL is the deflection in the cantilever or displacement of bead in the trap, in case of AFM or Optical tweezers, respectively. This force further can be used to have an estimate of membrane tension or the radius of the nanotube using the equations described in the next section. In our experiments, we

have used an optical trap to study the effect of cell spreading on static and dynamic membrane tension. The experiments related to explore the dynamics of a pulled or retracted tether were also done using the optical tweezers.

3.2 Tension in a membrane tether

The tension in tether, pulled from a bilayer, can be broadly divided into two parts: static tension and dynamic tension. The division is based upon, whether the tether has a fixed length or is constantly elongating. The description of the two tensions is as follow.

3.2.1 Static membrane tension

A tether formed by pulling a membrane tube from the bilayer plasma membrane gives an estimate of the steady state membrane tension in the static condition. The radius of the membrane tube in equilibrium is determined by the membrane tension and the bending modulus of the bilayer. The bending modulus of plasma membrane is a constant quantity which depends on the composition of the membrane. According to the formulation by Derenyi et al. [103] the equilibrium radius of the a membrane tube pulled from a bilayer is given by,

$$R_0 = \sqrt{\frac{B}{2T}} \tag{3.4}$$

where, T=membrane tension and B= bending modulus. The bending modulus of a lipid bilayer have been reported to be of the order of $10^{-19} N.m$ [10–12]. Pulling a tether from the bilayer of a living cell does not give the actual membrane tension in a true sense. It is an apparent tension because it has a contribution from the membrane cytoskeleton adhesion. Therefore, membrane tension resulting from extracting a tether, from a plasma membrane, can be written as [10, 104],

$$T = T_m + \gamma \tag{3.5}$$

where γ= adhesion energy per unit area and T_m = in plane membrane tension. The force F_0 required to maintain the equilibrium length of the tether is related to the apparent membrane tension by the following equation [103].

$$T = \frac{F_0^2}{8B\pi^2}. \tag{3.6}$$

The in plane tension of the membrane can be estimated by performing tether measurements on cell blebs. Blebs are formed by the detachment of cell membrane from the cell cytoskeleton. The tether force measurements done on cell blebs show that 75% of the apparent membrane tension is due to membrane-cytoskeleton adhesion [105].

3.2.2 Dynamic membrane tension

Dynamic membrane tension refers to the tension in a membrane tether elongating at a constant speed. As per Evans and Yeung,

1994 [106], if the length of a membrane tube is elongated with a constant speed v, then the instantaneous tether force in the case of a vesicle, is given by,

$$f_t = f_0 + 2\pi \left[\eta_m h^2 ln \left(\frac{R}{R_t} \right) v \right] \tag{3.7}$$

where f_0 = static tether force, R= radius of the vesicle, η_m= effective viscosity of the bilayer, h= bilayer thickness and R_t= tether radius. The second term in the right hand side of eq. 3.7 is due to the friction between the lipid monolayers of the bilayer. The outer lipid layer of the tether has a slightly greater radius than the inner layer, which cause a friction between the layers, when a membrane tube is pulled. This is because more of outer layer would be pulled as compared to the inner layer. According to the already reported behaviour of a dynamic tether, there is barrier force that exists for the formation of a membrane tube [107]. This barrier force depends on the area on which pulling force is being applied to pull the tether. Once the tether is formed, the tether force increases linearly with increasing rate of tether elongation. Recent experiments have put forward the evidences for the existence of membrane reservoirs that can supply extra membrane to the tether and hence can buffer the increasing dynamic membrane tension [108–110]. Caveolae on the plasma membrane, acting as membrane reservoirs, have been shown to open up in response to a sudden surge in the membrane tension, cause either by mechanical stretching or an osmotic sock [109, 110]. Opening up of these cup-like structures in a force dependent manner

act like membrane reservoirs.

3.3 Optical trap

An optical trap uses a highly energetic, focused laser beam and the mismatch of refractive index, to trap micron size dielectric particles. The working principle of an optical trap is based on the law of momentum conservation. Ray optics can be used to understand the trapping of a micron size bead by a laser beam. A parallel beam of light coming from a TEM-00 laser mode is known to have a gaussian intensity profile. Consider a micron sized dielectric bead in the path of the laser beam. When a light ray passes through the bead, it changes its path and momentum due to refraction. In accordance with Newton's third law, change in momentum in the ray causes an equal and opposite change in momentum of the bead. In case of an off centre bead, the light beam applies a force on the bead to pull it back into the centre. In fig. 3.5(b), the bead is displaced to the right of the beam centre. Due to the gaussian profile of the beam, the rays to the left of the bead centre would be stronger than the rays to the right of the bead centre. These rays after passing through the bead will have a change in momentum, as shown in fig. 3.5(a). The rays on the left will have larger change in momentum than the rays on the right. This will cause a net force acting on the bead directed towards the beam centre, as shown in fig. 3.5(b). Therefore, the bead will be trapped in the plane normal to the beam propagation

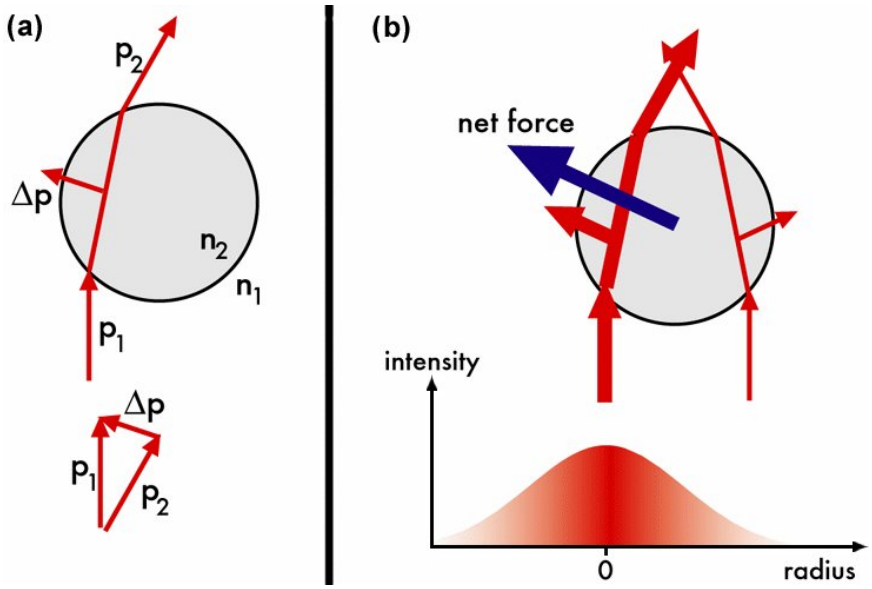

FIGURE 3.5: (a) When a light beam passes through the bead, which can be either of glass or latex or polystyrene, it changes it's path due to refraction. The refraction of the beam causes a change in momentum in the light rays passing through the bead. (b) The difference in the change in momentum of the two representative rays passing through the bead causes a net force acting on the bead, which pulls the bead towards the centre of the gaussian beam profile. Image courtesy http://www.rpgroup.caltech.edu/courses/PBL/tweezers.htm.

direction but not along it. The force component along the beam will cause a movement in the bead to push the bead away from the beam, as shown in fig. 3.6. In order to trap the bead in the third direction, a high numerical aperture lens has to be inserted to focus the beam as shown in fig. 3.7. The focused beam traps the bead in all three directions, i.e., the neck region. If a laterally centred bead displaced in upward or downward direction from the centre of the focus, it experiences a net force acting towards the neck of the trap, as shown in fig. 3.7(a) & (b). An optical trap can be used to apply force of typically on the order of piconewton.

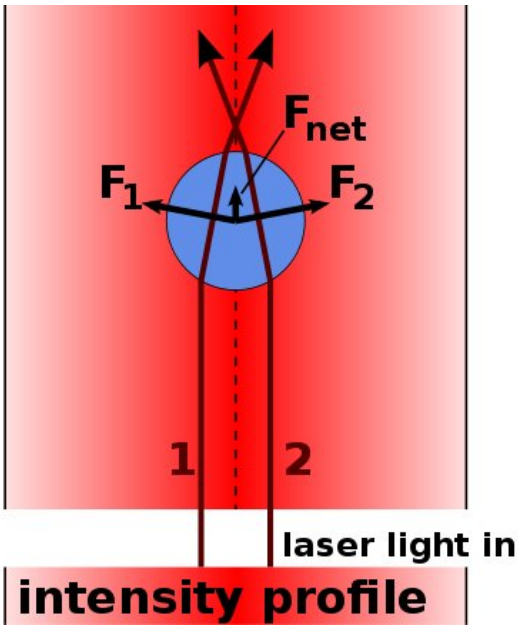

FIGURE 3.6: An unfocused beam of laser can trap the bead only in a plane. Any disturbance in the bead position with respect to the beam centre, pulls the bead back into the beam centre. A laterally centred bead in an unfocused beam will be forced to move away from the beam due to the component of force along the direction of bead propagation. The image is adopted from Wikipedia.

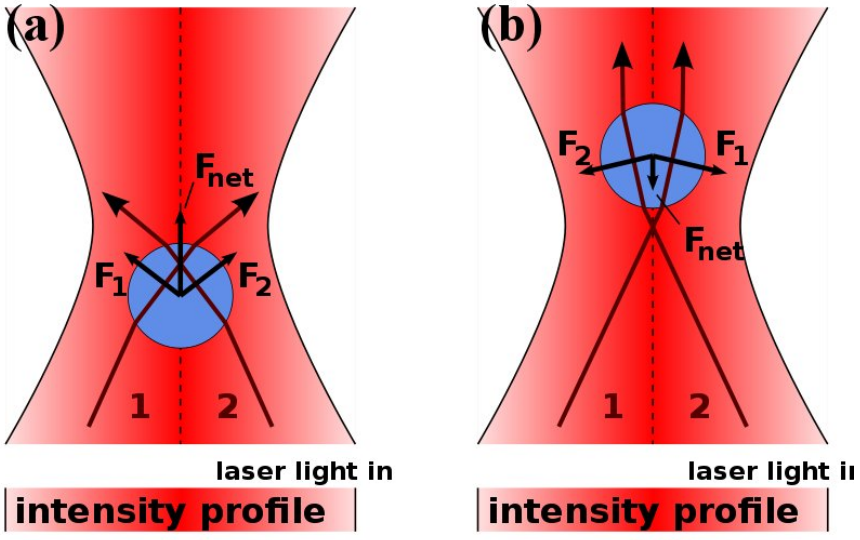

FIGURE 3.7: A focused beam has a catenoidal shape, and any disturbance in the position of the trapped bead from the centre of the catenoid leads to a net force acting on it to bring it back to the centre. This image is adopted from Wikipedia.

3.4 Cell spreading dependency of membrane tension

To understand the dependency of membrane tension on cell spreading, we performed tether pulling experiments on 3T3 fibroblast cells grown on fibronectin coated cover-glass. To study the role of cell spreading on membrane tension, static and dynamic membrane tensions were measured. For the static membrane tension a 15–20μm long tether was pulled from the lamellopodia, with the help of an optically trapped 2.8 μm size plastic bead. As the position of the trap was fixed in the set up we had used, the stage was moved to change the distance between the cell and the trapped bead. The tether tension was allowed to get stabilized to get the static membrane tension. For the dynamic tether force, an already existing tether of length around 10 μm was elongated to 40–50μm length, at different velocities. The results of these two measurements are as follows.

3.4.1 Static membrane tension

In order to find the dependency of membrane tension on cell spreading, we chose three different cell areas. Other than the well spread cells with an average area of 1800 μm^2 (as it was calculated for cells on fibronectin coated cover glass, in chapter 2), we did membrane tension measurements on cells grown on circular adhesive islands of diameter 40 μm and 20 μm. Details of the micro-contact

printing that we have used to pattern glass with adhesive circles are discussed in Appendix A. We found that the membrane tension increases with increasing cell area. The tether force measurements were taken for around 20 cells for each cell spreading area and the results are as shown in fig. 3.8. The average static tether force for the cells with spreading 1800 μm^2, 1300 μm^2 and 314 μm^2 were found to be 10.7±0.3 pN, 7.8±0.3 pN and 6.2±0.5 pN, respectively.

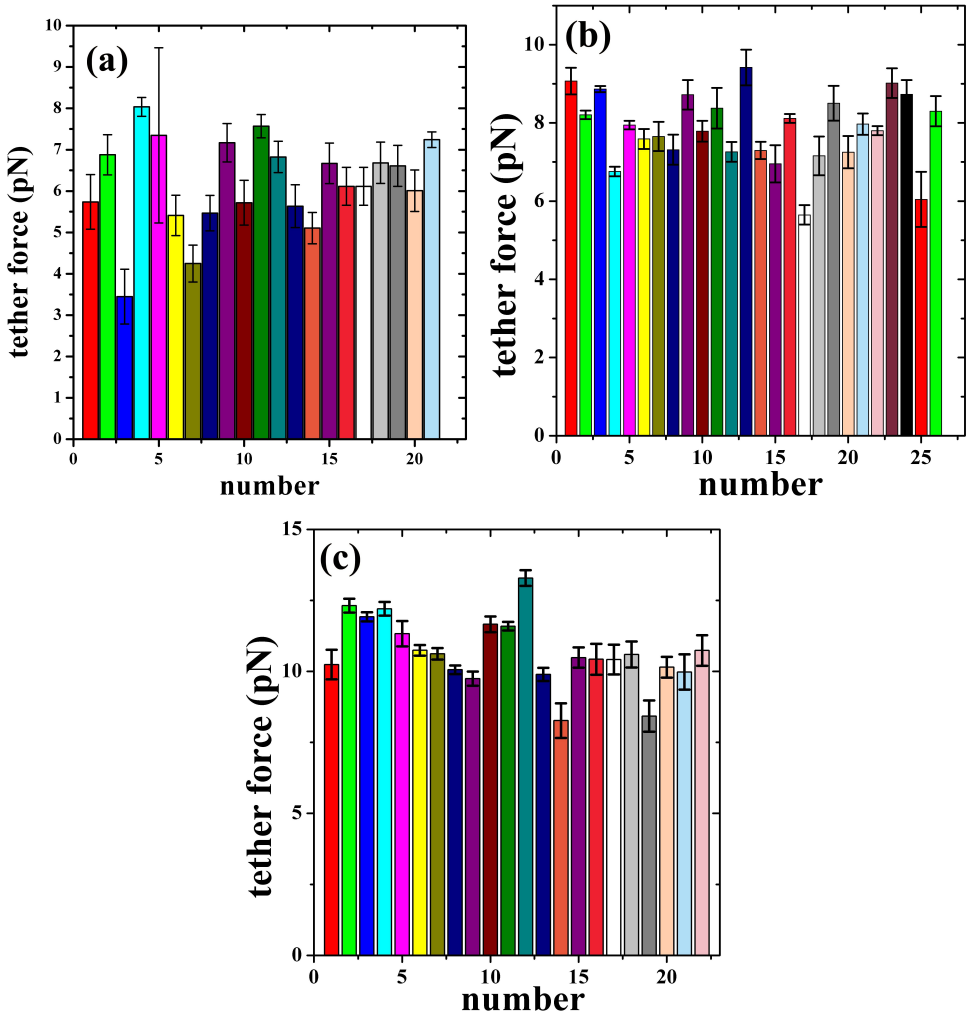

FIGURE 3.8: (a), (b) & (c) show the static membrane tension for around 20 cell for cell with cell spreading 1800 μm^2, 1300 μm^2 and 314 μm^2, respectively. The error bar on the individual bar, represents the fluctuations in the membrane tension, recorded by the trap for an individual cell.

The cells grown on circular patches of different area will have a limited area to make focal contacts with the surface as the other part of the surface is passivated. Even though the adhesion area is restricted, a cell is able to protrude a lamellopodia outside the adhesive island. It is this lamellopodia from where the tethers were pulled. No labelled focal adhesions were found under these lamellopodia when cells were immunostained for vinculin as shown in fig. 3.9.

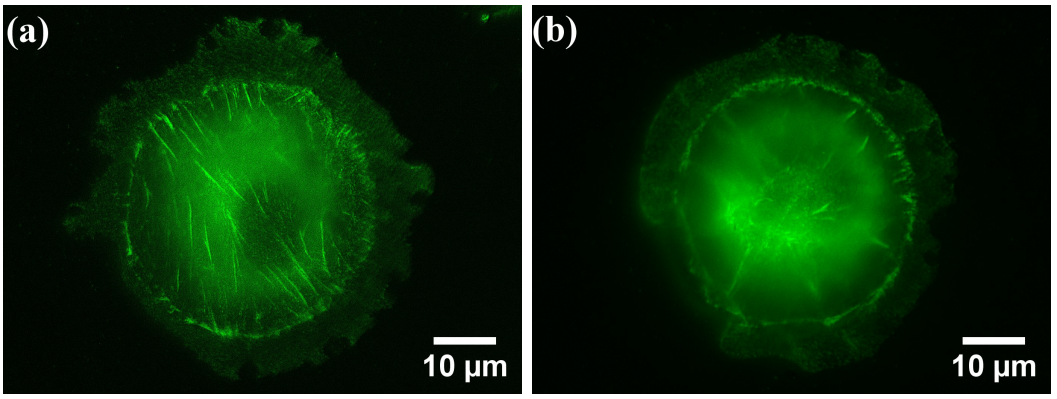

FIGURE 3.9: (a) & (b) Cell grown on adhesive circular patches were observed to extend their lamellopodia, beyond the patch on the passivated surface. The cell in the image were grown on circular patch of diameter 40 μm. The cells are labelled for focal adhesions with the help of Immunostaining for vinculin.

3.4.2 Dynamic membrane tension

According to the earlier work the tension in tether pulled with a constant velocity increases linearly till it reaches a plateau which is followed by an exponential increase in tether force [108], as shown in fig. 3.10. The existence of the plateau in the dynamic tether force curve has been presented as the proof of membrane reservoirs that act as buffer for membrane tension till they are depleted. The pulling experiments done in this reported work involved pulling a small tether

to a length of around 5–10 μm with a constant speed 4 $\mu m/sec$. In our experiments, the dynamic tether forces were recorded for an

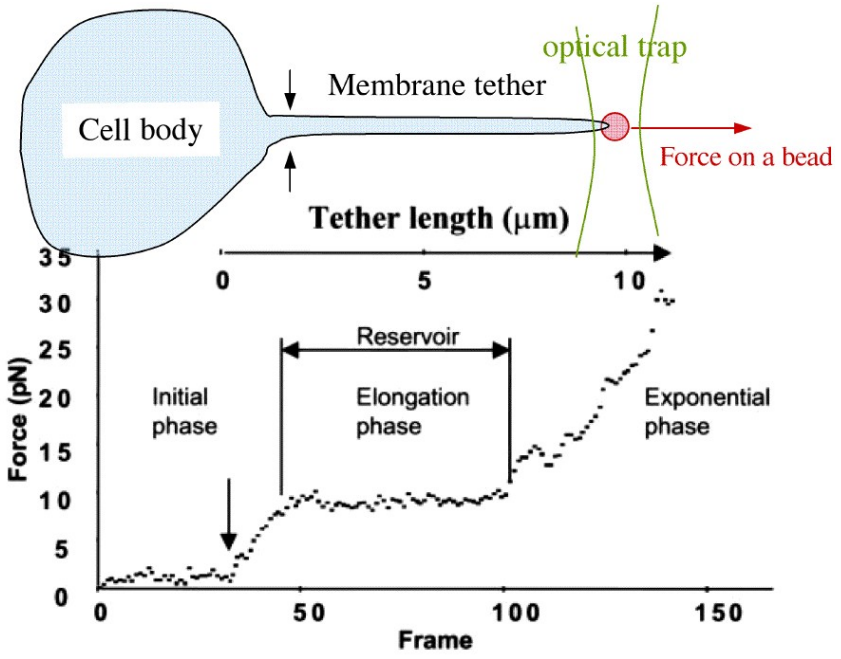

FIGURE 3.10: Membrane tension first increases till a point where it is high enough to open up the membrane reservoirs to give a plateau region. The membrane supplied to the tether maintains a constant tension in the tether till the local reservoirs are exhausted. Once the local reservoirs are exhausted, tether force shows an exponential increase, [108]. Image is taken from the article, Raucher and Sheetz, 1999.

already existing tether. A 10–15 μm long tether was first allowed to attain an equilibrium tether force and then pulled by 40 μm length, with a constant speed. The pulling was done for the well spread cells with average cell spreading area of 1800 μm^2 and cell on circular adhesive island of area 314 μm^2. We used two different speeds, for each of the cell spreading areas, to elongate the membrane tether and the force curves as a function of tether length are as shown in fig. 3.11. We observed that the tether force, for both cell area, first increases and then remains constant for a pulling speed of 0.6 $\mu m/sec$. At a pulling speed 10 times higher two types of force curves can be seen in

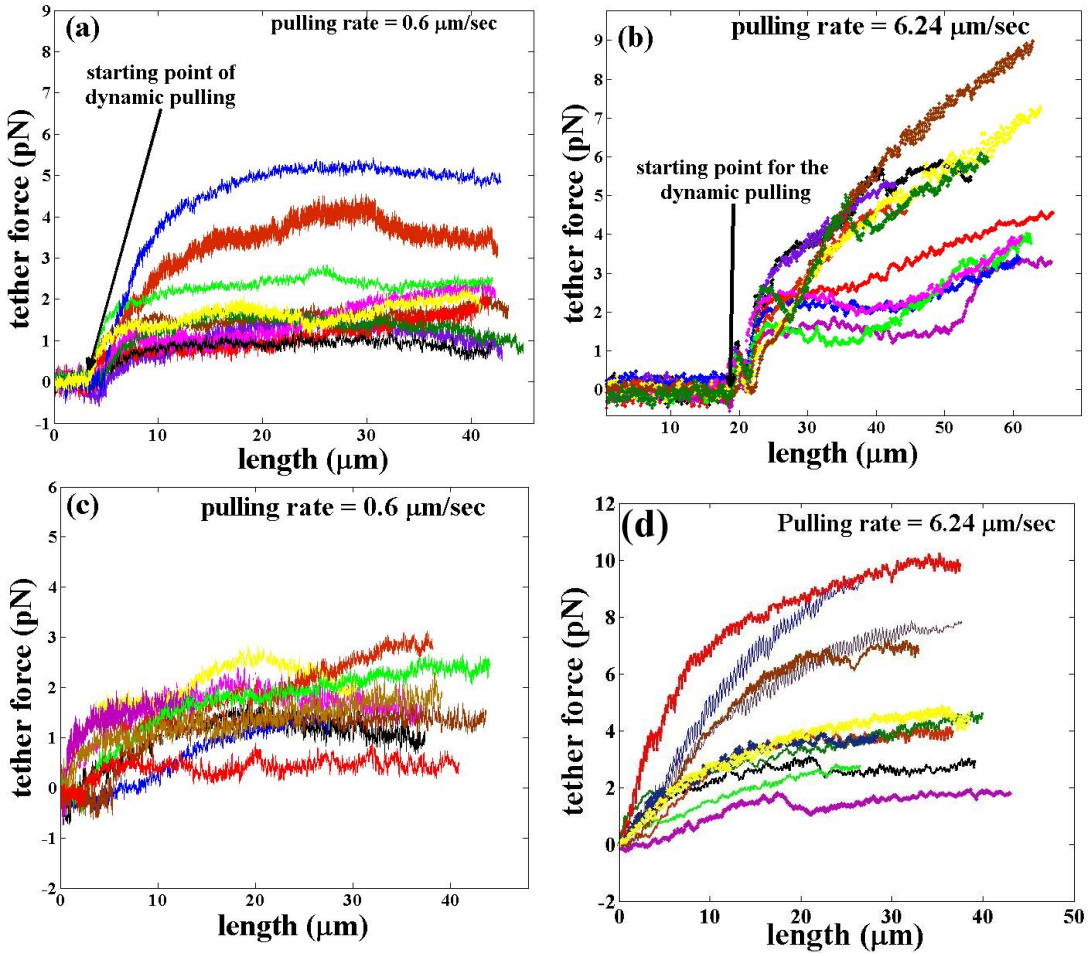

FIGURE 3.11: Force response to dynamic pulling at constant rate. The two speeds used to pull tether from the cell membrane were 0.6 $\mu m/sec$ and 6 $\mu m/sec$. (a) & (b) show the dynamics of tether force for the cells grown on adhesive patches of diameter 20 μm. (c) & (d) are the plots showing the tether force values as a function the length of constantly increasing tethers, for the cells grown on cover glass, without patterns. Force curves were rescaled to start from zero, by applying "$f - f_0$" on individual force curve.

fig. 3.11(b). One type show a plateau in their force curves after the linearly increasing regime followed by further linear increase. The other type showed a saturation behaviour within the studied tether length. The dynamic force in fig. 3.11(d), i.e, the well spread cells at high pulling speed were observed to attain a kind of saturation force value after an initial increase in force. The possible explanations for the dynamic force response at two different speeds for the cells with

cell spreading area 1800 μm^2 and 314 μm^2 are as follow.

It is known that a cell has a number of membrane reservoirs on its surface which are in the form of caveolae, membrane folds and protrusions. Other than these reservoirs, exocytosis is also a method which a cell deploy to regulate its membrane tension. Exocytosis rate has been reported to increase with increase in membrane tension. The reservoirs and exocytosis, together provide excess membrane to the cell for its membrane expansion during cell spreading, migration and phagocytosis [111].

For pulling rate 0.6 $\mu m/sec$, the flow of membrane from plasma membrane to the tether is very slow and therefore the cell has enough time to constantly supply the excess membrane through exocytosis or from the surface reservoirs once a threshold tension is reached. The extra membrane made available by the cell for a slow tether elongation helps in maintaining a steady dynamic force in tether as shown in fig. 3.11(a) & (c).

Tether force for dynamic pulling at speed 6 $\mu m/sec$ seemed to show a cell spreading dependency, as shown in fig. 3.11(b) & (d). There are two rates involved in the dynamic pulling of a tether: a) the rate at which the tether is being pulled, and b) the rate at which the cell can provide extra membrane to the tether. If the two rates are equal then there would not be any change in the dynamic force value, but if pulling rate is higher than the supply of membrane, there would be an increase in tether force. A cell can supply excess

membrane to the tether either by unfolding of membrane reservoirs or via exocytosis. Either one of the sources, or both of them could be responsible for the dynamic force response as a function of cell spreading. The possible explanation for the role of exocytosis and surface reservoirs is as follows.

- It is known that an increase in the membrane tension increases the exocytosis rate [18, 97]. We speculate that the dynamic pulling of the tether might induces a temporary change in the cell membrane tension which could lead to an increase in the exocytosis rate. A difference of nearly 5 pN in membrane tension was observed between cells with spreading area 314 μm^2 and 1800 μm^2, as mentioned in the previous section. This would lead to a difference in exocytosis rate also. Suppose we have two cells, one with spreading area 314 μm^2 and the other with area 1800 μm^2. If τ_1 and τ_2 are the exocytosis rates associated with cell, having spread area as 314 μm^2 and 1800 μm^2 respectively. Then according to the earlier reports, $\tau_1 < \tau_2$. If the dynamic pulling increase the exocytosis rates to $\tau_1^{'}$ and $\tau_2^{'}$ for the cells with spread area as 314 μm^2 and 1800 μm^2 respectively. $\tau_1^{'}$ would still be lower rate than $\tau_2^{'}$. This implies that the exocytosis rate, in case of cells with more spreading, might become equal to the rate at which the membrane is being pulled out which would make the force saturate. In case of cells with lower spreading, the increased exocytosis rate will not be enough to compensate for the rate at which the membrane is been pulled.

The initial increase in membrane tension may correspond to the response time taken by the cell to increase the exocytosis rate.

- The presence of actin supported reservoirs i.e., folds and protrusions, on the cell surface is well documented. The actin filaments that supports these reservoirs have their + ends towards the cell membrane. An increase in membrane tension stops the binding of actin monomers to the filament at the + end but due to treadmilling the − end keeps disintegrating [111]. This leads to a collapse of the actin filament supporting the membrane reservoir. This way an increase in membrane tension may lead to the unfolding of the membrane reservoirs. A reservoir is expected to have a threshold tension to unfold [112]. The initial increase in tension, in this case would correspond to that threshold tension.The increase in membrane tension due to dynamic pulling may open up more number of such reservoirs in a well spread cell as compared to a poorly spread cell, given that the pulling rate is same for both the cells. This is because the static, and the increased tension due to dynamic pulling, both would be higher in case of a well spread cell, than in a poorly spread cell. Therefore opening up of more number of reservoirs might lead to a saturation in case of well spread cells but no saturation in case of the less spread cell.

As mentioned earlier, these possibilities require further investigations. The first possibility, i.e., a temporary increase in the membrane tension can be tested using a duel trap, which is currently

not available in our lab. As for the second possibility electron microscopy would be a way to explore the extent to which the surface reservoirs are responsible for spreading dependent tether force response, in case of dynamic pulling at high pulling rate. Other way to find, if the temporary increase in membrane tension increases the exocytosis rate or not, could be to image the moving vesicles inside the cell. The possibility of stretch activated ion channels on cell surface, can also not be ruled out.

3.5 Step pulling

According to the earlier reports, a sudden increase in tether force due to a step like increase applied to the tether length is followed by a relaxation to the tether force, that happen over a finite time [113–115]. We performed similar step pulling experiments with the 3T3 fibroblast cells. A small tether of length around 10–15 μm was first pulled from the lamellopodia of well spread cells grown on fibronectin coated glass surface. The trapped bead attached to this tether was then given subsequent pulls of 5μm each, multiple times. The force on the trapped bead was allowed to relax to a stable value between two consecutive step pulls. Similar to the earlier reported works, we also observed a sharp increase in measured force followed by a decay after each step increment in the tether length. After the decay, the tether force relaxes back to the static force value again similar to earlier reports. The one interesting thing we observed in our

experiments was the varying height of the peak force. The height of the peak force value was found to be decreasing with increasing tether length as can be seen in fig. 3.12.

In order to find the contribution form the drag force in peak height, a trapped bead, not attached to any tether, was given steps of 5 μm. The drag force was detected to be around 4 pN. The drag force was found to be dropping back to zero in nearly 20 msec as shown in fig. 3.7. In our experiments, we have moved the stage to change the relative distance between the trapped bead and the cell. The speed at which the nano stage moves for a 5 μm step was found to be around 78 $\mu m/sec$. It means the observations taken for the dynamic force response will have negligible contribution in force due to fluid viscosity. The dependency of peak height on tether length is as shown in fig. 3.14. In order to investigate the role of actin cytoskeletal in controlling the peak height, we depolymerised the actin network by exposing the cells to 0.2 μM Lat-A for more than 30 min. We found that, even after actin depolymerization, the peak height of the force curve, decreases with increasing tether length.

3.5.1 Cyclic strain

A long tether of about 25-30 μm length, was pulled from the well spread cell and tether forces were allowed to reach the steady state. The trapped bead was then made to move forward and backward along the tether length in steps of 5μm. The force was allowed to

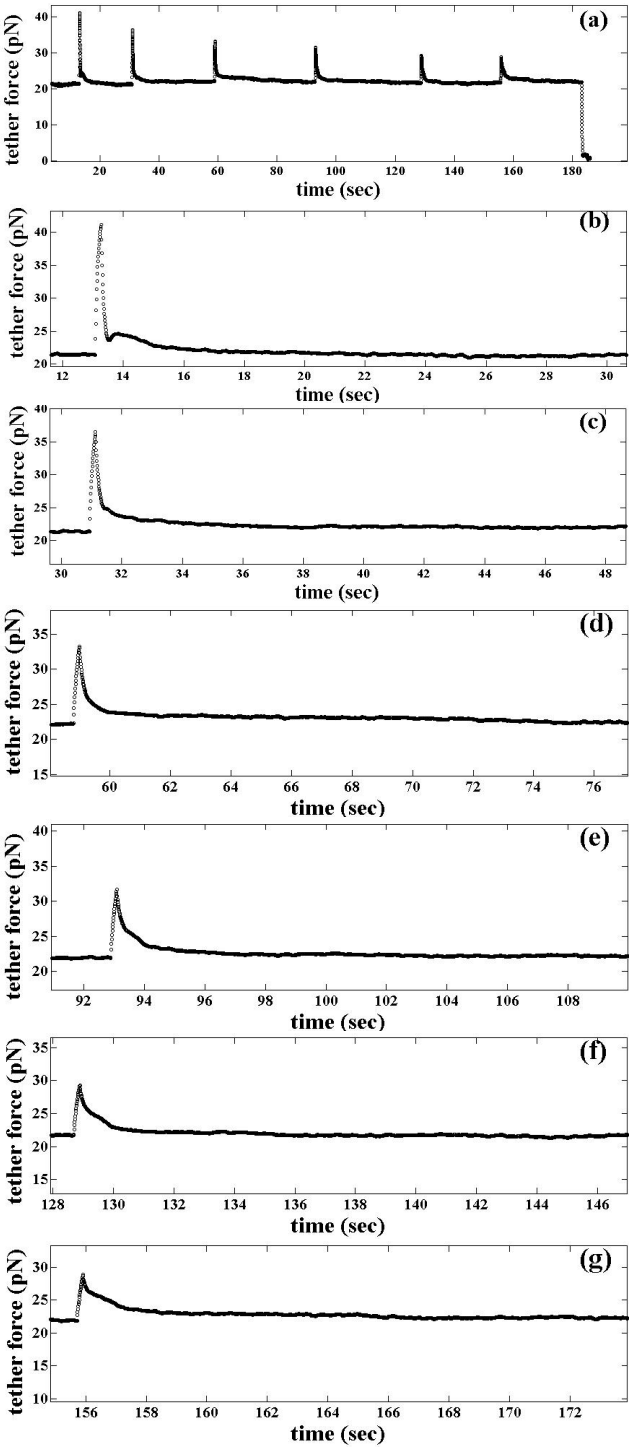

FIGURE 3.12: (a) The force relaxation curves of a membrane tether pulled multiple times in steps of 5μm. (b) to (h) are the zoomed in plots of the peaks in the same order as they appear in (a). (a) is a typical plot taken from 6 realizations giving similar trend but different static force as the force varies from cell to cell.

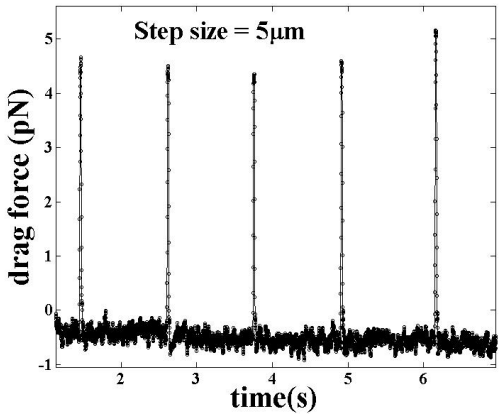

FIGURE 3.13: The force due to the sudden movement of the bead by 5 μm, was found to be around 4.5–5 pN. The force takes around 20 msec to drop down to zero force value.

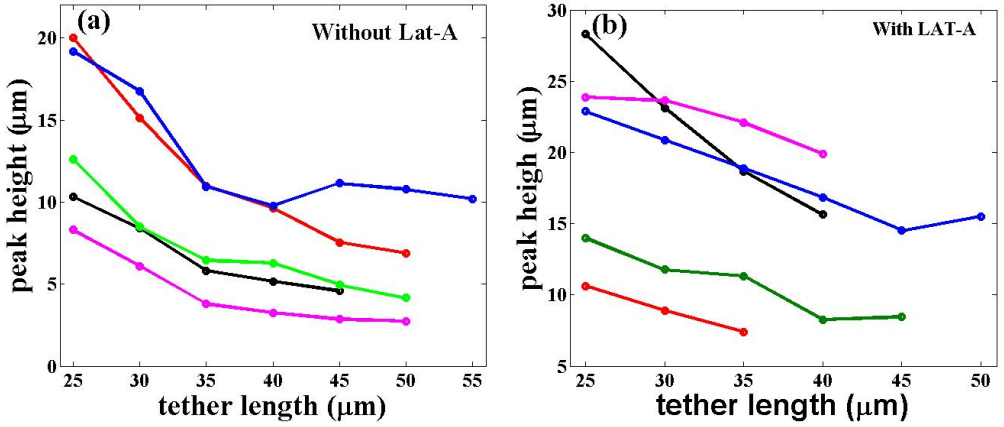

FIGURE 3.14: (a) Peak height for the multiple 5 /mum step pulls, decreases with increasing tether length. (b) The peak hight was also found to be decreasing with increasing tether length for Lat-A treated cells.

relax back or build up to a steady state value before every next step movement of the trapped bead. The result of this cyclic extension and relaxation can be seen in fig. 3.15. We observed that the force value decays down to the static value after each 5 μm step, for both forward and backward step, given repeatedly, as shown in fig. 3.15 without no sign of systematic change in peak heigh with pull number.

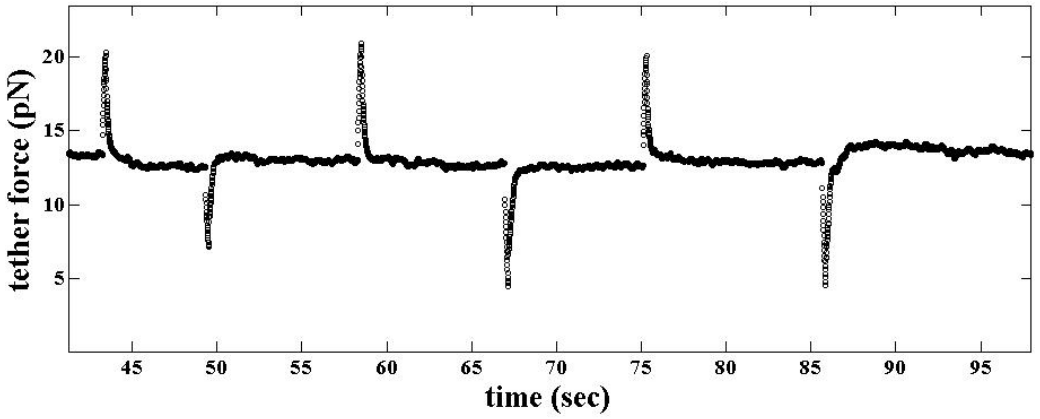

FIGURE 3.15: After pulling a tether of length 25–30 μm, we moved the bead back and forth in 5μm steps. The tether force was found to relax back to the steady state membrane tension after each cycle of pulling and retracing.

3.6 Tether retrieval

There have been extensive work done to understand the mechanism related to tether formation and pulling of a membrane tube from a bilayer, experimentally and theoretically. But the mechanisms by which the excess membrane is taken back by the cell remain poorly understood. In order to look at the force dynamics of a retracting tether we deployed the following two schemes–step retraction and continuous retraction, as discussed below

3.6.1 Step retraction

In order to explore the dynamics or building of the force in the retracting tether, the bead attached to the tether was made to move backward towards the source of the tether, along its initial length, in finite steps. The force was allowed to reach a nearly static value between two consecutive retracting steps. A long tether of 30-40μm

was first pulled from the cell. We then let the tether force relax to the static force value. Once the static force value is reached, the trapped bead attached to the tether end was allowed to move back along the tether length, towards the cell in 5 μm steps. The building up of force recorded at the trapped bead can be seen in fig 3.16. From the

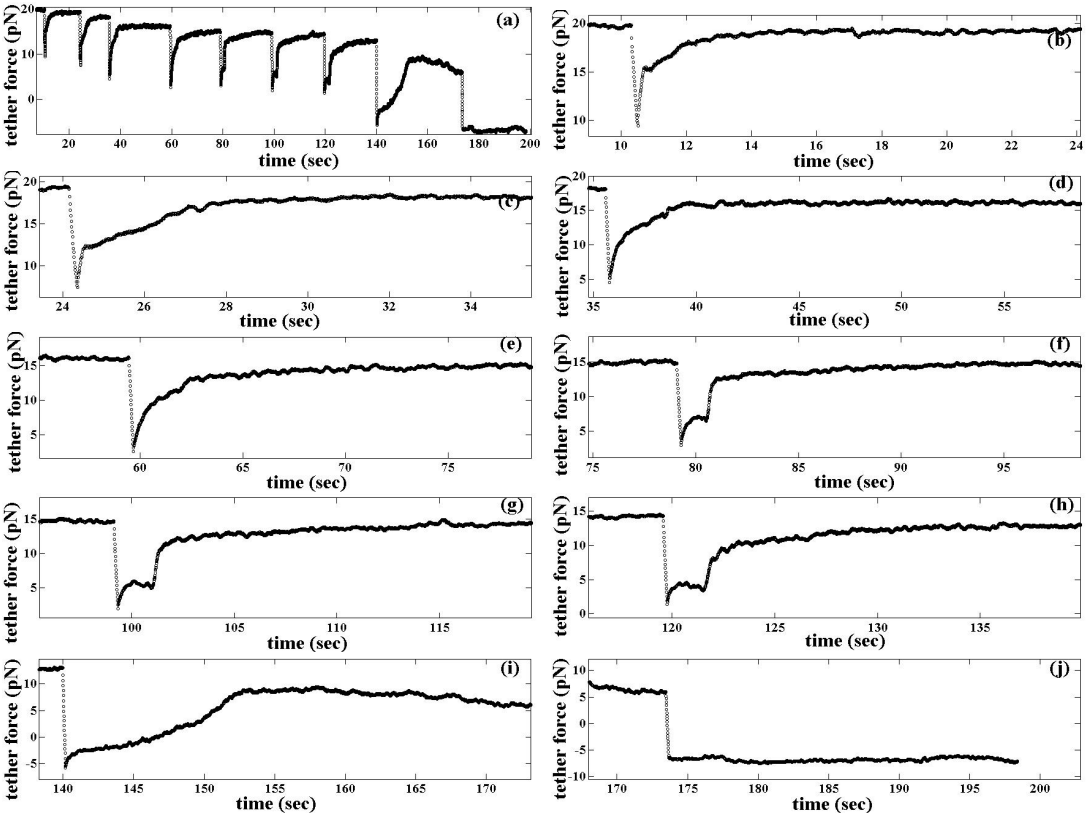

FIGURE 3.16: (a) The dynamics of a membrane tether retract in steps of 5μm. (b) to (j) are the zoomed in plots of the negative peaks in the same order as they appear in (a). (a) is a typical plot taken from 10 realizations giving similar trend but different starting force as the force varies from cell to cell.

general trend of the stepwise release of the tether, we make following conclusions.

- For the first few steps the force shows a clear, nearly monotonous increase just after the step displacement towards the cell.

- After a few steps a zone, i.e. zone 2 starts appearing in the force curve as shown in fig. 3.16 & fig. 3.17. The length of zone 2 was found to be increasing with the number of retraction step, i.e., the decreasing tether length.

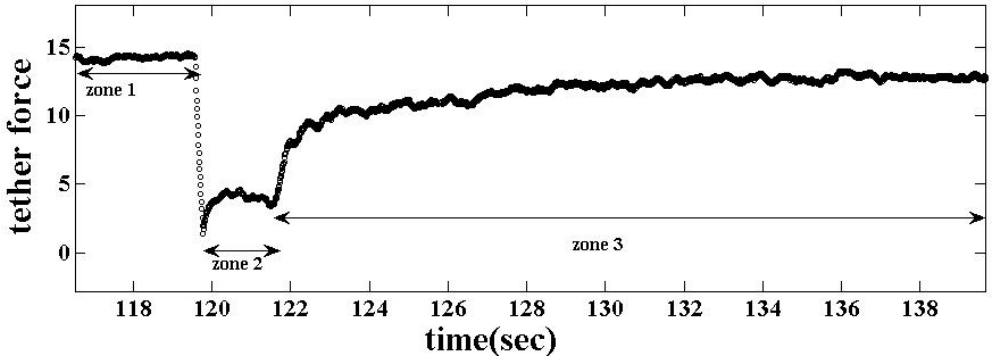

FIGURE 3.17: The force retrieval dynamics of a retracting tether when the trap is moved towards the cell in steps can be divided in three zones. Zone 1 represents the steady state tension of the tether before applying the step to the trap. Zone 2 is the duration for which the tether remains floppy, as seen in time lapse recording. Zone 3 shows how the force retrieves in the tether after the floppiness dies down.

- Together zone 2 and zone 3 showed two regimes of force retrieval in the tether retracted by the movement of the trap, towards the cell.

- After zone 3 relaxation, the force tends to stabilize at a value below the previous steady force and significantly below the equilibrium force. The force did not recover to the initial static force value for the cell during the observation time of 15-20 sec, which is much larger that the typical relaxation time seen in fig. 3.17.

Time lapse recording of the retracting tether was done to look at the changes that might be appearing in the tether geometry, as shown

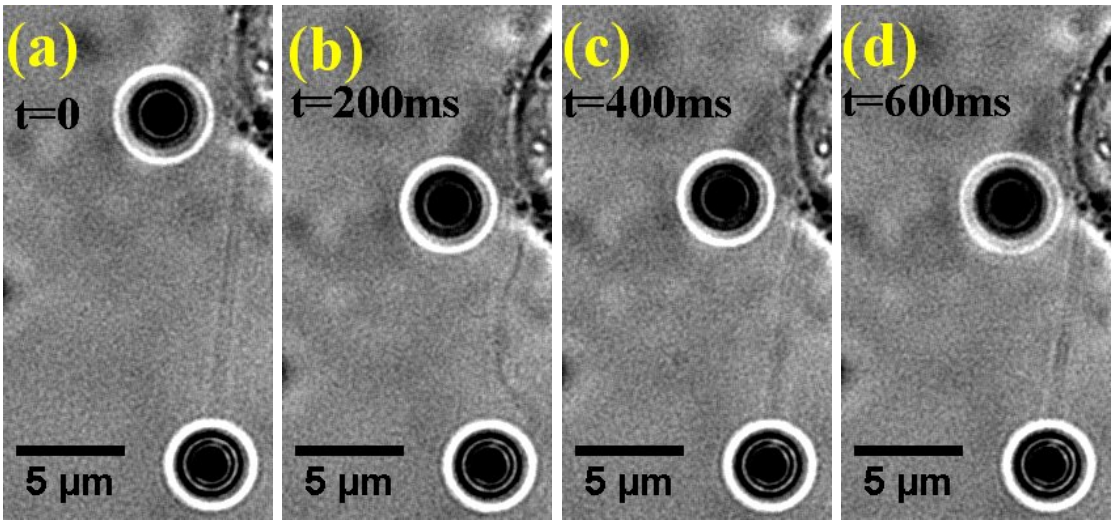

FIGURE 3.18: Time stamps taken from a time lapse recording of step tether retraction. (a) Tether with the steady state tension before the -ve step of 5μm. (b) floppy tether just after the step movement of the trap towards the cell. (c) & (d) floppiness stays for some time in the tether before the tether starts getting tensed again.

in fig. 3.18. In the time lapse recording, a very prominent floppiness was observed to be appearing in the tether as soon as the tether is moved back towards the cell as seen in fig. 3.18(b). This prominent floppiness disappeared fast in about 200 *ms* leaving little, non observable fluctuations in the tether as can be seen in fig. 3.18(c) & fig. 3.18(d). This corresponds to the first step force retrieval in the tether as seen in fig. 3.17 (c) & (d), i.e., zone 2.

The time lapse recording for these observations were done on cell treated with Lat-A for the following reason. The membrane tension of an unperturbed cell is higher than the cell without actin network. Due to a larger static force, the tether pulled from the unperturbed cell has smaller equilibrium radius as compared to the Lat-A treated cells, as per eq. 3.4. The thin tether in case of the unperturbed cells was most of the time found to be beyond the resolving power

of the microscope and could not be seen in bright field mode. As the force dynamics of the retracting tether were found to be the same, for both the unperturbed and Lat-A treated cell, as discussed in the next section. We could use the video recording done with a Lat-treated cell to see the changing configuration of the retracting tether.

3.7 Effect of actin depolymerization on retraction

Actin fibers of cell cytoskeleton were depolymerised to investigate the involvement of cytoskeleton in membrane tube retraction force dynamics. Actin depolymerization was done by incubating the cells at 37^oC with 0.2 μM for more than 30 min. Other that seeing a reduction in steady state tether force we did not observe any major qualitative change in the dynamics of tether retraction as can be seen in fig. 3.19. This indicates that the actin cytoskeleton does not play a role in the observed force dynamics of the retracting tether at a qualitative level. After the retraction of tether to a long length, cells allowed no further retraction of tether and the tether force remained close to zero. The length of this small tether for which the force remains zero, was found to be approximately the same in all the retraction experiments, as shown in fig. 3.20.

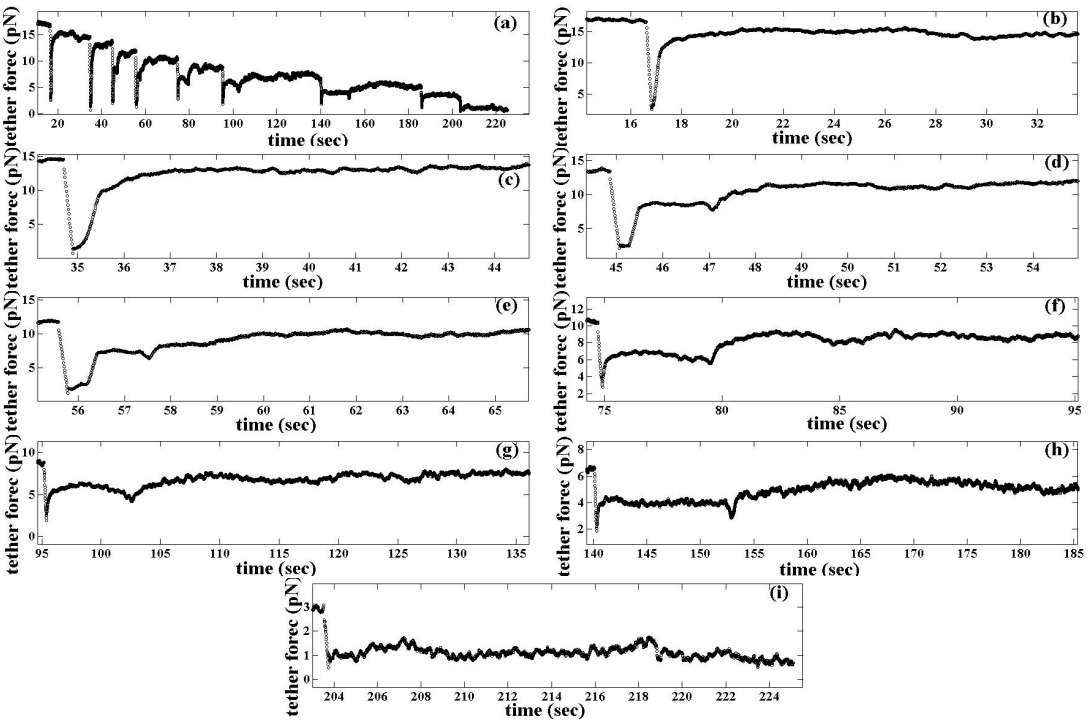

FIGURE 3.19: (a) The dynamics of a membrane tether on imposing backward steps of 5μm done on actin depolymerised cells. (b) to (i) are the zoomed in plots of the negative peaks in the same order as they appear in (a). (a) is the plot taken from 10 realizations giving similar trend but different starting force as the force varies from cell to cell.

3.7.1 Dynamic retraction

In order to look for the rate at which the cell membrane take the lipids from the tether back to the cell body we performed dynamic retraction experiments. In this experiments we had pulled a long tether from the cell body and let it relax to the steady state tension value. Once the steady state tension is reached, the trapped bead was taken back to the cell body with a constant speed of 0.2 μ/sec to get the retraction dynamics of the tether. The experiment was performed for three different initial tether length and the results are as shown in fig. 3.21. We observed a small length of tether remaining outside the cell body, which might be retracting at a time scale much

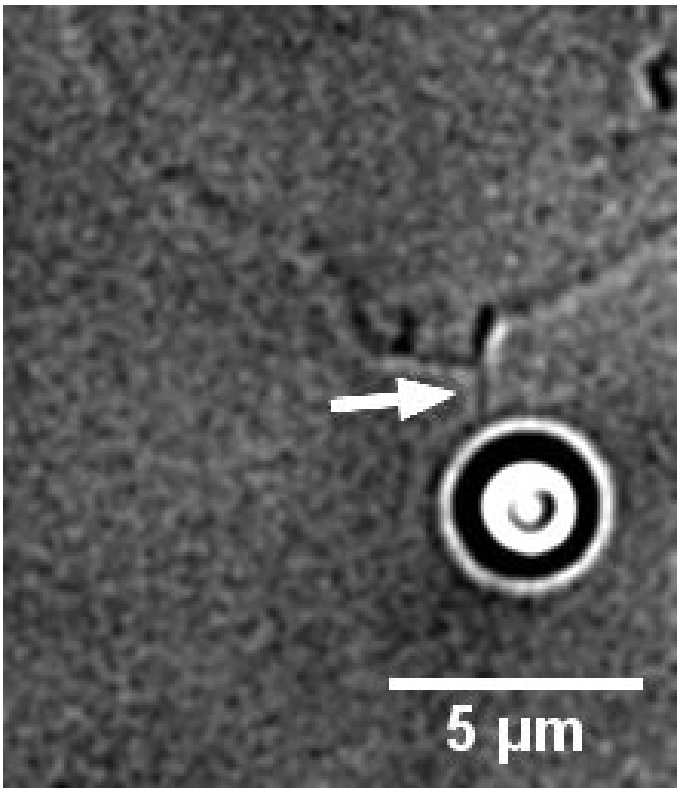

FIGURE 3.20: The length of tether that remains out and does not retract back easily into the cell membrane was found to be 10-15 μm.

larger than the time scale at which the observations were taken. This behaviour was seen for both step and continuous retraction of the tether.

3.8 Pulling multiple tethers from same cell

Raucher D. and Sheetz M.P., 1999 [108] reports that the extra membrane from the reservoirs used up in pulling tethers from one side of the cell affect the tension on the other side of the cell. In our experiments we sequentially pulled 5 tethers from different regions of the cell but did not find any change in the steady state membrane tension. For doing this experiment using the current set up with a

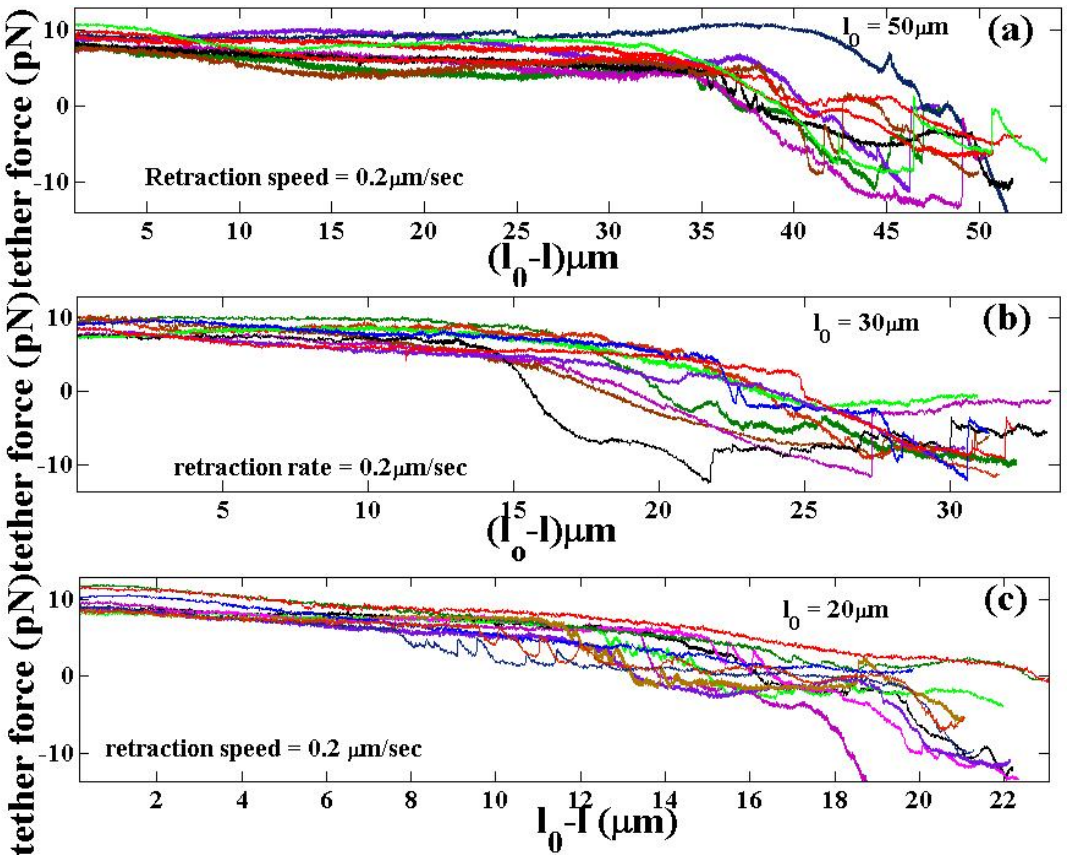

FIGURE 3.21: Tethers were retracted with speed 0.2 $\mu m/sec$, by moving the cell towards the trapped bead.The initial tether length before retraction is 50 μm, 30 μm and 20 μm in (a), (b) and (c) respectively.

single trap we pulled the tether and pinned the bead to the surface before proceeding to pull another tether. The initially pulled beads attach to the surface by non specific surface interactions. Fig. 3.22 show one such experiment where we have pulled three tethers from the same cell. We performed similar experiment with four different cells by pulling 4-5 tethers from the same cell but could not find a difference between the tension in first tether and the fifth tether.

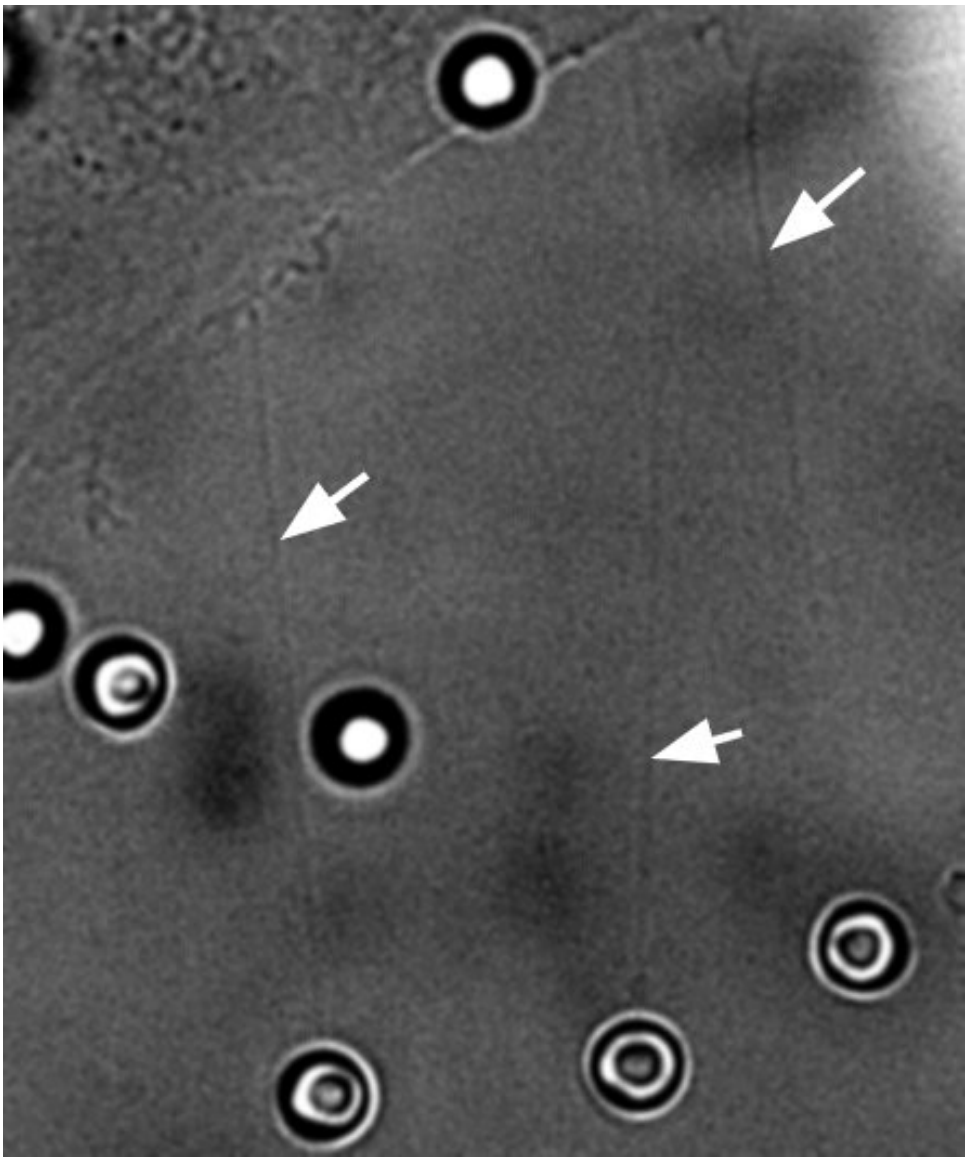

FIGURE 3.22: The beads are pined to the surface through surface interaction. The tether force is not sufficient to pull back the bead stuck on the glass surface where cell in grown.

3.9 Conclusion

This chapter includes a number of observations that to our knowledge, have never been reported earlier. There is a need for further experiments and theoretical modeling to have an insight of : a) Effect of cell spreading on static and dynamic tether force, b) dependency

of peak height on tether length for step pulling, and c) the mechanism to understand the different force relaxation regimes, in the force curve for step retraction. The summary and estimated conclusions that need testing, for the experiments discussed in previous sections, are as follow.

3.9.1 Spreading dependent static and dynamic membrane tension

The average static tether force for the cells with spreading 1800 μm^2, 1300 μm^2 and 314 μm^2 were found to be 10.7±0.3 pN, 7.8± 0.3 pN and 6.2±0.5 pN, respectively. The reason for the difference in membrane tension of cell with different spread area, could be the presence of more folds or reservoirs in a poorly spread cell than on well spread cell [116, 117]. The difference in number of surface reservoirs may cause a difference in adhesion of actin cortex to cell membrane. The difference in cortex-membrane adhesion strength might be the key factor for the observed cell spreading dependent difference in membrane tension as evident form eq. 3.5.

The dynamic tether pulling, for two different cell spreading showed similar tether force response for the slow pulling rate. The force curves showed at saturation after an initial increase in tether force. The saturation could appear if the rate at which the cell is providing membrane to the tether is equal to the rate at which the tether pulling is done. At the large pulling rates, the tether force first

increases fast, then show a slower increase for less spread cell and saturation for well spread cells. The reason for this cell spreading dependent behaviour of dynamic tether force can be explained by the involvement of either exocytosis rates or membrane reservoirs or both, as already discussed earlier in this chapter.

Inhibition of exocytosis, pulling two tethers using a duel trap to look for the temporary change in membrane tension and electron microscopy are the tools that can be used to investigate the validity of the possible mechanisms.

3.9.2 Retraction dynamics

In case of the cyclic 5 μm step movement of the trap, towards and away from the cell, we found that the force always relaxes or builds up back to the equilibrium force, f_0. The behaviour of the step pulling of a tether have been explored earlier but we could not found any experiment or theory related to the step retraction of the tether. In order to explore the dynamics of force in a retracting tether, we moved the trapped bead, attached to the tether, towards the cell in multiple steps 5 μm length. and we made the following observations.

For a tether of length about 40–50 μm, the first few retraction steps showed a very fast force build up in the tether. After a few retraction steps, the force retrieval was found to show two regimes marked as zone 2 and zone 3, as shown in fig. 3.23. Once the negative step is given to the trap to move it towards the cell the tether force drops

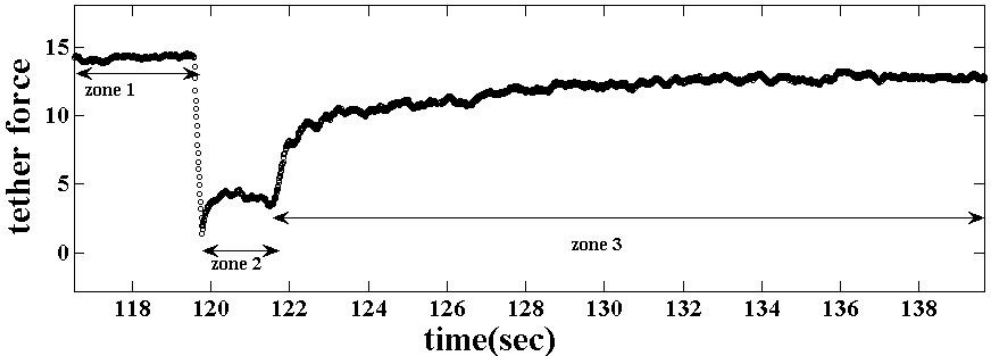

FIGURE 3.23: The force retrieval dynamics of a retracting tether when the trap is moved towards the cell in steps can be divided in three zones. Zone 1 represents the steady state tension of the tether before applying the step to the trap. Zone 2 is the duration for which the tether remains floppy, as seen in time lapse recording. Zone 3 shows how the force retrieves in the tether after the floppiness dies down.

down instantly. After the instant drop, force starts building up on the trapped bead. The force on the trapped bead due to the tether attached to it evolve in two steps, marked as zone 2 and zone 3 in fig. 3.17. Both, zone 2 and zone 3, showed that the force builds up to a steady value, but the duration for which the tether maintains this steady tension was shorter for zone 2 than zone 3. No further increase in force after zone 3, was observed over the time 15–20 sec. What happens to the tether when the bead attached to the tether is taken back to the cell was investigated by recording time lapse video of the retracting tether. We observed that as soon as the tether is taken back, a floppiness appears in the tether which remains till the end of zone 2. No floppiness was observed in the tether beyond zone 2.

The force evolution at the trapped bead due to the entropy of the floppy tether, attached to it can be explained by "Worm Like Chain

model (WLC model)" proposed by Marko and Siggia in 1995 [118]. According to this model the force due to entropy of a worm like chain is given by,

$$F = \left(\frac{K_B T}{L_p}\right)\left[\frac{1}{4(1-x/L_0)^2} - \frac{1}{4} + \frac{x}{L_0}\right] \tag{3.8}$$

Where, L_p= persistence length, x= distance between the two ends of the tether, L_0=contour length, K_B=Boltzmann constant and T= temperature.In our experiments, once the relative distance between the trapped bead and the cell is decreased, the contour length of the tether L_0 evolves as a function of time. This is because the excess membrane is being taken back by the cell (in zone 2). This happens at constant end–to–end distance. Assuming L_p= 100 μm and substituting the values for K_B and "T", the force as a function of monotonically decreasing contour length (from 35 μm–30 μm) is as shown in fig. 3.24.

From fig. 3.24, we can say that a shrinking length of the floppy tether is causing an increase in force on the trapped bead. But the shape of the force curve will depend on the functional form of $L_0(t)$, i.e., how the membrane is retrieved back to the cell. E.g., in our step retraction experiments, through time lapse recording, we observed that the decrease in contour length of the floppy tether is fast for first few milliseconds and very slow over the rest of the force retrieval. At the end of zone 2, the floppiness completely goes away and the second regime of force retrieval starts, i.e., zone 3. Force build up in zone 3 is to bring back the tether tension to an equilibrium with the

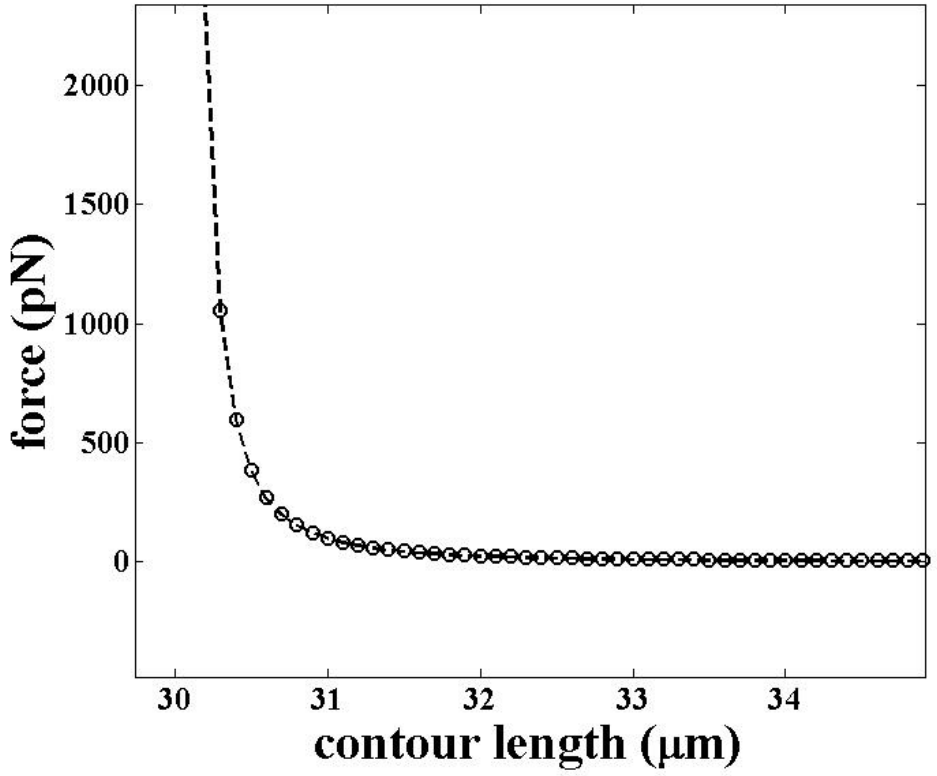

FIGURE 3.24: Force curve for a worm like chain with fixed ends, as a function of contour length. The force monotonically decreases with contour length of the floppy tether. The change in contour length of the tether is time dependent, as seen in the experiments.

cell membrane tension, just like force relaxation after tether pulling or the response seen in the first few backward steps. It might be that a gradient in membrane tension is generated in the cell membrane, locally, due to tether retraction giving a lower steady state force at the end of zone 3.

As it is observed that the retraction force dynamics remains intact after actin depolymerization, the force build up could be just due to the intrinsic properties of the plasma membrane. This can be tested by performing similar retraction experiments on lipid vesicles which is a future plan to understand tether retraction mechanism.

3.9.3 Redistribution of membrane reservoirs

Our multiple tether experiment suggests that there is no redistribution of the reservoirs as discussed in section 3.8. All the tethers pulled sequentially from the cells, detected same value of static membrane tension. The membrane given out in the form of tether is a very small fraction of the membrane available to cell in the form of reservoirs. Pulling from one side many times therefore should not give a different tension value at the other side of the cell.

Chapter 4

Design of a shearing device and its applications

Introduction

The bonding between a cell and its extracellular matrix (ECM) is what is called as cell adhesion. Cell adhesion is a non-uniform, dynamic, time and environment dependent process. It depends on the biochemical and mechanical nature of the ECM and the duration for which a cell is left to interact with the ECM. It is not uniform as the cell-ECM contact is not a direct type of contact but it is through some adhesion receptor proteins clustered on the cell surface. These adhesion receptors are called Cell Adhesion Molecules (CAMs) [119]. The cell adhesion involves anchoring of cells to the substrate through the transmembrane adhesion receptors called integrin [120]. Integrins act as both cell-ECM and cell-cell adhesion receptors and are known to play a crucial role in tumour progression,

cell migration, differentiation and development [121–124]. These adhesion units bind to the ECM proteins outside the cell and to the cell cytoskeletal through focal adhesion complexes, inside the cell [125], as shown in fig. 4.1(b).

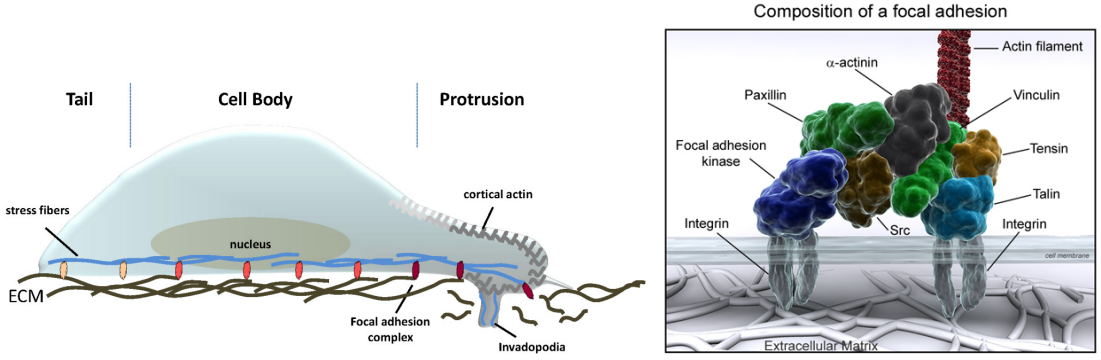

FIGURE 4.1: (a) A pictorial representation of a single cell. The contact between the cell and the ECM is not continuous and is through cell adhesion molecules (CAMs). The image is taken from [126] (b) Each unit of adhesion complex consists of a focal adhesion assembly that is connected to the cytoskeletal on one side and anchor to ECM at the other side. A typical mature focal adhesion assembly. Integrins are the plasma membrane proteins and the outermost structure of an adhered cell. Image is adopted from http://www.reading.ac.uk/cellmigration/adhesion.htm

Focal adhesions are the units that form a part of the force sensing machinery of the cell together with cell cytoskeletal [29]. Through these focal adhesion contacts, a cell tries to "feel" its surrounding and responds back through machanotransduction. As the functionality of the cell is now well known to depend on cell adhesion, it is important to have a measure of the strength of these adhesions. One way to have a measure of cell adhesion strength is to get hold of the stress value required to detach the cell. Detachment at a single cell level will give an estimate of the cell-substrate adhesion, whereas in case of the monolayers the detachment will be influenced by cell-cell adhesion

also. As cell-cell adhesion could not be quantified with the shearing device we are presenting in this chapter, we restrict ourself to the single cell detachments. As it was indicated in Chapter 1, here we aim to measure the adhesion strength of cells by using a cone and plate geometry based shearing device that we have designed in our lab. The basic designing part of the device and RPM control were done by Nidhi Pashine (Summer project student) and Chandrashekar Kuyyamudi (Visiting student program, RRI). The device is compact, easy to use and can be combined with different types of microscopy techniques (total internal reflection fluorescence (TIRF), confocal, traction force microscopy (TFM)).

Unlike a passive material, a cell under shear is able to reorganize its cytoskeleton and change the distribution of its adhesion sites to oppose the stress caused by the shear [127–131]. This happens when the applied shear is lower than the stress required to detach the cell. One of the advantage of the device that we have designed is the live recording at high magnification that can be done while the cells are under shear. This advantage can be exploited to study the cytoskeleton reorganization and focal adhesion redistribution in adherent cells due to fluid stress. This chapter includes the design of the shearing device with details of its control, detection, alignment methods involved and its applications.

4.1 Different methods to apply shear to adherent cells

Shear can be applied to an adherent cell by shearing a surface in contact with the cell surface. The surface in contact with the cell can be either a solid surface or the layer of fluid. The first two methods described in this section for applying shear to the cells, i.e., the magnetic tweezers and the shear cell, use a solid surface to be in contact with the cell. The other methods described in this section, use a moving fluid layer to apply shear to the cells. A fluid flowing between two surfaces has a parabolic velocity profile in its flow. This profile is due to the friction between the layers of fluid itself. The layer of fluid in contact with the surface has zero velocity. The velocity by which fluid is moving increases with increasing distance from the layer of fluid in contact with the surface. Depending on the flow rate, the flow can either be laminar or turbulent as can be seen in fig. 4.2. Subjecting adherent cells to the laminar fluid flow is a known method to measure the cell adhesion strength. Shear stress in a laminar flow, for the Newtonian fluids, at a point z on the surface element, parallel to the flat plat, is given by,

$$\tau(z) = \mu \frac{\delta v}{\delta z} \tag{4.1}$$

where, μ= dynamic viscosity and $\frac{\delta v}{\delta z}$= velocity gradient along z direction. Shear can also be used as a tool to study cytoskeletal reorganization under shear at low shear stress. There are many tools that

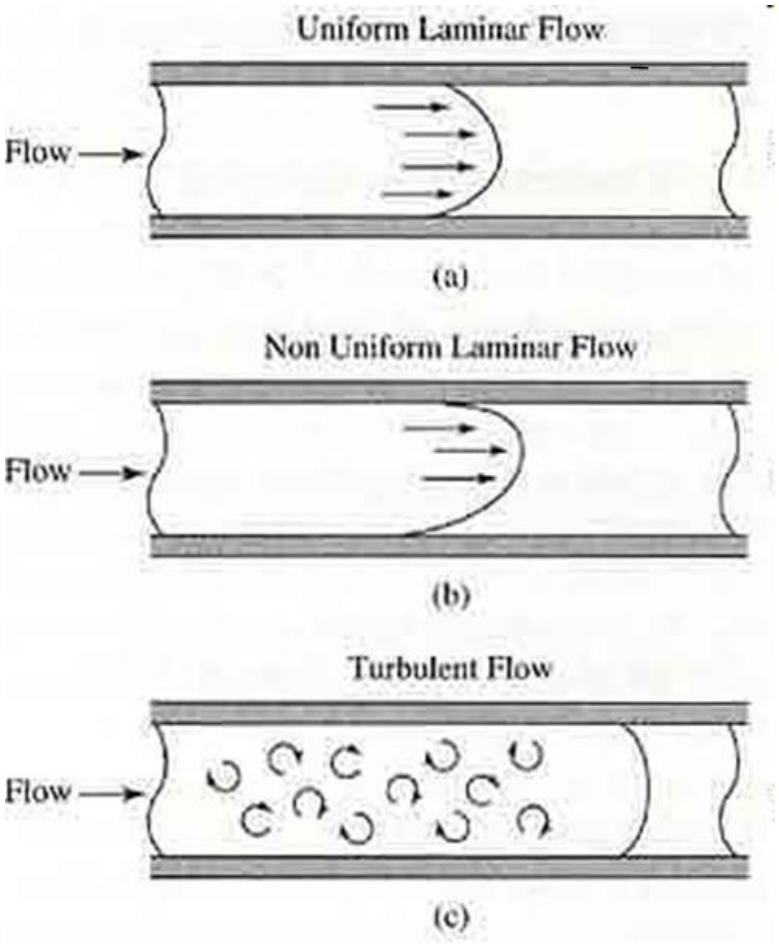

FIGURE 4.2: The arrows show the direction in which different layers moves in different flow conditions.

have been deployed so far to apply shear stress on adherent cells. For example, magnetic tweezers, cell monolayer rheometer, flow chambers, and parallel plate or cone plate rheometer. Each of these have certain advantages and disadvantage as discussed below.

4.1.1 Magnetic tweezers

Magnetic tweezers is a well established technique to apply shear to the adherent cells to measure the mechanical properties of cell

cytoskeleton [132]. In this method, a micro-magnetic bead is either injected inside the cell or attached to the cell membrane and then moved with the help of external magnetic field to apply shear. Schematic of a magnetic tweezers is shown in fig. 4.3.

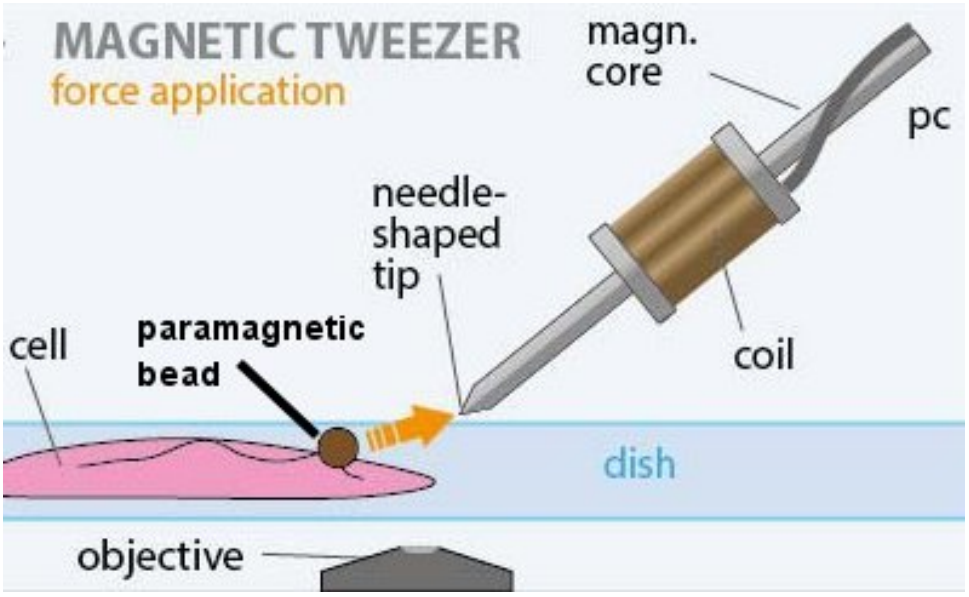

FIGURE 4.3: The magnetic bead attached to the cell surface, is moved using the external magnetic field. The bead movement is then recorded using various imaging techniques to get the mechanical properties of cell cytoskeleton. Image courtesy http://www.cellmechanics.de/Methods/Methods.html

A magnetic tweezer is generally used to know the effects of a local shear on the inside organization of the cell. Giving the viscoelastic properties of a small region in a cell is both advantage and disadvantage of this method of applying shear. This tool can only be used for the measurements at single cell level, and it can not be used as cell detachment assay to measure cellular adhesion strength or to study the dynamics of a monolayer of cells under shear. The rest of the methods that we are going to discuss in this chapter are useful for the studies in cell monolayers as well.

4.1.2 Cell Monolayer Rheology

In this method, a monolayer of cells is held between the two glass plates and the cell rheology measurements are done using a commercially available rheometer [133], (fig. 4.4). This device is capable of

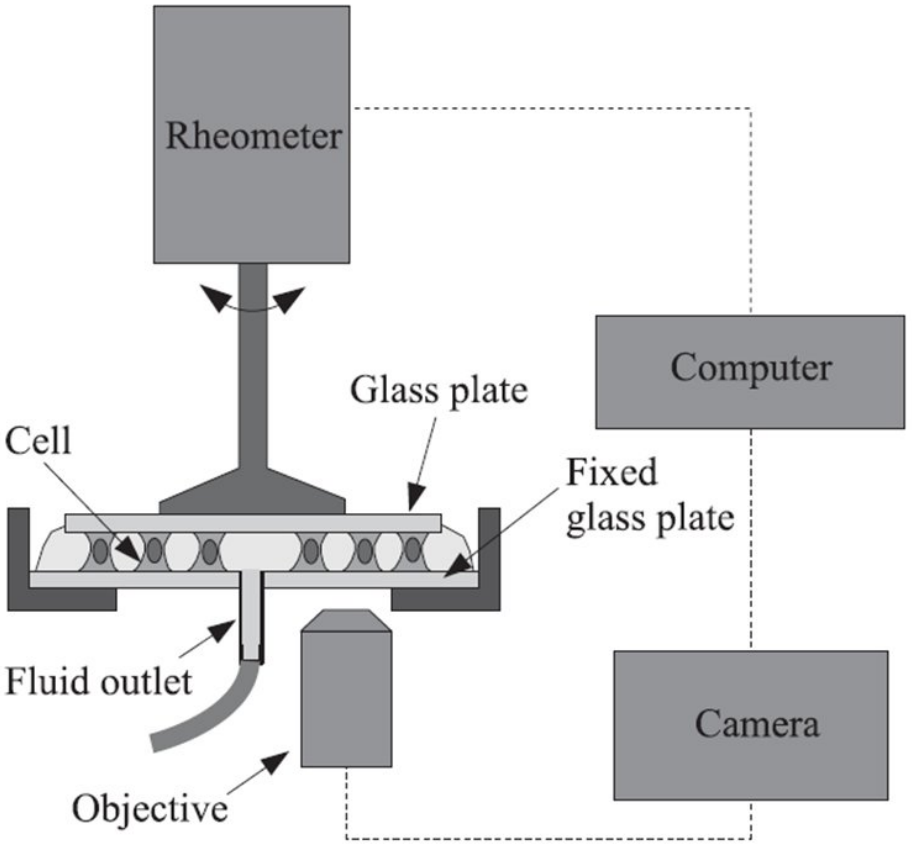

FIGURE 4.4: A monolayer of cells is held between two glass plates. The top plate is rotated using a commercially available rheometer to apply a constant or cyclic shear stress or strain to get the mechanical properties of the cell cytoskeleton. Image courtesy Fernández et. al., 2007 [133].

applying a constant or cyclic shear stress or strain to measure the viscoelastic properties of the cell cytoskeleton. This method does not give a freedom to easily combine the device with microscopy techniques such as confocal, total internal reflection or high resolution

microscopy due to its size and the method of detection (the bulky rheometer).

4.1.3 Flow chambers

It consists of a chamber with an inlet and an outlet for the flow of cell culture medium. It generally consists of two parallel plates with some spacer in between. There are many ways of making a flow chamber, lithography is one of them. Cells are cultured inside the chamber and the cell culture medium is flown through a channel to apply fluid shear, as shown in fig. 4.5.

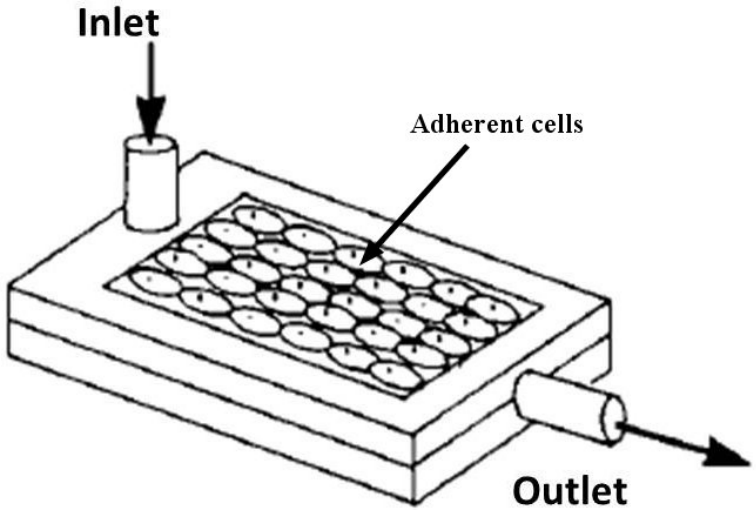

FIGURE 4.5: In a flow chamber, fluid is made to flow through a narrow channel to apply shear. The shear stress acting on the cell is nearly equal to the wall shear stress in this case. Image is adopted from Blackman et al., 2000 [134].

Due to small thickness of a cell, the shear stress experienced by the cell due to moving fluid is taken as the wall shear stress, which can be derived using the Navier-Stokes equations and continuity equation

[135], and is given by

$$\tau = \frac{6Q\mu}{wh^2} \tag{4.2}$$

where, Q=flow rate, μ= dynamic viscosity, w=chamber width and h=chamber height. This method of subjecting cells to fluid shear involves a continuous directional flow of fluid through the channel where cells are grown. Though the device is compact, low cost, easy to handle and can be used with different type of microscopy, it requires a huge amount of medium if the shear is to be applied for hours. One way to reduce the wastage of medium is to circulate it in a loop between a reservoir and the channel. This solution for avoiding wastage of cell culture medium requires an addition machinery like a water pump, to be deployed with the flow chamber.

4.1.4 Shear using a rotating fluid

Growing cells on a flat plate and making the fluid layer rotate over them is another method to apply fluid shear to the adherent cells. It involves two surfaces with fluid in between. One of the surfaces with cells on it, is fixed and another surface is made to rotate to create shear in the fluid layer. Depending on the shape of the rotating surface there can be three rotating shearing devices as shown in fig. 4.6

The cup and bob geometry, as shown in fig. 4.6(a), often requires a huge amount of the fluid to apply shear on the cells grown on the surface of the cup. Other than the wastage of large amount of

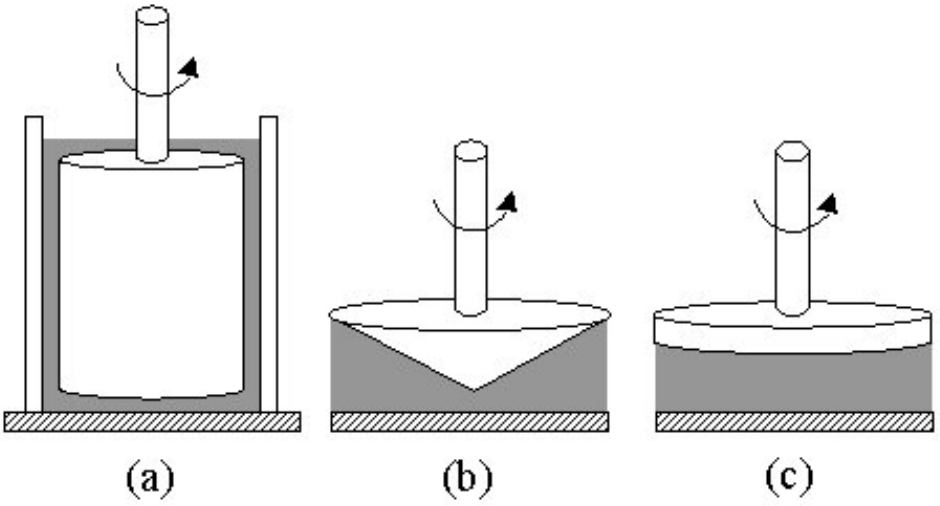

FIGURE 4.6: Depending on the set up either the surface on the top of the cells rotates or the plate with the cells rotate to make the thin layer of fluid rotate to apply a fluid shear on the cells. The advantage of the device in (a), (b) and (c), is in the less quantity of fluid it requires to apply a shear on the cell. The three devices can also be combined with different microscopes. As per the terminology (a) is called cup and bob, (b) is called cone-plate and (c) is called parallel plate viscometer.

expansive drugs, huge mass and large inertia are also the drawbacks of this geometry. Parallel plate and cone plate are the modifications to the cup and bob rheometer as shown in fig. 4.6 (b) and (c), to reduce the amount of fluid required, weight and inertia.

A parallel plate viscometer consists of two parallel flat surfaces with either one or both the surfaces rotating with a small amount of liquid between the plates. The equation that relates the rheometer's geometry, angular velocity and shear rate is given by

$$\tau = \frac{3\omega\mu}{4h}r \tag{4.3}$$

where ω=angular velocity, μ=dynamic viscosity, h=gap between the plates and r= radial distance from the centre of the plate. The

parallel plate geometry generates a fluid shear at the surface which depends on the radial distance. Fluid shear is less near the centre as compared to the periphery. This takes away the freedom to choose an observation point which is independent of radial distance. This is a big disadvantage in the case of single cell imaging as not all the cells in a culture are good and each observation might need different position with respect to the centre. To overcome the issue of position dependent shear stress the geometry of the top plate is modified to a cone.

The cone plate geometry requires minimum amount of the fluid among all other methods to apply fluid shear and hence a wastage of expensive drugs can be avoided. The cells grown on the bottom plate are subjected to fluid shear by rotating the cone which shears the fluid layers between the cone and the plate. The shear stress on

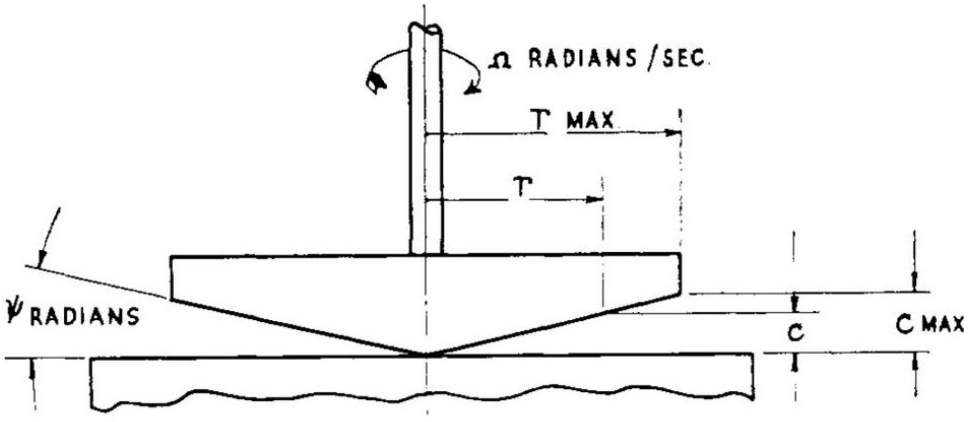

FIGURE 4.7: The cone plate design used to apply fluid shear on adherent cells (adopted from [136]).

the plate, in cone plate viscometer for a gap "c" between the cone

apex and the flat plate (see fig. 4.7) is given by,

$$\tau = \mu\omega \frac{r}{c + r\psi}, \tag{4.4}$$

where, τ=shear stress at plate (dyn/cm^2); μ=dynamic viscosity; ω=rotational speed (rad/sec); c=gap between cone apex and plate (cm); r= radial coordinates of the point of observation; and ψ=cone angle (degree). For a very small gap, shear stress is given by,

$$\tau = \frac{\mu\omega}{\psi}. \tag{4.5}$$

As stated in Mckennell Raynold, 1956 [137] in his comparison of cone-plate viscometer with coaxial viscometer, a cone plate viscometer can give a uniform shear stress with $\psi = 0.3^o$ and a gap of 50μm. It also says that $\psi = 6^o$ gives only 0.35% error from the uniform shear rate. The advantages a cone plate geometry gives in a shearing device are as follows: a) Uniform shear everywhere gives us the freedom to use large field of view objective for cell detachment experiment as all the cells are subjected to the same shear stress. b) For single cell imaging, in case of transfected cells, it gives the liberty to look for the cell showing best fluorescence without worrying about the distance from the centre and therefore position dependent shear stress.

4.2 Design of the Shearing Device

We chose a hard disk motor to rotate the cone of our cone-plate cell shear as it give smooth rotations with no detectable wobble, over a

broad range of RPM. It is also light weight and small in size which helps in keeping the entire set up light weight and therefore does not overload the microscope stage. The shearing device mounted on microscope can be seen in the Fig. 4.8. As the shear stress is same at all points on the plate under the cone, we could use the motorized stage for multipoint imaging at different positions, owing to the light weight of the shearing device. The main part of the device consists

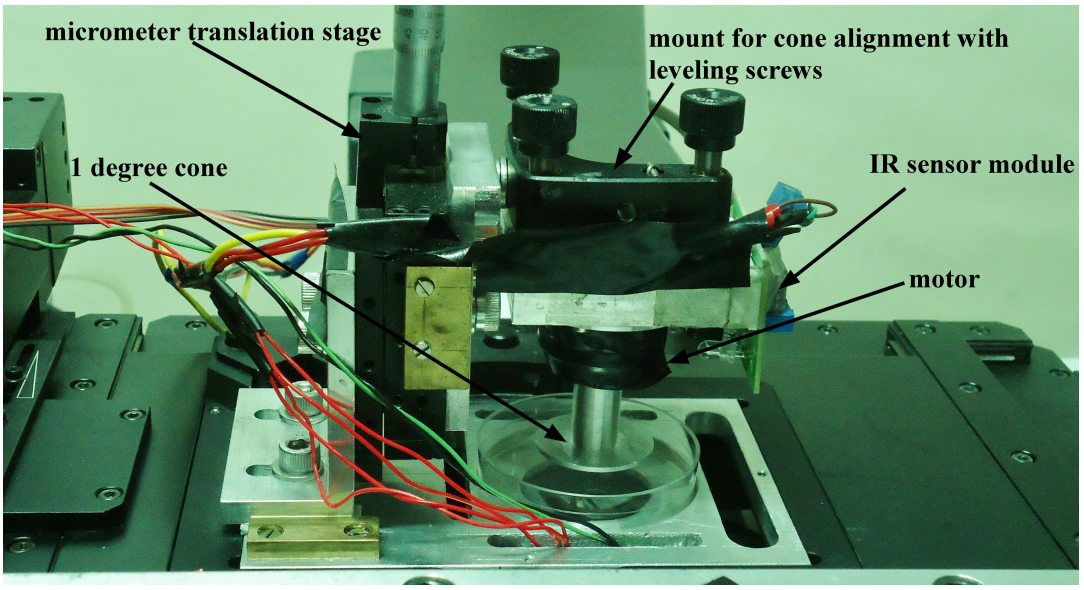

FIGURE 4.8: The shear device, designed in the lab to apply fluid shear on the adhered cells. The device is sitting on a motorized stage of a Axio Observer Z1 microscope. Imaging is done in fluorescence mode.

of the following components.

- A hard disk motor to rotate the cone.
- z-direction micrometer translation stage (PT1, Thorlabs).
- Alignment screws at the top of the cone (lens mount, KS1, Thorlabs).
- Electronic Speed Controller (ESC), 2 Amp rating.

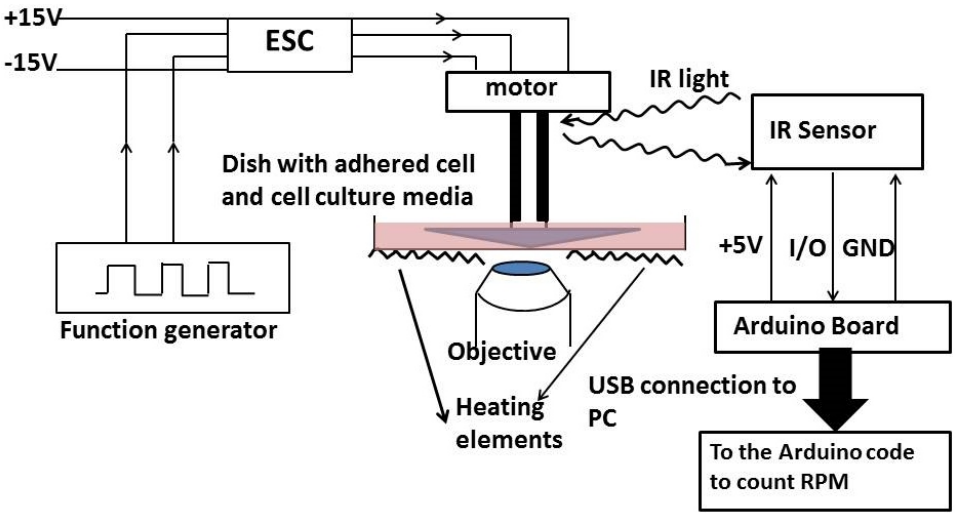

FIGURE 4.9: RPM of the motor is controlled by the electronic speed controller which gets pulse width modulated signals from the function generator. RPM of motor depends on the duty cycle of the pulse from the function generator. As for detection, the shiny metal part of the rod attached to the cone reflects the IR light at every rotation it makes. IR sensor generates electric pulse from this reflected IR light and pass it on to the Arduino board, which counts these pulses and gives RPM value with the help of a small code written in Arduino.

- A function generator.
- An inverted microscope.

The details on temperature control, RPM counting, cone alignment and the procedure followed to perform the experiments are given in the concerned sections and summarized in the schematic shown in fig. 4.9.

A 1° home-made cone was used to have a laminar flow between the plate and the cone. Pulse Width Modulation (PWM) signals were supplied to ESC with the help of a function generator, to drive the hard disk motor. The change in duty cycle of the pulse given to ESC was used to change the RPM of the motor. The plot showing dependency of RPM on duty cycle for a given load using a 15 Volt

power supply to 2 Amp ESC is as shown in Fig. 4.10. A hard disk motor is a Brushless DC motor with four terminals, but ESCs are with three output terminals. To connect the motor to ESC, the resistance between pairs of terminals of the motor was measured. The one with lowest resistance was left unconnected and rest three were connected to ESC output terminals. In general it is said that an ESC of any current rating higher that the motor's current rating works fine, but with our shearing device we observed that the ESC should be of comparable current rating. ESC of higher current rating was observed to have problems in feeding signals to the motor, which led to in between stopping and different duty cycle for the minimum RPM the motor could run at. We used function generator to feed

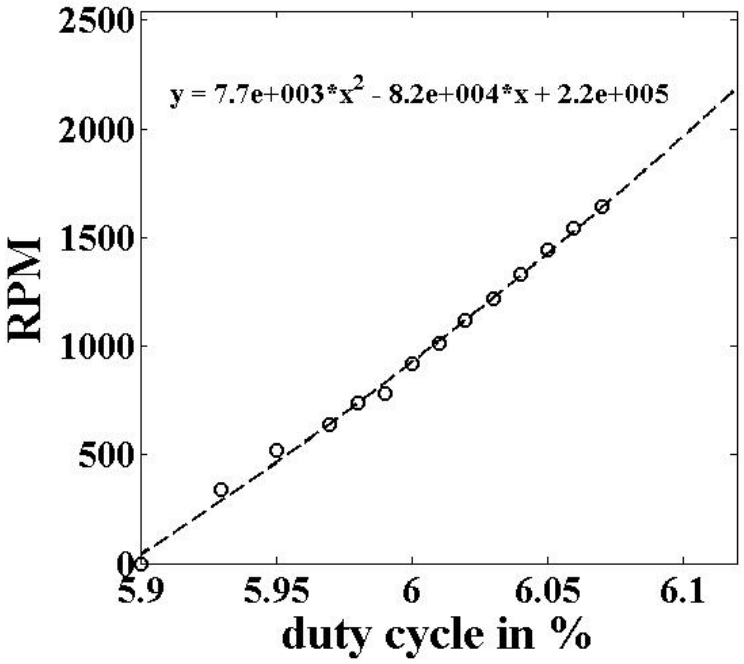

FIGURE 4.10: Calibration curve showing how RPM changes with changing duty cycle of the pulse from function generator. For a given duty cycle value, RPM value fluctuations were found to be ±10.

PWM signals of varying duty cycle to ESC.

4.2.1 RPM counting

To have a measure of the RPM value for the rotating cone, IR sensing module in combination with an Arduino board was used. The aluminium rod, connecting the cone and the motor was painted black with an unpainted slot on the rod as shown in Fig. 4.11.

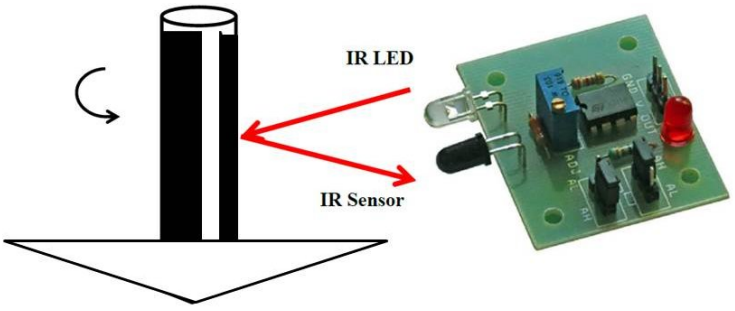

FIGURE 4.11: A commercially available IR sensor unit (Elementz Engineers Guild Pvt Ltd), was used to detect the number of rotations in a minute. Every time the cone make a rotation IR light gets reflected from the not-painted aluminium surface to give a signal to the chip which passes it to the Arduino board. The image of the IR sensor unit is taken from http://www.amazon.in.

The light reflected from the not-painted part of the rod was detected and converted into a pulse by the sensor. The electric output from the module is fed as the analog input to the Arduino board. A small code, written in Arduino software (Appendix B), makes an increment to the counter every time the analog input voltage makes a transition from low voltage to high voltage. The number of such transitions per minute gives the RPM of the shearing device. The RPM of the motor in the range 100 to 3000 can be detected using this method. Beyond this, the frequency of IR reflection goes very high and the module gives unreliable RPM values.

4.2.2 Temperature control

To control the temperature on microscope stage, thermofoil ribbon heaters (Minco ribbon heaters) were attached to the bottom aluminium plate of the shear device. Two such heaters each with resistance 17 Ω, connected in parallel were sandwiched between an aluminium foil and the bottom surface of the device. The temperature of the heaters was controlled by connecting the heaters to a temperature controller (Minco CT325 miniature DC temperature controller) in a circuit as shown in Fig. 4.12. A platinum resistor with resistance

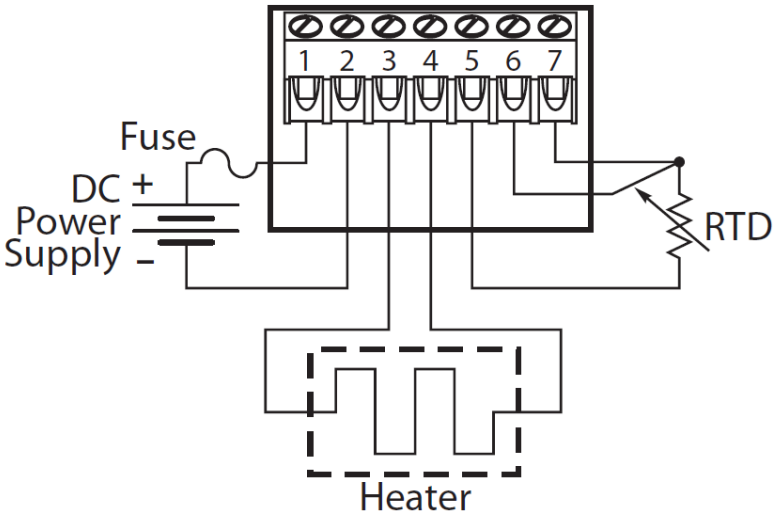

FIGURE 4.12: A 100 Ω platinum temperature detector was stuck to the bottom side of the device, close to the heating elements, to serve as temperature feedback.

of 100 Ω at 0^oC, was used as a sensor. The temperature controller compares the temperature of the platinum sensor stuck to the bottom plate of the shear device and the set temperature, to act like a switch. The current supply to the heater is stopped by the controller

if the sensor gets heated to the temperature equal to the set temperature. As soon as the sensor senses a temperature lower than the set temperature, current supply and therefore heating is restored. Temperature was controlled at $37^oC \pm 1^oC$ for the experiments.

4.2.3 Cone alignment

The alignment of the cone axis perpendicular to the tissue culture dish is very crucial as any tilt in the axis would cause different fluid shear at different point. In order to make the rotating axis of the cone perpendicular to the surface of the cell culture, a motorized stage of Axio Observer Z1 microscope along with Axio Vision software, was used. Alignment was done by focusing at the cone surface and the dish surface at four points which are equidistant from the cone centre. The steps we adopted to align the cone with respect to the plate are as following.

- Prepare a dish with fluorescent markers on it. In our case we took the labelled nucleus of the cell as the surface marker.
- Keep the dish in the slot made for it in the shearing device.
- Select four equidistant points on the dish, using the Mark and Find option of the microscope, and record their focus. The difference in the focus of the two opposite points will give a measure of the tilt in the dish, along that axis. Once the tilt is the plate is known, the same tilt should be introduce in the

axis of the cone to keep the cone axis perpendicular to the plate as shown in the fig. 4.13. To tilt the cone axis follow the next steps.

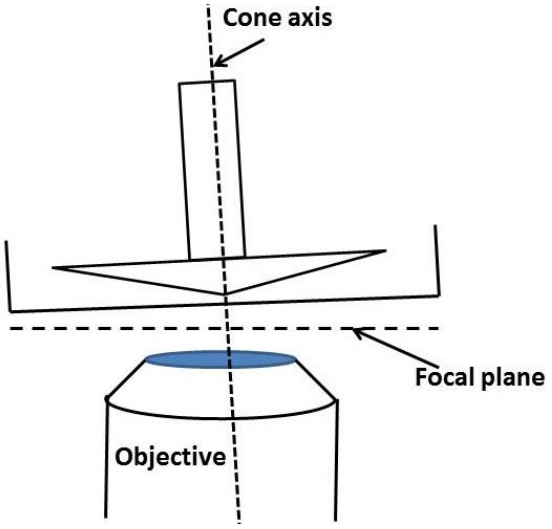

FIGURE 4.13: The first step in the aligning the cone is to find the tilt a plate with cells would have with respect to the objective focal plane, when it is inserted in the device. Once this tilt is known the cone can be tilted by the same amount in such a way the cone axis is perpendicular to the plate with cells.

- Remove the dish from the device and lower down the cone.
- As the cone surface was noticed to give fluorescence under UV illumination, we used UV light to visualize the cone surface in order to tilt the cone axis to make it perpendicular to the dish.
- Mark four equidistant points from the centre of the cone and make note of their focal distance. Tilt the cone using the alignment screws to make the cone axis perpendicular to the bottom plate.

Three separate tissue culture dishes were used to get an estimate of the tilt in the bottom plate, with respect to the focal plane.

4.2.4 Experimental protocol

The following steps were adopted to perform the experiments with the shear device.

- Switch on the heating unit at least half an hour before starting the experiment.
- Switch on the function generator and send pulses to the ESC as per the specification mentioned in the previous section.
- Set the duty cycle to 5.5% and switch on the power supply to feed 15 V to ESC. The motor will make rotations only if the duty cycle is more than 5.5%.
- Compile the arduino code, written to count the IR pulses from the IR sensing unit and open serial port to monitor the RPM value as shown in fig. 4.14.
- Take the cone down to get focused with the 40x objective and align the cone, as mentioned in the previous section. As the tilt in the bottom plate is fixed, only last two steps of cone alignment section should be followed.
- Once the cone is aligned, take the cone up and place the dish under the cone and bring back the cone down again.
- Cell nucleus was labelled by Hoechst33342 to use as the marker. The cone was lowered down to a point where it starts deforming the nucleus. The deforming of the nucleus was monitored

FIGURE 4.14: Screen shot of the code written in arduino software. The arrows show, from where to compile the code and open the serial port.

through the eye piece. The images of nucleus in non-deformed and deformed conditions are shown in fig. 4.15.

- When the cone tip compresses the nucleus, take the cone up by 20μm and increase the duty cycle of the pulse, from the function generator to start rotations in the cone.

4.3 Applications of the shearing device

In our lab, we have used the shearing device for mainly four purposes: 1) as detachment assay to measure the adhesion strength of 3T3

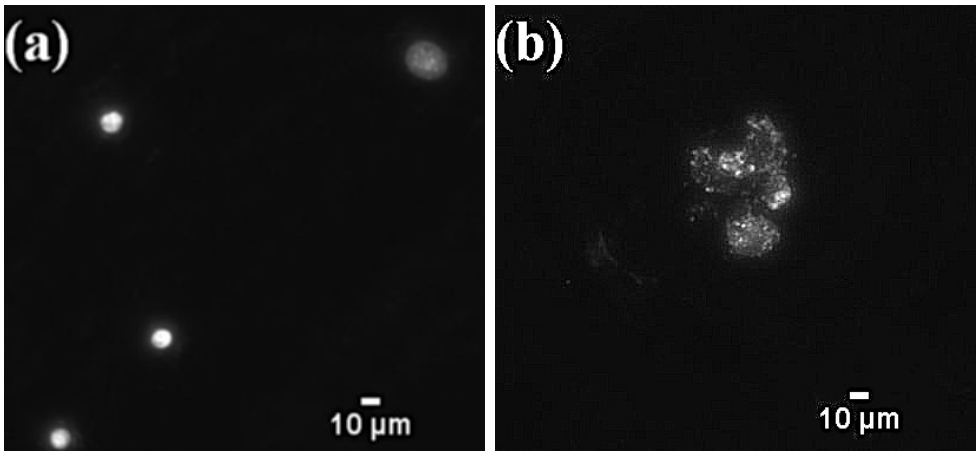

FIGURE 4.15: The cone was lowered down to touch the surface of the plate. Once the cone centre touches the plate surface the cell under the cone will get deformed. The stained nucleus indicates that the cone tip and the plate are in contact. (a) and (b) show the nucleus in the intact and deformed state respectively.

fibroblast cells and human embryonic kidney cells (HEKs), 2) to look at the change in adhesion strength of 3T3 fibroblasts under surface and drug treatment, 3) to study the mode of detachments of fibroblast cells under shear and 4) to study the shear induced shape changes in cells grown on triangular shape patterns. The discussion for the detailed experiment results that involved these applications of the shear device is as follows.

4.3.1 Cell detachment assays

The adhesion strength of a cell can be estimated by measuring the force required to completely detach the cell from the surface. Cells were cultured on fibronectin coated plastic surfaces for the detachment assays. The density of the cells was so chosen that there wouldn't be any cell to cell contact to avoid cell-cell adhesion in

the measurements. The experiments were performed with two cell lines, 3T3 fibroblasts and HEK293T. The average spread areas of a fibroblast and HEK cells growing on a plastic surface are around 1800 μm^2 and 1000 μm^2, respectively. Two types of experiments were performed to look at cell detachment dynamics: 1) cell detachment as a function of increasing shear stress, and 2) cell detachment as a function of time at a constant shear stress. The detachment curves for these two modes of experiments are as shown in fig. 4.16. Similar types of detachments curves have also been reported earlier

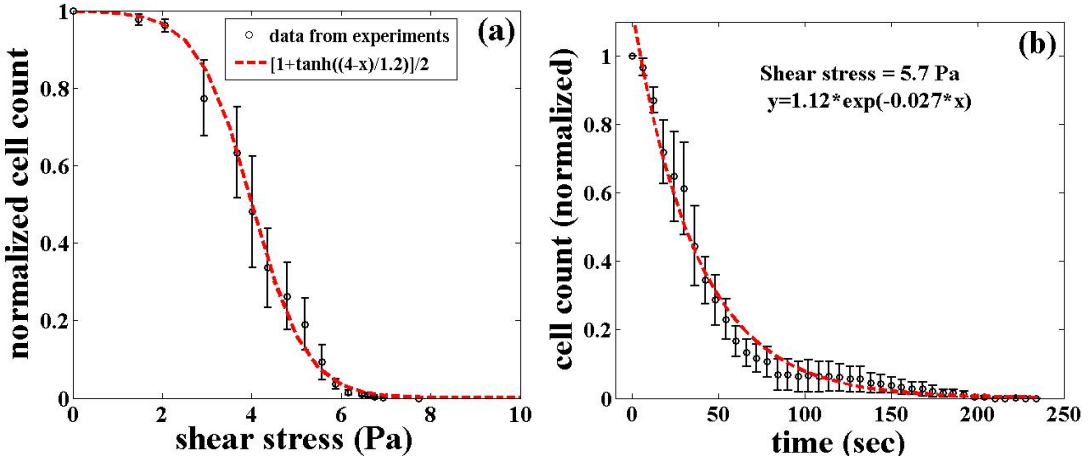

FIGURE 4.16: (a) Cell detachment dynamics for a varying shear stress. The time for which a particular shear stress was maintained in varying shear stress experiment was 1 min. (b) Cell detachment at a constant shear stress. The curves shown in both (a) and (b) represent an average detachment trend, taken over 4 independent runs. The starting number of cell count, taken for both, varying shear and constant shear mode experiments, was around 100. Error bars in the plot are ± standard deviation (SD).

in various experiments [138–140]. For cell detachment as a function of shear stress the detachment curve follows the following equation which shows a sigmoidal behaviour.

$$y = \frac{1}{2}\left[1 + tanh(\frac{a-x}{b})\right], \tag{4.6}$$

where, a= approximate mid point of the sigmoidal curve, which is around 4 for 3T3 fibroblasts, and b is the decay factor with value 1.2. The cell detachment as a function of increasing shear clearly shows a plateau where cells do not detach as the shear stress is less than the threshold stress required to detach the cells. We tried to fit an exponential to the data for detachment as a function of time but found that the detachment curve does not fit because of its non exponential tail. Even a double exponentials could not explain 3T3 detachment as a function of time.

We further explored the detachment dynamics of HEK293T with two approaches—detachment as a function of shear and at constant shear. HEK292T cells are known to have an average spread area much less than the fibroblast cells, as can also be seen from fig. 4.19. The detachment curves for the HEK293T cells as a function of shear stress and time are shown in fig. 4.17. The detach-

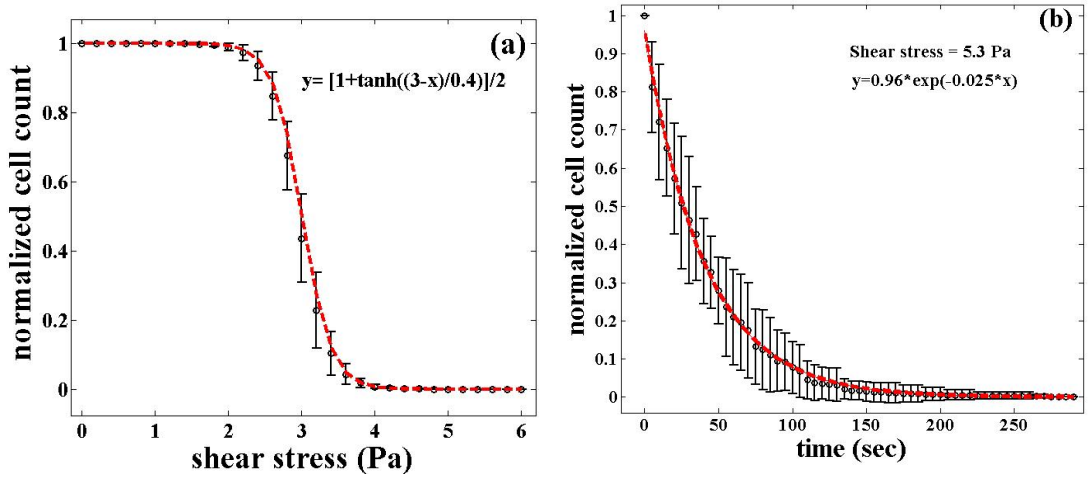

FIGURE 4.17: (a) Detachment of HEK cells as a function of increasing shear stress. (b) Detachment as a function of time for HEK cells at a constant shear stress of 5.4 Pa. Error bars here represent $\pm SD$

ment curves as a function of shear (fig. 4.17(a)) and as a function of time (fig. 4.17(b)), for HEK293T cells, show a sigmoidal and good exponential behaviour, respectively. The comparison of the detachment dynamics of 3T3 fibroblast and HEK293T is shown in fig. 4.18. Following are the observations made by comparing the detachment

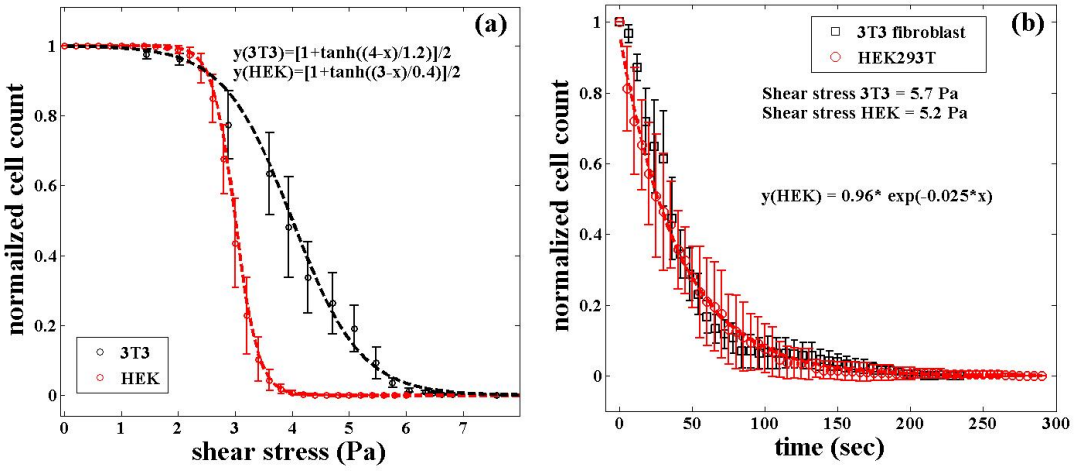

FIGURE 4.18: (a) Detachment of the HEK cells is faster than 3T3 cells as can be seen by comparing the half time and the decay constant. (b) Detachment for HEK cells gives exponentially decreasing number of cells as a function of time at a constant shear which was absent for 3T3 fibroblast cells. The constant shear stress used for the detachment as function of time is different for 3T3 and HEKs due to different half times that can be seen in (a). Error bars here represent $\pm SD$.

of 3T3 fibroblast cells and HEK293T cells.

- Detachment as a function of shear follows a sigmoidal trajectory for both 3T3 fibroblast and HEK293T. The difference is in the value of shear at the mid-point of the sigmoidal curve. For 3T3 cell it was found to be 4 Pa as compared to 3 Pa for HEK cells. The decay constant was also found to be different by a factor of 3 for the two cell lines, as seen in fig. 4.18(a). A difference of around 800 μm^2 in an average cell spreading area

between fibroblasts and HEK could be the reason for a faster detachment, in case of HEKs.

- Detachment as a function of time at a constant shear is a clear exponential for HEK cells but deviates from exponential in the tail region for the 3T3 fibroblast cells. This could be due to a very small population of enormously spread cells in case of 3T3 fibroblast cells, as can be seen in fig. 4.19(a).

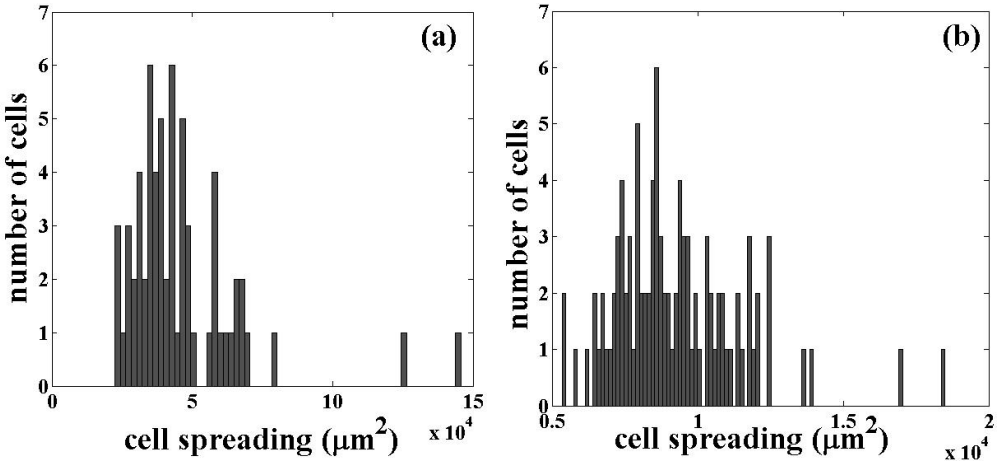

FIGURE 4.19: (a) Cell spreading area distribution plot for the fibroblast cells shows a small fraction of cells with enormously high cell spreading. (b) Distribution in cell spreading area for HEK cells. The distribution in cell size could be either due to the inherent size of the cell or due to the fact that different cells in a culture are at the different stages of the cell cycle at a given time. The total number of cells taken for the distribution is 64 for 3T3 fibroblasts and around 100 for HEKs.

4.3.2 Effect of surface and drug treatments on adhesion strength

The second application for which we have used the device is to look at the effect of surface and drug treatment on the deadhesion dynamics of the cells. For all our detachment assays we had used fibronectin

coated plastic dishes. These tissue culture dishes are treated with plasma for cell adhesion by the manufactures. The aim of the experiment here was to look for the effect of fibronectin coating on adhesion strength of the 3T3 fibroblast cells grown on these plasma-treated tissue culture dishes. Detachment as a function of time was recorded on the cells grown on tissue culture dishes with and without fibronectin coating, and the result is shown in fig. 4.20. We did not see any significant difference between the two detachment curves as shown in fig. 4.20, which may be due to the fact that the dishes used were already plasma treated for cell adhesion.

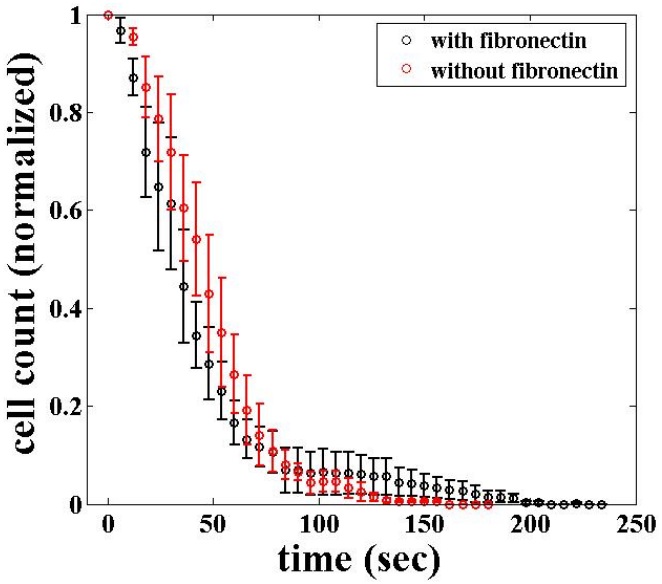

FIGURE 4.20: Detachment curves for cells grown on substrates with and without fibronectin coating. Error bars in the plot are $\pm SD$.

In order to see the effect of Myosin II inhibition on cell adhesion strength, cells were treated with 10 μM blebbistatin, for 30 min at 37 °C. The nuclear label (Hoechst33342) was used as a marker to count the number of cells to study detachment. A constant shear

stress was applied to the cells in the presence of Blebbistatin and number of remaining cells were recorded as a function of time. We

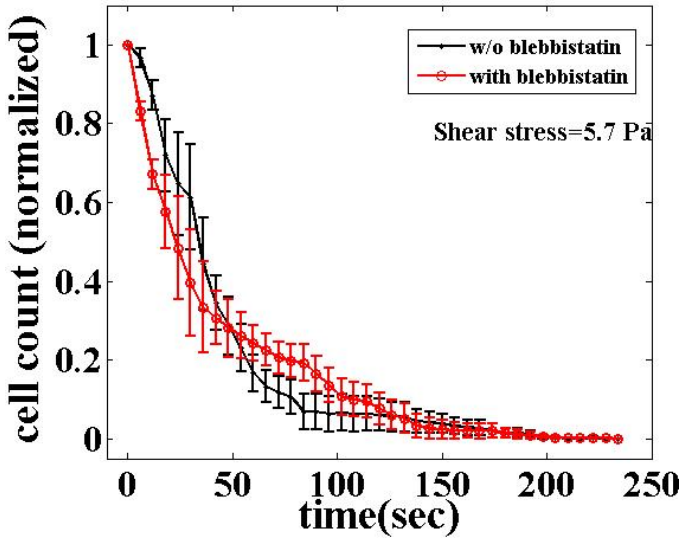

FIGURE 4.21: Compared to the cells without blebbistatin the detachment was found to be faster and slowed down later for the blebbistatin treated cell. The detachment curves are the average taken over four independent runs. $\pm SD$.

compared the cell detachment curve of blebbistatin treated cells to that of the non treated cells and found that the initial cell detachment rate of myosin inhibited cells was higher than that of the non treated cell. Later as the time increases, the detachment rate decreases and becomes lower than the non treated cells as shown in fig. 4.21. The experiments were done in the presence of ascorbic acid to avoid phototoxicity. This behaviour can be explained by tracing the movement of the nucleus of individual cell, as done in fig. 4.22 and discussed below.

The conclusions that can be drawn from the difference in detachment curves from the control experiment and the myosin II inhibition experiment using figure 4.22 are as follows. The time lapse movie of

the cell detachment for a constant shear shows that the detachment starts after some time from the time t=0 for non treated cell. That is why a plateau appear in fig. 4.16 before the cell count starts decreasing. In order to have an estimate of the fraction of cells detaching instantly over the cells detaching after some time, we used the following scheme.

Suppose we have a time lapse recording of cell detachment with 10 frames in total. We gave one color, i.e., red to the nuclei in the first frame and another color, i.e., green to the nuclei in the rest of the frames. In order to look at the movement in the nuclei before detachment, we overlapped all the frames. Fig. 4.22(a) is the image obtained after overlapping all the frames, including first frame. Therefore, if a cell does not show any change in the position of its nucleus, it will appear as a yellow spot in fig. 4.22(a) due to the overlapping red and green color. Similarly a red spot in the image resulted after overlapping will represent the cell which was present in the first frame but got detached before the recording of the second frame in the time lapse recording. We would call this instant detachment as the clean detachment from now onwards. The time duration between the two frames for the recording was around 5 second.

If the nucleus in the first frame has moved from its position in the second frame under shear, it would appear as a red spot followed by the green spot. Similarly, if the nucleus maintains its position for some time and then move before detachment, it would appear

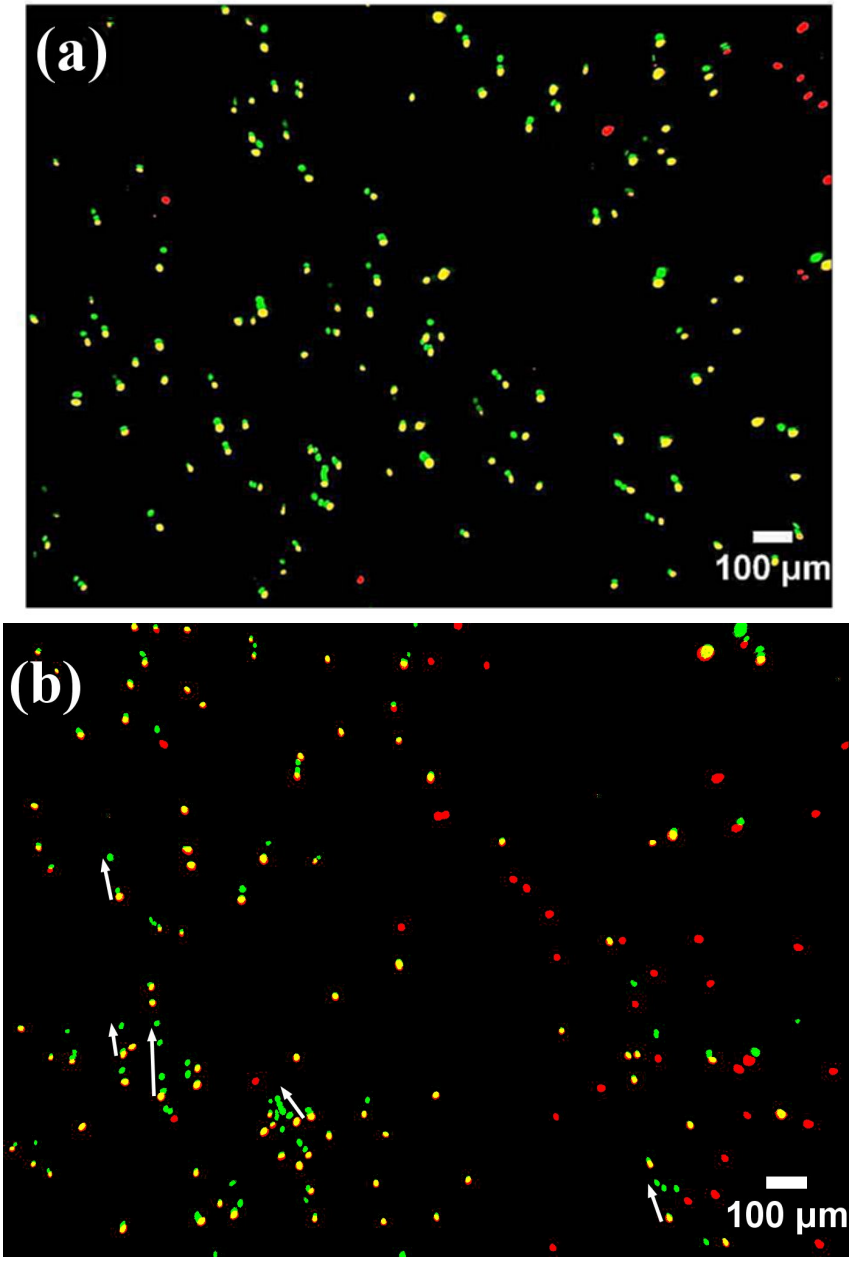

FIGURE 4.22: All the frames of the time lapse recording for cell detachment are overlapped together. The nuclei in all the frames except the first frame were made green using the look up table (LUT), of Image J. The nuclei in the first frame were given the red color. A red dot not followed by a green dot represents clean detachment. A yellow or red spot/nuclei, with a green streak represents a cell that does not detach cleanly but maintain its position for some time and is displaced along the flow before detachment. (a) In the case of cells with unperturbed acto-myosin contractility, cells showing clean detachment are very less in number as compared to the cells that maintains their position for some time, gets displaced a little bit and then detach. (b) A larger number of red spots and absence of green streaks were observed for blebbistatin treated cells. This means a larger fraction of cell detach cleanly and the distance by which the nuclei move before detachment is also larger for blebbistatin treated cells.

as a yellow spot, followed by a green spot. If the nucleus maintains its position for some time an then shows an increase in its displacement before detachment, for a few frames, it would appear as a green streak. The distance between the red or yellow nucleus and the green nucleus or the length of the green streak, represents the length for which the nucleus gets displaced in the direction of flow before detachment. Looking at fig. 4.22(b), one can say that almost all the nuclei maintain their position for some time and then get displaced by almost same length before complete detachment. The time required for the complete detachment was observed to vary from one cell to another.

Inhibition of myosin II using blebbistatin does not only dissolve mature focal adhesion [32–34] but also lowers down the membrane tension by reducing the cell contractility [141] and cell spreading area (as observed in chapter 2). The decrease in contractility after blebbistatin treatment was found to reduce the membrane tension, and increased contractility resulted in an increased membrane tension. The membrane tension measurement were done using an optical trap to quantify the dependency of membrane tension on cell contractility in the above mentioned observations by Lieber et al., 2013.

Due to an overall decrease in cell spreading, cells having weaker adhesion than required to counter balance the shear stress will detach faster than the cells without myosin II inhibition. This can also be seen in fig. 4.22(b), which shows a larger number of cells detaching cleanly as compared to the cells in fig. 4.22(a). This results in a

faster detachment rate in the beginning, as observed in fig. 4.21. The remaining cells, that have the adhesions strong enough to counter the shear stress for some time, will get stretched along the flow due to low membrane tension and hence will show a little slower detachment. as can be seen by large displacement of nuclei in fig. 4.22(b) as compared to fig. 4.22(a). What happens to a cell when it is under shear stress before its complete detachment from the surface is explored in the next subsection.

4.3.3 Cell detachment modes

In order to find out the reason for the movement of nucleus under shear, we imaged cells under shear by tagging cell cytoplasm with fluorescent dyes. Calcein AM, was used to make cells visible to understand the cell detachment modes. We found that there are three ways by which a cell can detach. a) Clean detachment: cells having adhesion strength less than the applied shear stress were found to detach cleanly, i.e., they were either at there position or not, b) Peeling from the surface (fig. 4.23(a) &(b), (c) &(d)), and c) Movement of the whole cell along the flow and then detach (fig. 4.23(e)-(f), (g)-(h)). In case of the cells with adhesion strength large enough to counter the shear stress for some time were found to be either changed in shape to different lengths before detachment or getting peeled like a sheet. Stretching and detaching mode of cell detachment have been observed previously by Irmscher et.al., in 2013 [142] in human monocytic THP-1 cells. They have explained how a cell

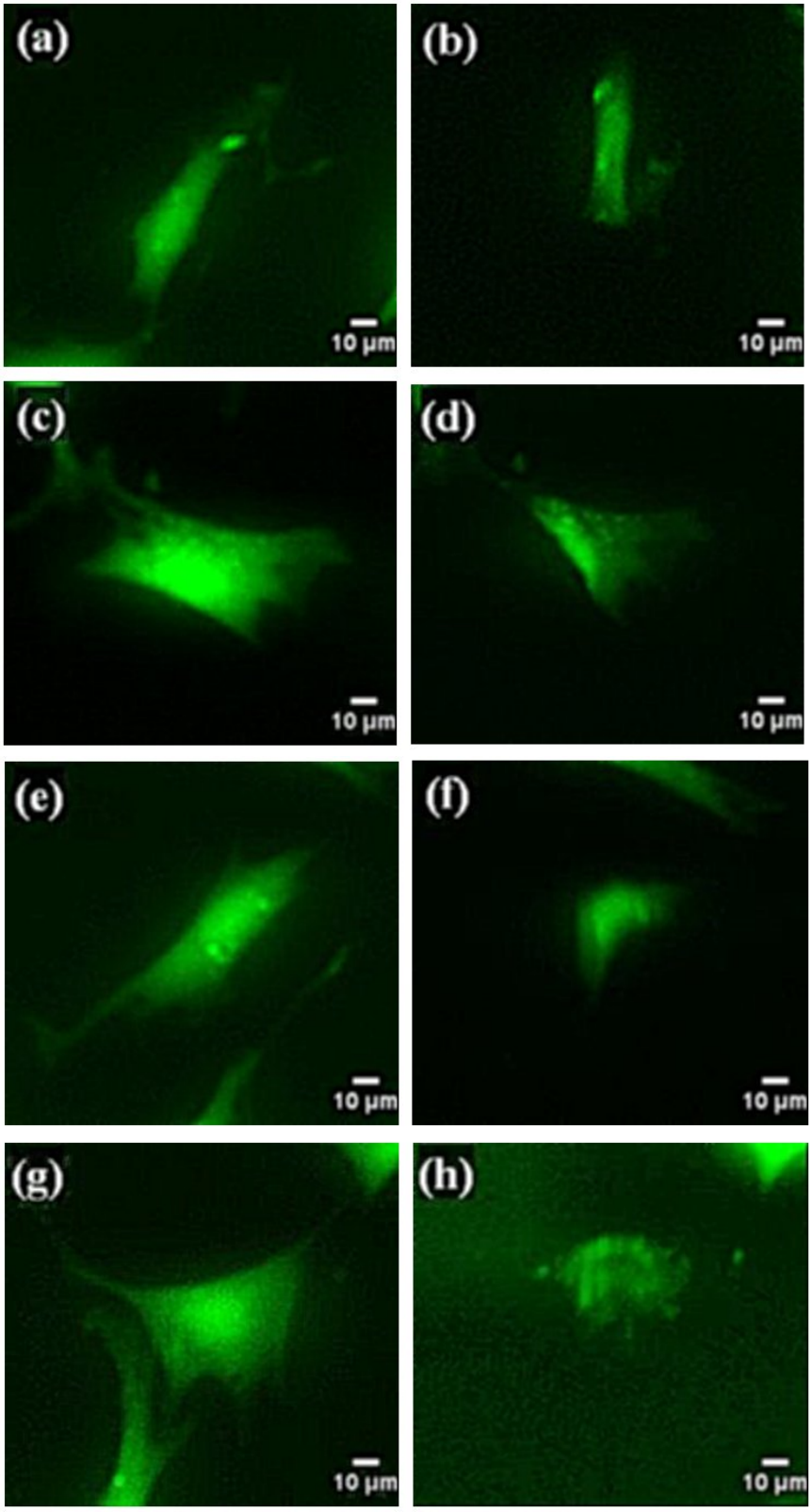

FIGURE 4.23: (a) & (b), (c) & (d) Peeling mode of cell detachment. (e) & (f), (g) & (h) cell gets dragged or moved along the flow direction before complete detachment from the surface.

gets dragged in the direction of flow with tethers left behind and how peeling of these tethers one by one makes cell detach from the surface. The peeling we have observed in our experiments is different from the one explained in the article mentioned above. In our experiments, peeling corresponds to the detachment of a few adhesion site to make some part of the cell being dragged along the flow. This dragged part stretches and applies an additional stress on the remaining adhesion sites, finally leading to complete peeling of the cell from the surface. In order to explore the possibility of a clear detachment of cells to reduce the range of time scales at which different cells detach, we used patterned substrates for the detachment assays. Triangular shape patterns were stamped on plastic surfaces, using micro-contact printing, to restrict cell spreading. The details of micro-contact printing have been explained in appendix A, section A.1. We observed that the cells remain at their positions for some time and then detach without much stretching. We could not do experiments with cells on pattern substrates to get the detachment curves due to the problem of multiple cells sitting on several of the adhesion sites thereby reducing the single cell count. This may be overcome in future by choosing smaller patterns. Cell synchronization can also be used to reduce the standard deviation in the detachment curves.

4.3.4 Modulation in cell shape below threshold shear needed for detachment

The shearing device designed here can also be used for the studies related to, cell alignment along flow, redistribution or reorganization of focal adhesions or actin stress fibers. According to the previous findings a cell under shear due to a laminar flow shows alignment [127] and strengthening of actin filaments [128], redistribution of focal adhesion and reorganization of actin cap [129]. Migration speed of the cells as well as the distribution of traction forces were also observed to get altered under fluid shear [130]. A cell under fluid shear also shows change in stiffness when observed using Atomic Force Microscopy (AFM), before and after an exposure to shear stress [131]. Cellular response under fluid shear plays a crucial role in th functionality of the endothelial cell (EC) that lines the interior surface of blood vessels, and are always under fluid shear. A change in blood flow can affect, vascular tone, remodelling, cell migration, platelet adhesion, permeability of the ECs. Change in the functionality of ECs leads to vascular diseases. Here we grow cells on micro-patterns of triangular geometry to see if our device can also be used for the studies related to cytoskeletal reorganisations. Adhesive islands of triangular shape were made using micro contact printing. We observed a reorientation and reorganization of cells when they were subjected to fluid shear stress of 1Pa as can be seen in fig. 4.24.

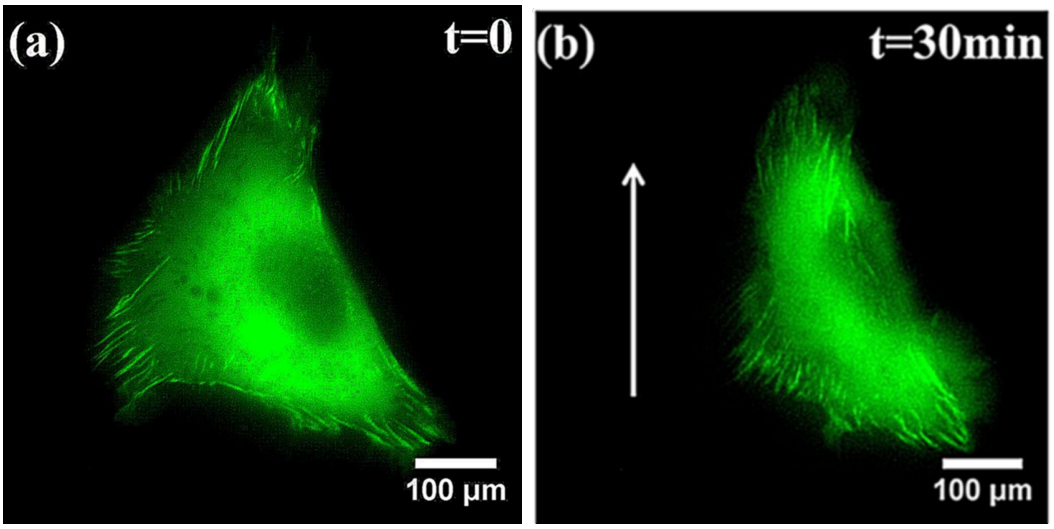

FIGURE 4.24: (a) The triangular cell grown on micropattern with labelled focal adhesions. (b) A change in cell shape and redistribution in focal adhesion was observed after 30 min of 1 Pa fluid shear stress. The direction of arrow represents the direction of flow. Cells were transfected with vinculin GFP for fluorescence microscopy.

4.4 Conclusion

We developed a compact, versatile, easy to handle and an inexpensive cell shearing device which can be used as a tool to study multicellular or single cell detachment dynamics. The device can be easily mounted on a microscope and therefore can be used in combination with different types of fluorescent microscopy techniques, e.g., confocal microscopy or total internal reflection microscopy (TIRF). The applications for which the shearing device can be used are much more than what we have listed in this chapter. For example our shearing device can be used in combination with TIRF microscopy to study focal adhesion dynamics over a range of shear stress. As a cancerous cell is know to have difference in adhesion than a non-cancerous cell,

the device can also be used as a detection method to detect cancerous cells. It can also be used to look at the shape modulation in cell/nuclear shape under the fluid shear. As a detachment assay, the shearing device gave us the following information.

- Different cell lines have different cell detachment curve and different threshold values for shear to initiate detachment.
- Can be used to detect differences in adhesion strength of different cell lines.
- The cell spreading distribution of fibroblast cells includes some enormously spread cells which gives a tail in the detachment curve as a function of time, deviating from the exponential behaviour. The HEK cells having no such issue showed an exponentially decreasing cell count as a function of time for a constant shear.

Use of micropatterns for cell detachment dynamics and synchronization of the cell cycle are two techniques that can be employed to reduce the size of the error bars observed in the detachment curves.

Inhibition of myosin II lead to a change in detachment dynamics. The detachment curves for control and myosin II inhibition showed a cross over. The cross over was due to the lower detachment threshold and decreased membrane tension after myosin II inhibition. Further, we used our shearing device to look at the redistribution of focal adhesions under fluid shear. We observed that other than reshaping

of cell the focal adhesions distribution also changes. The number of focal adhesions seemed more at the front of the cell along the direction of flow as compared to the rest of the cell outline. Together all these experiments give a number of applications the shearing device that we have designed can be used for.

4.5 Transfection Protocol

In order to study the single cell dynamics, in terms of changes in focal adhesion and actin organization cells were transfected with vinculin Venus and LifeAct RFP respectively. The tranfection was done using two equally efficient protocols, electoporation and Lipofactamine. The details of the two protocols are as follows.

4.5.1 Electroporation

- Detach the cells using 1x trypsin and pellet down the cells.
- Re-suspend the pellet in Opti-Mem medium to have 10^5 cells per ml of medium.
- Prepare a solution of 10μl of 1$\mu g/ml$ of plasmid DNA, 40 μl of Opti-MEM and 50 μl of cell suspension.
- Pass an electric pulse using Nepa gene electroporation unit, to force the DNA inside the cells.

- 100 μl Fresh Opti-MEM was added to the transfected cells immediately after the electroporation and cells were incubated at room temperature for 1 minute before being seeded onto the cell culture dish.

4.5.2 Lipofactamin transfection

This protocol is to transfect cells that have been grown overnight in medium without antibiotic, with 60-70% confluency.

- Remove the medium from the dish, add Opti-MEM and incubate the cells at 37^oC for 20 min.
- Take 100 μl Opti-MEM in two 0.5μl centrifuge tubes. Add 1μg plasmid DNA to one and 5μl of lipofactamin in the other tube, and let the solutions stand for 5 min at room temperature.
- Gently mix the contents of the two tubes in one and let the DNA-lipofectamin complex form for 15 min at room temperature.
- Add the content of the tube to the cell culture and incubate at 37^oC for 3–5 hours. Add fresh medium or change the medium completely after this incubation time.

In both the protocols, the expression was observed after 36–48 hours.

Chapter 5

Summary and Outlook

Introduction

Receiving a mechanical signal from the ECM and responding back to it, is what is known as mechanosensitivity of a cell. This thesis explores a few cellular response to the stresses received from ECM using different experimental techniques. The thesis mainly constitutes of three projects. The brief summary of the experiment, conclusions and the future directions for each project, are as follow.

5.1 Role of Actin in correlating nuclear shape and cell spreading

The influence of cell spreading on nuclear geometry was investigated through a number of experiments, in the first project, i.e., chapter II of this thesis. The earlier observations that the cell spreading

is influenced by the substrate rigidity, which in turn regulates nuclear geometry were tested first. We found a correlation between the cell spreading and the nuclear projected area and we quantified it, which was never done before. The correlation between cell and nuclear projected area was then tested for its robustness against various cytoskeletal and nuclear perturbations. We found that the coupling between the cell area and nuclear projected area remains unperturbed under these perturbations. It does not matter how a change in cell spreading is induced, nuclear geometry also changes accordingly to follow a master curve. The existence of mechanical connection responsible for the coupling of the two area mentioned above was investigated through the confocal microscopy. Actin was found to be changing its organization from cortical to bundles of stress fibres as the cell spreading increases. The stress fibres passing over the nucleus, known as perinuclear stress fibres, were observed to become more strong and well defined as the cell spreading increases. This provided a base for the hypothesis that the nuclear compression via perinuclear stress fibres in responsible for the correlated changes in cell spreading and nuclear projected area. The hypothesis was then tested with the help of theoretical estimates and our novel nuclear compression experiment. All the experiments along with the theoretical modeling provided enough strength to the nuclear compression argument to say the following: Rigidity of a substrate induces, rigidity specific spreading in a cell. A nucleus is like an elastic inclusion inside the cell. In order to spread, cell will have

to change its shape from ellipsoid or spherical to disk like. Cell develops, perinuclear stress fibres to apply compressive forces to press on the nucleus. Larger the extent by which cell wants to spread, more is the compressive force it applies on the nucleus. Though the role of a certain organization of actin in correlating the nuclear shape and cell spreading has been explored in this chapter, there are a number of interesting questions that remain unanswered. The list of such questions, are as follow.

- Why and how the actin organization gets influenced by the substrate rigidity? We had observed, through confocal microscopy, that a poorly spread cell has all its actin in the form of cortex compared to a well spread cell which has actin in the form of bundles, known as stress fibres. The cell with intermediate spreading, were found to have some actin in the form of cortex and some in the form of stress fibres. It suggests that amount of actin that changes from cortical to stress fibres, is spreading dependent. The mechanism for this dependency, needs to be explored through further experiments.

- What will happen if the cell fragments, devoid of nuclei, are made to adhere to the substrates with different rigidity? Will they also show rigidity dependent spreading?

  A cell fragment can be prepared by removing nucleus from the cell. It can by done by depolymerizing actin and centrifuging the cells adhered on a cover glass, at high RPM. Unfortunately,

we could not get a success in preparing cell fragments using this technique even after a number of attempts but the experiment can lead to a number of interesting findings.

5.2 Dynamics of step pulling and retraction of a membrane tether

This chapter can be divided into a number of sections. Each section reports a novel experiment, with a possible mechanism which can be tested through further experiments and theoretical modeling. The brief discussions of these experiments are as follow.

- The initial experiments reported in this chapter, were aim at investigating the effect of cell spreading on static and dynamic membrane tension. We observed that the static membrane tension increases with increasing cell spreading. It is known that a poorly spread cell has more number of folds and protrusions as membrane reservoirs on its surface as compared to the well spread cells. It is also known that the measurements from tether pulling experiments, give apparent membrane tension due to membrane cortex adhesion. 75% of this apparent membrane tension is from the membrane cortex adhesion [105]. Therefore, this is a possibility that the cell spreading effects membrane-cortex adhesion which in turn might result in difference in membrane tension between the poorly spread cell and well spread cell.

To investigate the dynamic force response, of an elongating tether, two pulling speeds were used on the cells grown to two different cell spreading. We found that, for both the spreading, at slow speeds, the cell is able to supply membrane to the tether to maintain a constant force in tether. In case of high speed the rate at which the cell can supply membrane to the tether was found to be lower in cells with less spreading as compared to the well spread cells. We think that for a cell with less spreading, the increase in exocytosis rate or number of reservoirs unfolding, are low as compared to the well spread cells, due to the difference in spreading dependent static membrane tension. We suggest that the dynamic tether pulling at high speed leads to a temporary increase in membrane tension, which may cause a transient increase in exocytosis rate. This temporary increase in exocytosis rate may also be cell spreading dependent. This can be tested using a dual trap, currently not available in our lab. Using a dual trap, one can observe the change in force for a tether of constant length while a second tether is being pulled.

- Set of experiments were done to explore the force response of a tether for sudden step extension and relaxation. These experiments had shown a tether length dependent peak hight for step pulling and a two step force build up for step retraction. The observations in both the case need a lot of work to be done to have an insight of the mechanism(s) involved, as both the observations were found to be independent of actin organization.

As actin depolymerization does not affect the force dynamics of the step retraction, therefore the two regimes in force build up may be due to the inherent property of the plasma membrane. This can be tested by repeating the step relaxation experiment with giant vesicles. Pulling a long tether from a giant vesicle and then retracting it in step should also show a similar behavior in the force build up. The experiments are being done in the lab currently to look at the mechanisms by which a cell takes back the extra membrane pulled out in the form of tether once the tether is released.

5.3 Design of a compact device to measure cell adhesion and cellular response to shear stress

This part of the thesis includes the design, and a few application of a compact shear device that we have developed in our lab. The shearing device is based on the principle of a cone plate viscometer. The device uses a hard disk motor to rotate the cone on the top of a flat plate. The rotating cone shears the cells attached to the plate, by rotating the layers of the fluid between the cone and the plate surface. The advantages of the device are: a) compact size, b) easy to align, operate and design, c) compatible for use with different microscopy techniques, such as, confocal, TIRF, high resolution microscopy and d) very low manufacturing cost.

The device was used for the following applications

- For comparing the adhesion strength of 3T3 fibroblasts and HEK293T cell lines.
- The effect of detachment dynamics of cell after myosin II inhibition.
- Reorganization of focal adhesion of cells grown on triangular patterns.

There are a number of studies the device can be used for, which we are including in the future directions of this project. The list is as follows.

- In the experiment reported in this chapter, we had just looked at the effect of myosin II inhibition on cell deadhesion dynamics. The shearing device can be used for a number of such studies to investigate the effect of various surface treatments or drug treatments on cell adhesion strength. Investigating the role of different adhesion proteins could also be possible using siRNA knockdown.
- It can be used to study the reorganization and turn over of focal adhesions, under fluid shear. To do such experiments, the shearing device should be combined with TIRF microscopy.
- Coating PDMS with fluorescent beads on the bottom plated can help in traction force related studies, under fluid shear.
- One of the most important use of the shearing devise could be in the field of cancer detection. As it is known that the adhesion,

migration and stiffness of the cancerous cells are different than a healthy cell. Applying fluid shear stress could help in telling if a cell is cancerous or healthy.

Appendix A

Making adhesive islands

A.1 Micropatterning

It is been seen that controlling cell spreading by changing the substrate stiffness or by using micropatterns gives similar effects on cell lineage specification. Therefore, we chose to control cell spreading using micropatterns rather than using gels of different rigidity. We used optical tweezer to do the measurements on cell membrane. Use of gel could interfere with this procedure and that is one more reason for not using gels to change cell spreading. Other than the above two reasons, a culture on any substrate gives a distribution of cell spreading and therefore it becomes necessary to take sufficiently large number of observations to get correct statistical measures. The use of micropatterns helps as all the cells are of almost identical shape and size. A description of the method to prepare stamps with patterns and imprinting them on glass is as follows.

A.1.1 Stamp preparation

In order to get circular adhesive islands of different sizes on glass to control cell spreading we used Polydimethylsiloxane (PDMS) stamps. These stamps were prepared using silicon wafers manufactured at The Centre for Nano Science and Engineering, IISc, Bangalore. A chrome mask was designed in-house and fabricated by Bonda Technology, Singapore. To prepare the silicon wafer, lithography with Deep Reactive-Ion Etching (DRIE) was used. For photolithography, a negative photoresist was spin coated on silicon wafer and patterned by a photomask (custom made) and UV light. The wafer is then baked, developed and cleaned before DRIE. The si-wafers were etched to the depth of 20 μm, using DRIE. After DRIE, the photoresist was removed from the wafer using a suitable solvent. The wafer with permanent micro-patterns on it is called master, which was used to prepare PDMS stamps. The pictorial presentation is given in fig. A.1. The steps involved in preparing stamps and then microcontact printing are as follows.

- Treat the silicon wafer with hydrophobic silane in a desiccator for 10 min to make the wafer hydrophobic. For this treatment, take few drops of trichlorodimethyl silane in a small vial, and keep the vial with the wafer in a plastic dish of 100 mm diameter (for the reason given later), inside the desiccator. The

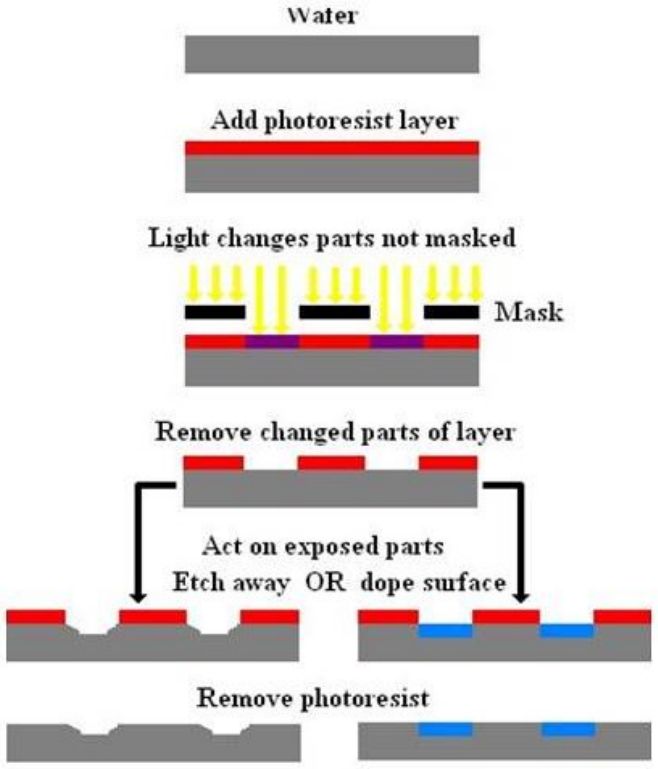

FIGURE A.1: Steps involved in preparing a silicon wafer from a chrom mask with patterns of different sizes and shapes. The image is adopted from http://anh.cs.luc.edu/150summer11/notes/notes.html.

Silane vaporizes and gets deposited on the surfaces kept in desiccator and makes them hydrophobic. Silane coating facilitates the removal of the mould after casting.

- Wash the wafer with milipore water thoroughly using a sprayer and dry in sterile, dust free condition.

- Mix the prepolymer and the curing agent in 10:1 (V/V) ratio and pour it on the silane treated silicon wafer kept in the silane treated dish. The dish was used to have a thick layer of PDMS on silicon wafer by stopping the PDMS from flowing. The Dish was made hydrophobic to not let the wafer stick to the dish.

- Degas the PDMS till all the air bubbles disappear.
- Incubate overnight at 65 °C to cure the PDMS. After curing, peel off the stamps from the wafer. The typical size of the stamps prepared was 1 by1 cm.

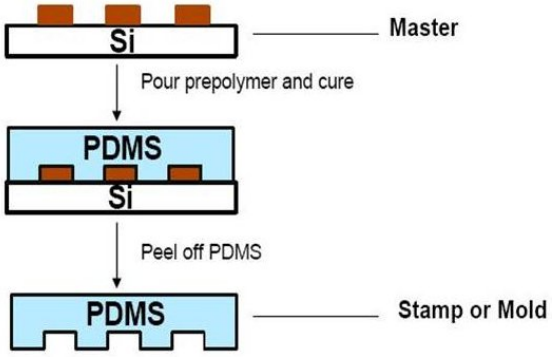

FIGURE A.2: Steps involved in preparing a PDMS Stamp from a silicon mould with patterns of different sizes and shapes http://www.pharmafocusasia.com/research-developement/unconventional-micro-nanofabrication.

A.1.2 Micro-contact printing (MCP)

The steps taken to print the patterns on a glass surface are the following.

- Cover the stamp surface with 50 μg/ml of fibronectin solution and let the fibronectin bind to PDMS for 1 minute.
- Aspirate the fibronectin solution and let the stamp dry.
- As soon as the stamp dries, stamp the pattern on the surface where patterns are desired as shown in fig. A.3.
- To make the non-patterned part inert for cell adhesion, use 0.1% solution of Pluronic 127 (Sigma) for plastic surfaces and 0.1

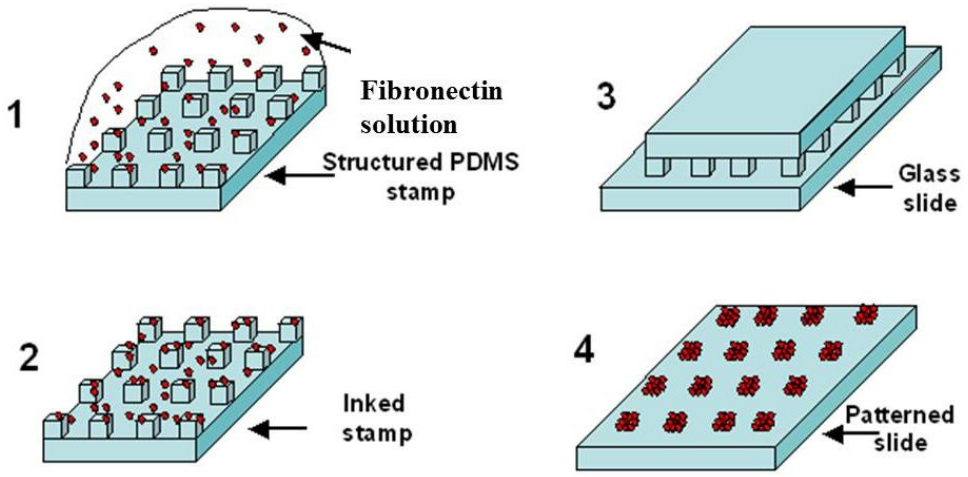

FIGURE A.3: pictorial representation of stamping a glass surface. Image is adopted from Thibault et al. [143].

mg/ml solution of PLL-g-PEG (Surface solutions-Chemicals) for glass surfaces. For Pluronic acid 1hr and for PLL-g-PEG overnight incubation is required before culturing cells on the surface.

We prepared stamps for different patterns, four if then can be seen in fig. A.4.

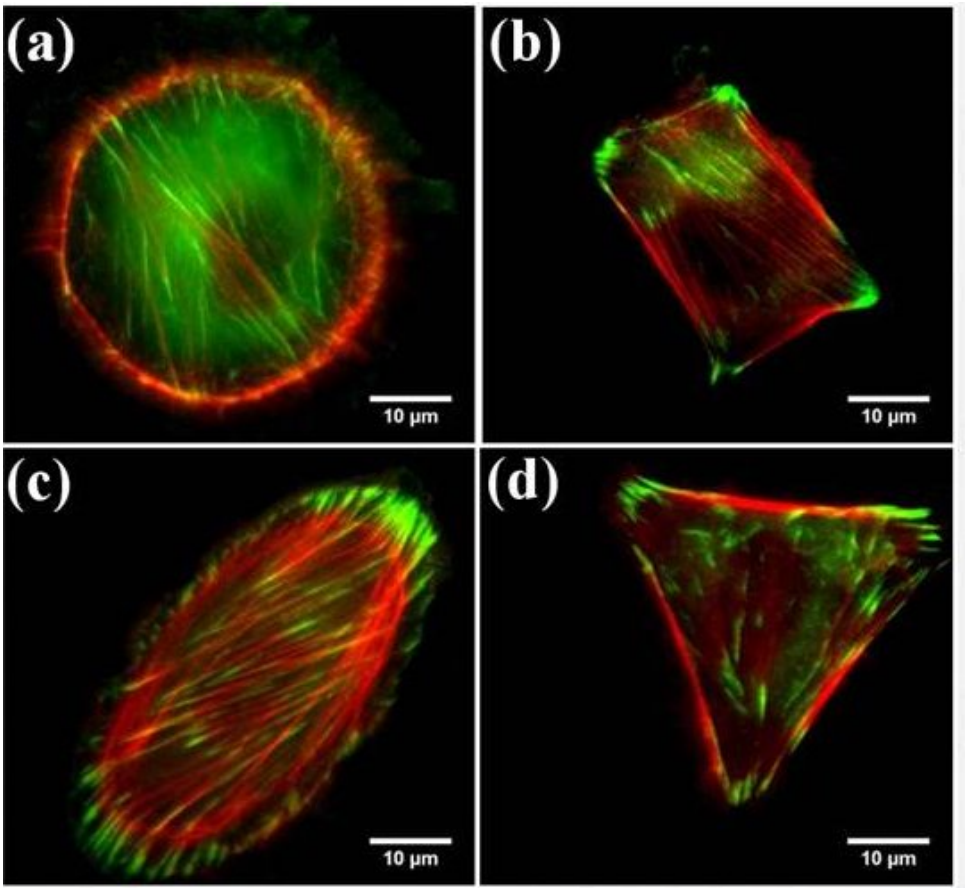

FIGURE A.4: The cell on the patterns in all the images were labelled for actin and focal adhesions with rhodamin phalloidin and anti-vinculin antibody, respectively. Red is actin and green in focal adhesions.

Appendix B

Tether force plots and aurodino code to count RPM

B.1 RPM counting code

```
//-----------------------------------------------
 volatile byte rpmcount;

 unsigned int rpm;
 unsigned long timeold ;
 float sstress;
 void setup()

 {
   Serial.begin(9600);
   attachInterrupt(0, rpm_counter, RISING);
   rpmcount = 0;
```

```
   rpm = 0;
   timeold = 0;
 }
 void loop()
 {
   if (rpmcount >= 5) {
     //Update RPM every 5 counts, increase this for better
.....//RPM resolution, decrease for faster update

     rpm = (30*1000/(millis() - timeold))*rpmcount*2;
     sstress = rpm * 0.0048;
     timeold = millis();
     rpmcount = 0;
     Serial.print("RPM = ");Serial.println(rpm,DEC);
     Serial.print("Shear Stress = ");Serial.println(sstress,DEC);
   }
 }
 void rpm_counter()
 {
   rpmcount = rpmcount + 1;

   //Each rotation, this interrupt function is run once.
 }
//------------------------------------------------
```

B.2 Plots for step retraction

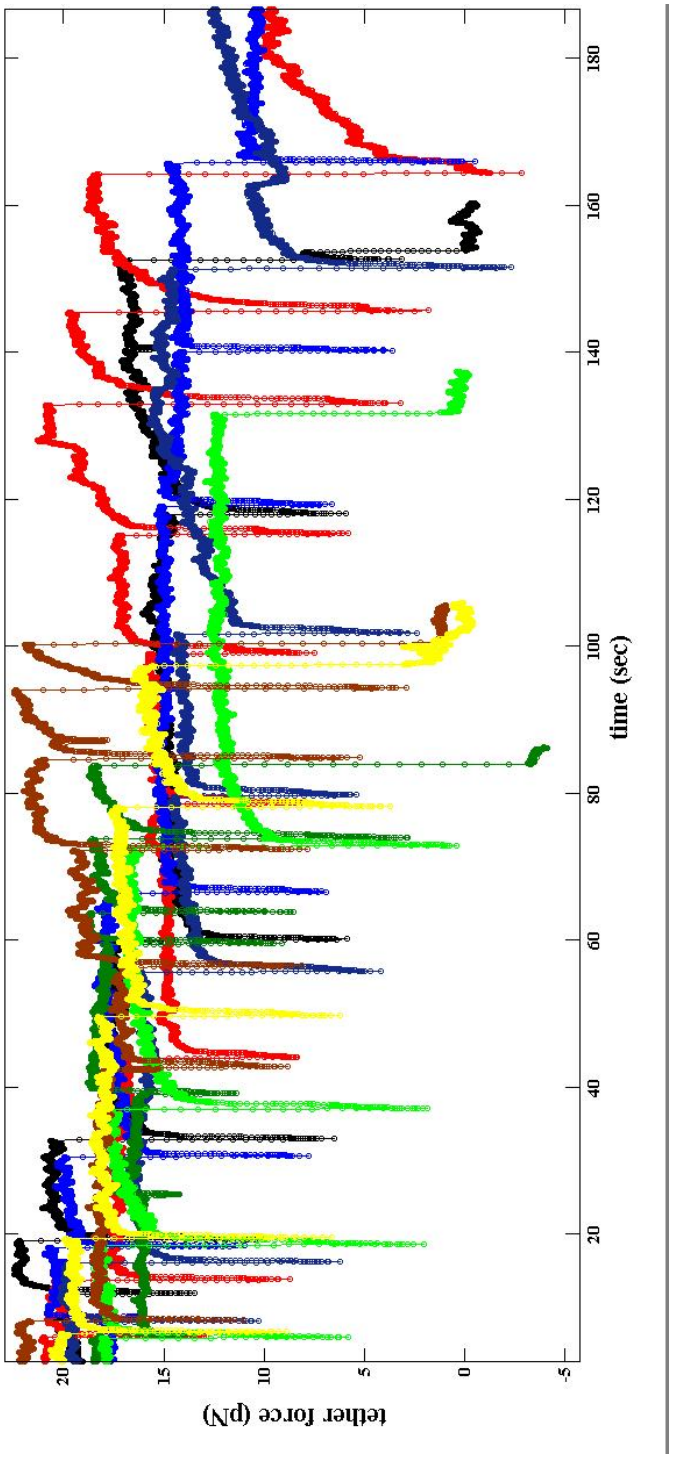

FIGURE B.1: Force curves for step retraction.

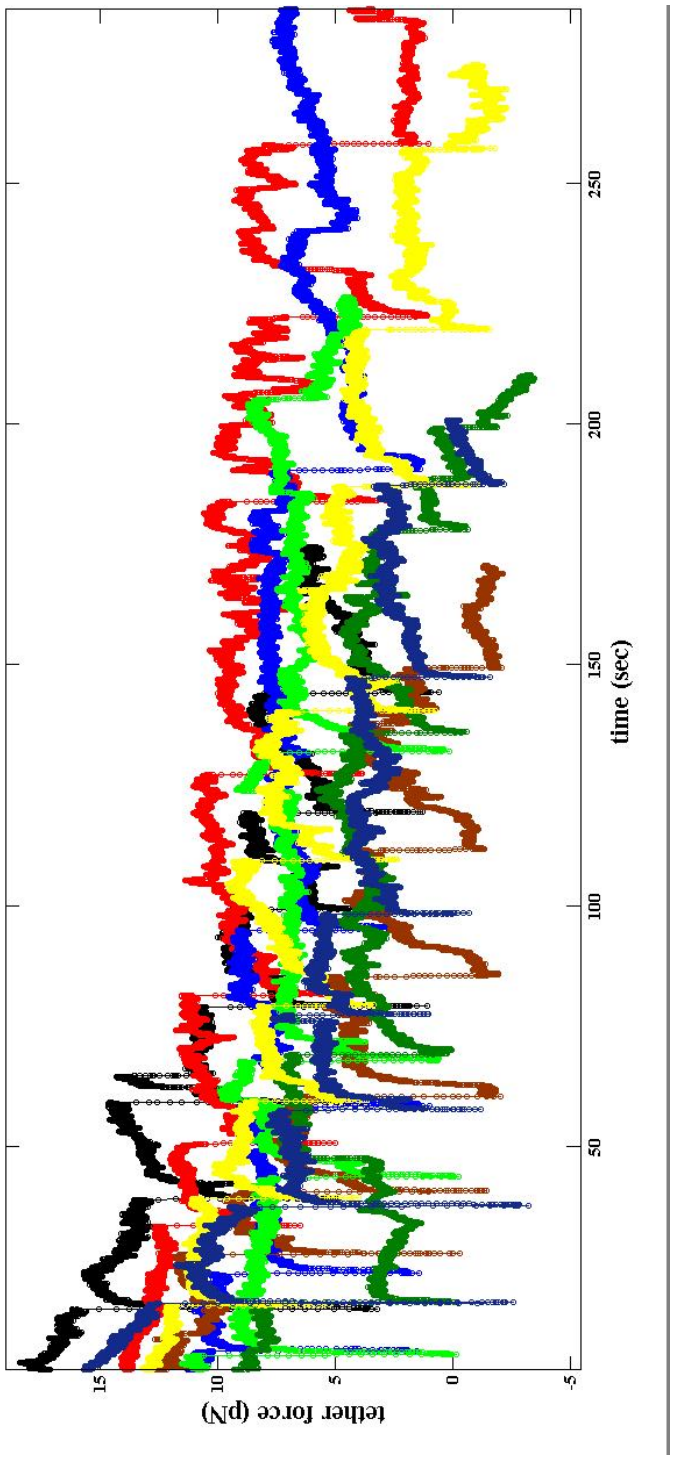

FIGURE B.2: Force curves for step retraction after actin depolymerization.

Bibliography

[1] S. Mitalipov and D. Wolf. Totipotency, Pluripotency and nuclear reprogramming. *Adv. Biochem. Eng. Biotechnol*, 114:185–199, 2008.

[2] O. P. Hamill and B. Martinac. Molecular basis of mechanotransduction in living cells. *Physiol. Rev.*, 81:685–740, 2001.

[3] J. Helms and C. Zurzolo. Lipids as targeting signals: lipid rafts and intracellular trafficking. *Traffic*, 5:247–254, 2004.

[4] G. van Meer and H. Sprong. Membrane lipids and vesicular traffic. *Curr. opin. Cell Biol.*, 16:373–378, 2004.

[5] E. Evans. New membrane concept applied to the analysis of fluid shear- and micropipette-deformed red blood cells. *Biophys. J.*, 13(9):941–954, 1973.

[6] H. Engelhardt and E. Sackmann. On the measurement of shear elastic moduli and viscosities of erythrocyte plasma membranes by transient deformation in high frequency electric fields. *Biophys. J.*, 54(3):495–508, 1988.

[7] S. Hénon, G. Lenormand, A. Richert, and F. Gallet. A new determination of the shear modulus of the human erythrocyte membrane using optical tweezers. *Biophys J.*, 76(2):1145–1151, 1991.

[8] R. Hochmuth, N. Mohandas, and P. Blachshear. Measurement of the elastic modulus for red cell membrane using a fluid mechanical technique. *Biophys. J.*, 13(8), 1973.

[9] R. Hochmuth and R. Waugh. Erythrocyte membrane elasticity and viscosity. *Ann. Rev. Physiol.*, 49(8), 1987.

[10] R. M. Hochmuth, J. Y. Shao, J. Dai, and M. P. Sheetz. Deformationand flow of membrane into tether extracted from neuronal growth cones. *Biophys. J.*, 70:358–369, January 1996.

[11] L. Bo and R. E. Waugh. Determination of bilayer membrane bending stiffness by tether formation from giant, thin-walled vesicles. *Biophys. J.*, 55(3):509–517, 1989.

[12] J.-Y. Shao and J. Xu. A modified micropipette aspiration technique and its application to tether formation from human neutrophils. *J. Biomech. Eng.*, 124:388–396, 2002.

[13] D. Raucher and M. P. Sheetz. Cell spreading and lamellipodial extension rate is regulated by membrane tension. *J. Cell Biol*, 148:127–136, 2000.

[14] A. R. Houk, A. Jilkine, C. O. Mejean, R. Boltyanskiy, E. R. Dufresne, S. B. Angenent, S. J. Altschuler, L. F. Wu, and O. D.

Weiner. Membrane tension maintains cell polarity by confining signals to the leading edge during neutrophil migration. *Cell*, 148:175–188, 1991.

[15] N. C. Gauthier, M. A. Fardin, P. Roca-Cusachs, and M. P. Sheetz. Temporary increase in plasma membrane tension coordinates the activation of exocytosis and contraction during cell spreading. *PNAS*, 108(35):11467–11472, 2011.

[16] E. L. Batchelder, G. Hollopeter, C. Campillo, X. mezanges, P. Jorgensen, E. M. Nassoy, P. Sens, and J. Plastino. Membrane tension regulates motility by controlling lamellipodium organization. *PNAS*, 108(4):114429–114434, 2011.

[17] K. Keren, Z. Pincus, G. Allen, G. Marriott, A. Mogilner, and J. A. Theriot. Mechanism of shape determination in motile cells. *Nature*, 453:475–480, 2008.

[18] G. Apodaca. Modulation of membrane traffic by mechanical stimuli. *Am. J. Physiol. renal. Physiol.*, 282(2):F179–190, 2002.

[19] F. Sachs. Stretch-Activated Ion Channels: What Are They? *Physiology (Bethesda)*, 25(1):50–56, Aug 2010. doi: 10.1152/physiol.00042.2009.

[20] D. A. Fletcher and R. D. Mullins. Cell mechanics and the cytoskeleton. *Nature*, 463(7280):485–492, January 2010.

[21] G. M. Cooper. *The Cell: A molecular approcah, 2nd edition.* McGraw–Hill, 2000.

[22] F. Korobova and T. Svitkina. Arp2/3 complex is important for filopodia formation, growth cone motility, and neuritogenesis in neuronal cells. *Mol. Biol. cell*, 19(4):1561–1574, April 2008.

[23] R. Domiquez. Structural insights into de novo actin polymerization. *Curr. opin. struct. Biol.*, 20(2):217–225, Apr 2010.

[24] T. D. Pollard and G. G. Borisy. Cellular motility driven by assembly and disassembly of actin filaments. *Cell*, 112:453–465, 2003.

[25] B. Wickstead and K. Gull. The evolution of the cytoskeleton. *JCB: Review*, 194(4):513–525, August 2011.

[26] E. W. Flitney, E. R. Kuczmarski, S.A. Adam, and R. D. Goldman. Insight into the mechanical properties of endothelial cell: the effect of shear stress on the assembly and remodeling of keratin intermediate filaments. *FASEB J*, 23:2110–2119, 2009.

[27] M. Y. Tsai, S. Wang, J. M. Heidinger, D. K. Shumaker, S. A. Adam, R. D. Goldman, and Y. Zheng. A mitotic lamin B matrix induced by RanGTP required for spindle assembly. *Science*, 311(5769):1887–1893, March 2006.

[28] E. A. Cox, S. K. Sastry, and A. Huttenlocher. Integrin-mediated adhesion regulates cell polarity and membrane protrusion through the Rho family of GTPases. *Mol. biol. of the cell*, 12:265–277, 2001.

[29] B. Geiger, J. P. Spatz, and A. D. bershadsky. Environmental sensing through focal adhesions. *Nat. Rev. Mol. Cell Biol.*, 10: 21–33, 2009.

[30] H. Wolfenson, A. Bershadsky, Y. I. Henis, and B. Geiger. Actomyosin-generated tension controls the molecular kinetics of focal adhesions. *J. Cell Sci.*, 124:1425–32, May 2011.

[31] A. M. Pasapera, L. C. Schneider, E. Rericha, D. D. Schlarpfer, and c. Waterman. Myosin II activity regulates vinculin recruitment to focal adhesions through FAK-mediated paxillin phosphorylation. *J. Cell Biol*, 188:877–890, 2010.

[32] T. Volberg, B. Geiger, S. Citi, and A. D. Barshadsky. Effect of protein kinasei nhibitor H-7 on the contractility, integrity, and membrane anchorage of the microfilament system. *Cell motil. Cytoskeleton*, 29:321–338, 1994.

[33] M. Chranowska-Wodnicka and K. Burridge. Rho-stimulated contractility drives the formation of stress fibers and focal adhesions. *J. Cell Biol.*, 133:1403–1415, 1996.

[34] M. Kovacs, J. Toth, C. Hetenyi, A. Malnasi-Csizmadia, and J. R. Sellers. Mechanism of blebbistatin inhibition of myosin II. *J. Biol. Chem.*, 279:35557–35563, 2004.

[35] D. Riveline, E. Zamir, N. Q. Balaban, U. S. Schwarz, T. ishizaki, S. Narumiya, Z. kam, B. Geiger, and A. D. Bershadsky. Focal contacts as mechanosensors: externally applied

local mechanical force induces growth of focal contacts by an mDia1-dependent and ROCK-independent mechanism. *J. Cell Biol.*, 153:1175–1186, 2001.

[36] M. Vicente-manzanares, J. Zareno, L. Whitmore, C. K. Choi, and A. F. Horwitz. Regulation of protrusion, adhesion dynamics, and polarity by myosins IIA and IIB in migrating cells. *J. Cell Biol.*, 176:573–580, 2007.

[37] A. del Rio, R. Perez-Jimenez, R. Liu, P. Roca-Cusachs, J. M. Fernandez, and M. P. Sheetz. Stretching single talin rod molecules activates vinculin binding. *Science*, 323:638–641, 2009.

[38] C. T. Mierke. The role of vinculin in the regulation of the mechanical properties of cells. *Cell Biochem. Biophys*, 53:115–126, 2009.

[39] S. E. Lee, R. D. kamm, and M.R. Mofrad. Force-induced activation of talin and its possible role in focal adhesion mechanotransduction. *J. Biomech.*, 40(9):2096–106, August 2007.

[40] N. O. Deakin and C. E. Turner. Paxillin comes of age. *J. Cell Sci*, 121(pt15):2435–2444, Aug 2008.

[41] S. H. Lo, E. Weisberg, and L. B. Chen. Tensin: a potential link between the cytoskeleton and signal transduction. *Bioessays*, 16:817–23, November 1994.

[42] A. G. Petrov and P. N. Usherwood. Mechanosensitivity of cell membranes. Ion channels, lipid matrix and cytoskeleton. *Eur. Biophys J.*, 23(1):1–19, 1994.

[43] B. Ladoux and A. Nicolas. Physically based principles of cell adhesion mechanosensitivity in tissues. *Rep. Prog. Phys*, 75: 116601(25pp), 2012. doi: 10.1088/0034-4885/75/11/116601.

[44] A. J. Engler, S. Sen, H. L. Sweeney, and D.E. Disher. Matrix elasticity directs stem cell lineage specification. *Cell*, 126:677–689, 2006.

[45] A. J. Engler, C. Carag-Krieger, C. P. Johnson, M. Raab, H. Y. Tang, D. W. Speicher, J. W. Sanger, J. M. Sanger, and D.E. Disher. Embryonic cardiomyocytes beat best on a matrix with heart-like elasticity: scar-like rigidity inhibits beating. *J. of Cell Science*, 121:3794–3802, 2008.

[46] K. J. Aitken and D. J. Bägli. The bladder extracellular matrix. Part II: regenerative applications. *Nature Reviews urology*, 6: 612–621, 2012. doi: 10.1038/nrurol.2009.202.

[47] N.D. Leipzig and K.A. Athanasiou. Static Compression of Single Chondrocytes Catabolically Modifies Single-cell Gene Expression. *Biophys J.*, 94:2412–2422, 2008.

[48] R. McBeath, D. M. Pirone, C. M. Nelson, et al. Cell Shape, Cytoskeletal tension, and RhoA regulates stem cell lineage commitment. *Developmental Cell*, 6:483–495, 2004.

[49] S. A. Ruiz and C. S. Chen. Emergence of patterned stem cell differentiation within multicellular structures. *Stem Cells*, 26 (1):2921–2927, 2008.

[50] K. A.. Kilian, B. Bugarija, B. T. Lahn, and M. Mrksich. Geometric cues for directing the differentiation of mesenchymal stem cells. *PNAS*, 107(11), 2010.

[51] A. Manzanares, D. J. Webb, and A. R. Horwitz. Cell migration at a glance. *J. of cell science*, 118:4917–4919, 2005.

[52] C. L. Clainche and M. F Carlier. regulation of actin assembly associated with protrusion and adhesion in cell migration. *Physiological Reviews*, 88(22):489–513, 2008.

[53] S. Even-Ram, A. D. Doyle, M. A. Conti, K. Matsumoto, R. S. Adelstein, and K. M. Yamada. Myosin IIA regulates cell motility and actomyosinmicrotubule crosstalk. *Nat. Cell Biol.*, 9: 299–309, 2007.

[54] R. J. Pelham and Y. L. Wang. Cell locomotion and focal adhesions are regulated by substrate flexibility. *PNAS*, 94(25): 13661–13665, 1997.

[55] J R. Tse and A. J. Engler. Stiffness Gradients mimicking Invivo Tissue Variation Ragulate Mesenchymal Stem Cell Fate. *PLoS ONE*, 6(1):e15978, 2011.

[56] T. A. Ulrich, E. M. D. J Pardo, and S. Kumar. The mechanical rigidity of the Extracellular matrix regulates the structure,

motility and proliferation of glioma cells. *Cancer research*, 69: 4167, 2009.

[57] J. D. Mih, A. Marinkovic, F. Liu, A. S. Sharif, and D. J. Tschumperlin. Matrix stiffness reverses the effect of actomyosin tension on cell proliferation. *J. of Cell Science*, 125:5974–5983, 2012.

[58] A. I Caplan. Mesenchymal Stem cells. *J. of orthodaedic Res.*, 9:641–650, 1991.

[59] S. B. Khatau, C. M. Hale, P.J. Stewart-Hutchinson, M. S. Patel, C. L. Stewart, P.C. Searson, D. Hodzic, and D. Wirtz. A perinuclear actin cap regulates nuclear shape. *Proc. Natl. Acad. Sci.*, 106:19017–19022, 2009.

[60] C. M. Lo, H. B. Wang, M. Dembo, and Y. L. Wang. Cell Movement is Guided by the Rigidity of the substrate. *Biophys J.*, 79:144–152, July 2000.

[61] T. Yeung, P. C. Georges, L. A. Flanagan, B. Marg, M. Ortiz, M. Funaki, N. Zahir, W. Ming, V. Weaver, and P.A. Janmey. Effects of Substrate Stiffness on cell Morphology, cytoskeletal Structure, and Adhesion. *Cell Motility and the Cytoskeleton*, 60:24–34, 2005.

[62] M. Ghibaudo, A. Saez, L. Trichet, A. Xayaphoummine, J. Browaeys, P. Silberzan, A. Buguin, and B. Ladoux. Traction forces and rigidity sensing regulate cell functions. *Soft Matter*, 4:1836–1843, 2008.

[63] S. Y. Tee, J. Fu, C. S. Chen, and P.A. Janmey. Cell Shape and Substrate Rigidity Both Regulate Cell Stiffness. *Biophys J.*, 100:L25–L27, 2011.

[64] Y. B. Lu, K. Franze, G. Seifert, C. Steinha user, F. Kirchhoff, H. Wolburg, J. Guck, P. A. Janmey, E. Q. Wei, J. Ka s, and A. Reichenbach. Viscoelastic properties of individual glial cells and neurons in the CNS. *Proc. Natl. Acad. Sci., USA*, 103(47): 17759, 2006.

[65] N. D. Evans, C. Minelli, E. Gentleman, V. LaPointe, S. N. Patankar, et al. Substrate Stiffness affects early differentiation events in Embryonic Stem Cells. *European Cells and materials*, 18:1–14, 2009.

[66] P. Roca-Cusachs, J. Alcaraz, R. Sunyer, J. Samitier, R. Farre, and D. Navajas. Micropatterning of single Endothelial cell shape reveals a tight coupling between nuclear volume in G1 and proliferation. *Biophys J.*, 94:4984–4995, 2008.

[67] M. V. Mazumdar and G.V. Shivashankar. Emergence of a prestressed eukaryotic nucleus during cellular differentiation and development. *J.R. Soc Interface, supplementary (3)*, 7:S321–330, 2010.

[68] M. Versaeval, T. Grevesse, and S. Gabriele. Spatial coordination between cell and nuclear shape within micropatterened endothelial cells. *Nat. Commun.*, 3:671, 2012.

[69] T. Khiara, S. M. Haghparast, Y. Shimizu, S. Yuba, and J. Miyake. Physical properties of mesenchymal stem cells are coordinated by the perinuclear actin cap. *Biochem Biophys Res commun*, 409:1–6, 2011.

[70] K. Nagayama, Y. Yahiro, and T. Matsumoto. Stress fibers stabilize the position of intrenuclear DNA through mechanical connection with nucleus in vascular smooth muscle cells. *FEBS Letters*, 585:3992–3997, 2011.

[71] R. P. Jean, D. S. Grar, A. A. Spector, and C. S. Chen. Characterization of the nuclear deformation caused by changes in endothelial cell shape. *Transactions of the ASME*, 126:552–558, 2004.

[72] D. E. Ingber, J. A. Madri, and J. Folkman. Endothelial growth factors and extracellular matrix regulate DNA synthesis through modulation of cell and nuclear expansion. *In Vitro Cellular and Development Biology*, 23(5):387–394, July 1987.

[73] S. Sen and S. Kumar. Cell-Matrix De-Adhesion Dynamics Reflect Contractile Mechanics. *Cellular and Mol. Bioengineering*, 2(2):218–230, June 2009.

[74] J. Lammerding, L. G. Fong, K. Reue, C. L. Stewart, S. G. Young, and R. T. Lee. Lamin A and C, but not Lamin B1 Regulate Nuclear Mechanics. *J. of Biol.Chem.*, 281(35):25768–25780, 2006.

[75] J. Swift, I. L. Ivanovska, A. Buxboim, T. Harada, P. D. Dingal, J. Pinter, J. D. Pajerowski, K. R. Spinler, M. Shin, J. W. Tewari, F. Rehfeldt, D. W. Speicher, and D. E. Discher. Nuclear Lamin-A Scales with Tissue Stiffness and enhances matrix-directed differentiation. *Science*, 341(6149):1240104, 2013.

[76] J. Schäpe, S. Prußе, M. Radmacher, and R. Stick. Influence of lamin A on the mechanical properties of Amphibian oocyte nuclei measured by Atomic Force Microscopy. *Biophys J.*, 99: 4319–4325, 2009.

[77] A. Saez, A. Buguin, P. Silberzan, and B. Ladoux. Is the Mechanical Activity of Epithelial Cells Controlled by Deformations or Forces? *Biophys J.*, 89(6):L52–L54, Dec 2005. doi: 10.1529/biophysj.105.071217.

[78] J. Fu, Y. K. Wang, M. T. Yang, R. A. Desai, X. Yu, Z. Liu, and C.S. Chen. Mechanical regulation of cell function with geometrically modulated elastomeric substrates. *Nat. methods*, 5:733–736, 2010.

[79] S. S. Hur, Y. Zhao, Y. S. Li, E. Botvinick, and S. Chien. Live cells Exert 3-Dimentional Traction forces on Their Substrata. *Cell and molecular Bioengineering*, 2(3):425–436, 2009.

[80] J. P. Butler, I. M. Tolic-Norrelykke, B. Fabry, and J. J. Fredberg. Traction fields, moments, and strain energy that cell

exerts on their surroundings. *Am. J. Physiol*, 282:C595–C605, 2002.

[81] Y. Tatara. On compression of rubber elastic sphere over a large range of displacements – part 1: Theoretical study. *J. Eng. Matter. Technol.*, 113:285–291, July 1991.

[82] Y. Tatara, S. Shima, and J. C. Lucero. On compression of rubber elastic sphere over a large range of displacements – part 2: Comparision of theory and experiment. *J. Eng. Matter. Technol.*, 113:292–295, july 1991.

[83] S. J. Han, K. S. Bielawski, L. H. Ting, M. L. Rodriguez, and N.J. Sniadecki. Decoupling substrate stiffness,spread area, and micropost density: A close spatial relation between traction forces and focal adhesions. *Biophys J.*, 104(4):640–648, 2012.

[84] Y. Yan, Z. B. Zhang, J. R. Stokes, Q. Z. Zhou, G. H. Ma, and M.J. Adams. Mechanical characterization of agarose microparticles with a narrow size distribution. *Powder Tech*, 192: 122–130, 2009.

[85] R. Budyna and K. Nisbett. *Shigley's Mechanical Engineering Design.* McGraw–Hill, 2008.

[86] F. P. Beer and E. R. Jhonston. *Mechanics of Materials.* McGraw–Hill, 1992.

[87] Q. Li, A. Kumar, A. Makhija, and G. V. Shivashankar. The regulation of dynamic mechanical coupling between actin cytoskeleton and nucleus by matrix geometry. *Biomaterials*, 35: 961–969, 2014.

[88] D. Cuvelier, M. Théry, Y. S. Chu, S. Dufour, J.P. Thiéry, M. Bornens, P. Nassoy, and L. Mahadevan. The Univarsal Dynamics of Cell Spreading. *Curr. Biol.*, 17:694–699, 2007.

[89] M. A. Fardin, O. M. Rossier, P. Rangamani, P. D. Avigan, N. C. Gauthier, W. Vonnequt, A. Mathur, J. Hone, Iyengar R., and M.P. Sheetz. Cell spreading as a hydrodynamic process. *Soft Matter*, 6:4788–4799, 2010.

[90] S. Tojkander, G. Gateva, and P. Lappalainen. Actin stress fibers assembly, dynamics and biological roles. *J. of cell science*, 125:1–10, 2012.

[91] S. Tojkander, G. Gateva, G. Schevzov, P. Hotulainen, P. Naumanen, C. Martin, P. W. Gunning, and P. Lappalainen. A Molecular Pathway for Myosin II Recruitment to Stress Fibers. *Curr. Biol.*, 21:539–550, 2011.

[92] J. Y Tinevez, U. Schulze, G. salbreux, J. Roensch, J. F. Joanny, and E. Paluch. Role of cortical tension in bleb growth. *Proc. Natl. Acad. Sci, USA*, 106(44), 2009.

[93] T. Lecuit and P. F. Lenne. Cell surface mechanics and the control of cell shape, tissue patterns and Morphogenesis. *Nat. Reviews, Mol. cell Biol.*, 8:633–644, August 2007.

[94] T. Choudhary, F. Rehfeldt, H. L. Sweeney, and D.E. Disher. Preparation of collagen-Coated Gels that Maximize In Vitro Muscle. *Methods in mol. Bio.*, 621:185–202, 2010.

[95] U. Chippada, B. Yurkea, and N.A. Langranaa. Simultaneous determination of Young's modulus, shear modulus, and Poisson's ratio of soft hydrogels. *J. of Materials Research*, 25:545–555, 2010.

[96] K. Saha, J. Kim, E. Irwin, J. Yoon, F. Momin, V. Trujillo, D. V. Schaffer, K. E. Healy, and R. C. Hayward. Surface Creasing instability of soft Polyacrylamide cell Culture Substrate. *Biophys J.*, 99(12):L94–L96, December 2010.

[97] J. Dai and M. P. Sheetz. Regulation of endocytosis, exocytosis, and shape by membrane tension. *Cold Spring Harb Symp. Quant. Biol.*, 60:567–571, December 1995.

[98] K. S. Cole. Surface Forces of the Arbacia egg. *J. Cellular and comparative physiol.*, 1:1–9, 1932.

[99] A. Diz-Muñoz, D. A. Fletcher, and O. D. Weiner. Use the force: membrane tension as an organizer of cell shape and motility. *Trends in Cell Biology*, 23(2):47–53, 2013.

[100] J. Dai and M. P. Sheetz. Cel membrane mechanics. *Methods Cell Biol*, 55:157–171, 1998.

[101] A. Diz-Muñoz, M. Krieg, I. Ibarlucea-Benitez, D. J. Muller, and C.-P. Plauch, E. Heisenberg. Control of Directed Cell Migration In Vivo by Membrane-to-Cortex Attachment. *PLoS Biol.*, 8(11):e1000544, 2010.

[102] R. M. Hochmuth, H. C. Wiles, E. A. Evans, and J. T. McCown. Extensional flow of erythrocyte membrane from cell body to elastic tether. II. Experiment. *Biophys. J.*, 39(1), 1973.

[103] I. Derényi, G. Koster, M. M. van Duijn, A. Czövek, M. Dogterom, and J. Prost. Membrane Nanotubes. *Lect. Notes Phys.*, 711:141–159, 2007.

[104] Sheetz. M. P. Cell control by membrane-cytoskeleton adhesion. *Nature reviews Mol. cell Biol.*, 2:392–396, May 2011.

[105] J. Dai and M. P. Sheetz. Membrane tether formation from blebbing cells. *Biophys. J.*, 77(6):3363–3370, December 1999.

[106] E. Evans and A. Yeung. Hidden dynamics in rapid changes of bilayer shape. *Chemistry and physics of lipids*, 73(12):39–56, 1994.

[107] G. Koster, A. Cacciuto, I. Derényi, D. Frenkel, and M. Dogterom. Force barriers for membrane tube formation. *Phys. Rev. lett.*, 94:068101, Feb 2005.

[108] D. Raucher and M. P. Sheetz. Characteristics of a membrane Reservoir Buffering membrane Tension. *Bio. Phys. J.*, 77:1992–2002, 1999.

[109] O. L. Gervásio, W. D. Phillips, L. Cole, and D. G. Allen. Caveolae respond to cell stretch and contribute to stretch-induced signaling. *J. Cell Sci.*, 124:3581–3590, 2011.

[110] B. Sinha, D. Ḱoster, R. Ruez, P. Gonnord, M. Bastiani, D. Abankwa, R. V. Stan, G. Butler-Browne, B. Vedie, L. Johannes, N. Morone, R. G. Parton, G. Raposo, P. Sens, C. Lamaze, and P. Nassoy. Cells respond to mechanical stress by rapid disassembly of caveolae. *Cell*, 144(3):402–413, 2011.

[111] L. Figard and A. M. Sokac. A membrane reservoir at the cell surface. *BioArchitecture*, 4(2):39–46, 2014. doi: 10.4161/bioa.29069.

[112] S. Pierre and M. S. Turner. Budded membrane microdomains as tension regulators. *Phy. Rev. E*, 73:031918, 2006. doi: 10.1103/PhysRevE.73.031918.

[113] W. C. Hwang and R. E. Waugh. Energy of dissociation of lipid bilayer from the membrane skeleton of red blood cells. *Bophys. J.*, 72:2669–2678, June 1997.

[114] Z. Li, B. Anvari, M. Takashima, P. Brecht, J. H. Torres, and W. E. William. Force-induced activation of talin and its possible role in focal adhesion mechanotransduction. *J. Biomech.*, 82(3):1386–1395, August 2002.

[115] L. Jauffred, T. H. Callisen, and L. B. Oddershede. Visco-Elastic Membrane Tethers Extracted from Escherichia coli by Optical Tweezers. *Biophys. J.*, 93:4068–4075, December 2007.

[116] E. A. C. Follett and R. D. Goldman. The occurrence of microvilli during spreading and growth of BHK21/C13 fibroblasts. *Experimental Cell Research*, 59(1):124–136, 1970.

[117] C. A. Erickson and J. P. Trinkus. Microvilli and blebs as sources of reserve surface membrane during cell spreading. *Experimental cell research*, 99(2):375–384, 1976.

[118] J. F. Marko and E. D. Siggia. Stretching DNA. *macromolecules*, 28:8759–8770, 1995.

[119] S. M. Albelda and C. A. Buck. Integrins and other cell adhesion molecules. *The FASEB Journal*, 4(11):2868–2880, August 1990.

[120] J. D. Humphries, A. Byron, and M. J. Humphries. Integrin ligands at a glance. *J. Cell Sci.*, 119:3901–3903, October 2006.

[121] K. E. Brown and K. M. Yamada. The role of integrins during vertebrate development. *Seminars in Developmental Biology*, 6(2):69–77, April 1995.

[122] C. Bokel and N. H. Brown. Integrins in development: moving on, responding to, and sticking to the extracellular matrix. *Dev. Cell*, 3:311–321, 2002.

[123] D. Bouvard, C. Brakeebusch, A. Gustafsson, E. Aszodi, T. Bengtsson, A. Berna, and R. Fassler. Functional consequences of integrin gene mutations in mice. *Circ. Res.*, 89: 211–223, 2001.

[124] S. M. Albelda and C. A. Buck. Role of integrins and other cell adhesion molecules in tumor progression. *The Journal of Technical Methods and Pathology*, 68(1):4–17, 1993.

[125] R. O. Hynes and Q. Zhao. The evolution of cell adhesion. *J. Cell Biol.*, 150(2):F89–F96, July 2000.

[126] S. Wassler, M. Gimona, and G. Rieder. Regulation of the actin cytoskeleton in Helicobacter pylori-induced migration and invasive growth of gastric epithelial cells. *Cell communication and signaling*, 9:27, 2011. doi: 10.1186/1478-811X-9-27.

[127] B. L. Langille, J. J. K. Graham, D. Kim, and A. I Gotlieb. Dynamics of shear-induced redistribution of F-actin in endothelial cells In Vivo. *Arteriosclerosis and Thrombosis.*, 11:1814–1820, 1991.

[128] M. Yoshigi, L. M. Hoffman, C. C. Jensen, H. J. Yost, and M. C. Beckerle. Mechanical force mobilizes zyxin from focal adhesions to actin filaments and regulates cytoskeletal reinforcement. *JCB: Report*, 171(2):209–215, October 2005.

[129] A. B. Chambliss, S. B. Khatau, N. Erdenberger, D. K. Robinson, D. Hodzic, D. G. Longmore, and D. Wirtz. The LINC-anchored actin cap connects the extracellular milieu to the nucleus for ultrafast mechanotransduction. *nature, Scientific Reports*, 3:1087, 2013.

[130] Y. T. Shiu, S. Li, W. A. Marganski, S. Usami, M. A. Schwartz, Y. L Wang, M. Dembo, and S. Chien. Rho mediates the shear-enhancement of endothelial cell migration and traction force generation. *Biophys J.*, 86:2558–2565, 2004.

[131] A. B. Mathur, M. W. Reichert, and G. A. Truskey. Flow and High Affinity Binding Affect the Elastic Modulus of the Nucleus, Cell Body and the Stress Fibers of Endothelial Cells. *Annals of Biomedical Engineering*, 35(7):1120–1130, 2007.

[132] I. D. Vlaminck and C. Dekker. Recent Advances in Magnetic Tweezers. *Annu. Rev. Biophys*, 41:453–72, 2012.

[133] P. Fernández, L. Heymann, A. Ott, N. Aksel, and P. A. Pullarkat. Shear rheology of a cell monolayer. *New J. of Phy.*, 9:419, 2007.

[134] B. R. Blackman, K. A. Barbee, and L. E. Thibault. *In Vitro Cell Shearing Device to Investigate the Dynamic Response of cells in a controlled Hydrodynamic Environment. Annals of Biomed. Eng.*, 28(4):363–372, 2000.

[135] H. Bruus. *Theoretical microfluidics*. Oxford Unversity Press, 2008.

[136] M. Mooney and R.H. Ewart. The coincylindrical viscometer. *Physics*, 5:350–354, 1934.

[137] R. McKennell. Cone plate viscometer comperison with coaxial cylinder viscometer. *Anal. Chem.*, 28(11):1710–1714, 1956.

[138] J. S. Mitchell, W. S. Brown, D. G. Woodside, P. Vanderslice, and B. W. McIntyre. Clustering T-cell GM1 lipid rafts increases cellular resistance to shear on fibronectin through changes in integrin affinity and cytoskeletal dynamics. *Immun. and cell Biol.*, 87:324–336, 2009.

[139] C. Christophis, M. Grunze, and A. Rosenhahn. Quantification of the adhesion strength of fibroblast cells on ethylene glycol terminated self-assembled monolayers by a microfluidic shear force assay. *Phys. Chem. Chem. Phys.*, 12:4498–4504, 2010. doi: 10.1039/b924304f.

[140] L. S. L. Cheung, X. Zheng, A. Stopa, J. C. Baygents, R. Guzman, J. A. Schroeder, R. L. Heimark, and Y. Zohar. Detachment of captured cancer cells under flow acceleration in a biofunctionalized microchannel. *Lab Chip*, 9:1721–1731, 2009. doi: 10.1039/b822172c.

[141] A. D. Lieber, S. Yehudai-Resheff, E. L. Barnhart, J. A. Theriot, and K. Keren. Membrane Tension in Rapidly Moving Cells Is Determined by Cytoskeletal Forces. *Curr. Biol.*, 23(15):1409–1417, August 2013.

[142] M. Irmscher, K.A. V. Laarhoven, A. M. D. Jong, and M.W.J. Prins. The influence of inhomogenious adhesion on the detachmnet dynamics of adhering cells. *Eur Biophys J*, 2013. doi: 10.1007/s00249-013-0891-3.

[143] C. Thibault, V. Le Berre, S. Casimirius, E. Trévisiol, J. Francois, and C. Vieu. Direct microcontact printing of oligonucleotides for biochip applications. *J. of Nanobiotechnology*, 3: 7, 2005. doi: :10.1186/1477-3155-3-7.